UNDERSTANDING WEAK BINDING FOR PHOSPHO(ENOL)PYRUVATE TO THE ALLOSTERIC SITE OF PHOSPHOFRUCTOKINASE FROM *Lactobacillus delbrueckii* SUBSPECIES *bulgaricus*

A Dissertation

by

SCARLETT BLAIR FERGUSON

Submitted to the Office of Graduate Studies of
Texas A&M University
in partial fulfillment of the requirements for the degree of

DOCTOR OF PHILOSOPHY

August 2011

Major Subject: Biochemistry

Understanding Weak Binding for Phospho(enol)pyruvate to the Allosteric Site of Phosphofructokinase from *Lactobacillus delbrueckii* Subspecies *bulgaricus*

UNDERSTANDING WEAK BINDING FOR PHOSPHO(ENOL)PYRUVATE TO THE ALLOSTERIC SITE OF PHOSPHOFRUCTOKINASE FROM *Lactobacillus delbrueckii* SUBSPECIES *bulgaricus*

A Dissertation

by

SCARLETT BLAIR FERGUSON

Submitted to the Office of Graduate Studies of
Texas A&M University
in partial fulfillment of the requirements for the degree of

DOCTOR OF PHILOSOPHY

Approved by:

Chair of Committee,	Gregory D. Reinhart
Committee Members,	J. Martin Scholtz
	Vladislav Panin
	Donald W. Pettigrew
Head of Department,	Gregory D. Reinhart

August 2011

Major Subject: Biochemistry

ABSTRACT

Understanding Weak Binding for Phospho(enol)pyruvate to the Allosteric Site of Phosphofructokinase from *Lactobacillus delbrueckii* subspecies *bulgaricus*.

(August 2011)

Scarlett Blair Ferguson, B.S., Angelo State University

Chair of Advisory Committee: Dr. Gregory D. Reinhart

Phosphofructokinase (PFK) from the lactic acid bacterium *Lactobacillus delbrueckii* subspecies *bulgaricus* (LbPFK) is a non-allosteric PFK with weak binding affinity for both the allosteric ligands phospho(enol)pyruvate (PEP) and magnesium adenosine diphosphate (MgADP). PEP and MgADP bind to the same allosteric binding site but exhibit opposite effects, PEP acting as an inhibitor and MgADP an activator. In 2005, Parichatttanakul, et al. solved the first crystal structure of LbPFK to 1.87 Å resolution and allowed for a structural comparison of LbPFK to the allosteric forms of PFK from *E. coli* (EcPFK) and *Bacillus stearothermophilus* (BsPFK). Two additional structures of LbPFK have been determined with the first having phosphates bound at the four active sites and four allosteric sites solved to 2.20 Å resolution. The second structure solved to 1.83 Å resolution contains phosphates at all eight sites with the addition of the substrate fructose-6-phosphate (F6P) in the active sites. These structures are similar to the published sulfate-bound LbPFK structure. Overall, the secondary, tertiary and quaternary structure is conserved with the exception of the residues in the

allosteric site. E55, H59, S211, D214, H215 and G216, as well as the long cassettes of residues 52-61 (PFKs1) and 206-218 (PFKs2) were mutated to the corresponding residue/residues in *Thermus thermophilus* PFK (TtPFK). PFKs1 and PFKs1 were also combined to form PFKs1s2. The single mutations along with PFKs1 and PFKs2 showed no enhancement in PEP binding, but PFKs1s2 enhanced PEP binding 10-fold with no change in MgADP binding compared to LbPFK.

D12, located along the active site interface 15 Å away from the allosteric site, was mutated to an alanine and exhibited enhanced binding 9-fold for both PEP and MgADP to the allosteric binding site. A crystal structure of D12A was solved to 2.30 Å resolution with sulfate bound to all eight binding sites, and showed no major changes in secondary, tertiary or quaternary structure when compared to the sulfate-bound wild-type LbPFK structure. Combining D12A with PFKs1s2 (PFKs1s2/D12A) further enhanced PEP binding with a 21-fold tighter binding compared to LbPFK with MgADP binding being similar to D12A. PEP inhibition was also quantitated in PFKs1s2/D12A with a $Q_{ay} = 0.007 \pm 0.0008$. Coupling between PEP and F6P in PFKs1s2D12A is 2-fold stronger than the coupling measured in EcPFK and 7-fold stronger than the coupling measured in BsPFK. The coupling measured in PFKs1s2D12A is the first measured in any of the LbPFK variants.

DEDICATION

To my parents and husband: Terry and Mellissa Blair and Brent Ferguson. Mom and Dad, I could not have done any of this without your continued love and support. You always taught me to believe in myself, work hard to achieve my goals and to be thankful for the many blessings my God has given me. Thank you for providing a home for me to escape to, for always being there to listen about the ups and downs of graduate school and for your unconditional love. Because of all you have done for me, for which I am truly grateful, I dedicate this dissertation to my parents.

Brent, you are the love of my life and the most loving, gentle and patient man I have ever known. Your never-ending love and support have made this process a success and the last seven years would not have been the same without you in my life. Meeting you was the best thing that ever happened to me and without you I don't think I could have made it through the toughest times. God has blessed me by giving me a wonderful husband who is not only an amazing scientist but a great listener and friend. Your continued support and advice have made me a better person and scientist. For all this, I dedicate this work to my husband.

ACKNOWLEDGEMENTS

I would first like to thank my advisor, Dr. Gregory D. Reinhart, for his support, guidance and patience throughout my graduate career. He is an amazing mentor and never gave up on me even when my experiments just wouldn't work. Thanks to all my committee members, past and present, for all the advice and support over the last eight years. Dr. Scholtz has been a constant figure throughout my graduate career and has always pushed me to be my best. Dr. Fitzpatrick and Dr. Kladde helped me start out and helped me through my preliminary exams. Dr. Panin and Dr. Pettigrew stepped in to be a part of my committee when I needed them the most. All together my committee members helped me become the scientist I am today. I would also like to thank Dr. Sacchettini and Dr. Reddy for their work and help in solving the crystal structures of LbPFK discussed in chapters III and V of this dissertation.

Thanks to my lab mates, past and present, for great conversations and making the lab a great place to work. To the many friends I have made over the last eight years, you are all amazing people and I am a better person for having all of you in my life. Thanks for making me laugh, being by my side when times were tough and helping me celebrate all the accomplishments along the way. Thanks to my family for all being such a great support system and praying for me over the years. Mom, thanks for helping me move in the heat of August, for the many visits and for always answering the phone to hear about my day. Dad, thanks for all the advice you have given me about life and science. You are a brilliant person and have taught me so much during my life. Brent, thanks for

marrying me and loving me with all your heart. You are the love of my life and an amazing scientist. I would like to thank Sam, Tracy and Jordan Fulton for being wonderful friends and giving me a place to sleep these last few months. You guys are great and have always been there to help Brent and me over the years.

Last but certainly not least, I want to thank my God for blessing me with the knowledge to make it through graduate school, the family and friends to support me, and a wonderful husband. Thanks for listening to the many prayers and I give you all the glory for accomplishments I have achieved.

NOMENCLATURE

ABC	ATP binding cassette
BCA	Bicinchoninic acid
BsPFK	PFK from *Bacillus stearothermophilus*
CcpA	Catabolite control protein A
CCR	Carbon catabolite repression
Cre	Catabolite response element
Crp	cAMP binding protein
DHAP	Dihydroxyacetone phosphate
DTT	Dithiothreitol
EcPFK	PFK from *E. coli*
EDTA	Ethylenediamine tetraacetic acid
EPPS	N- [2-Hydroxyethyl] Piperazine-N‟-3-Propanesulfonic Acid
F6P	Fructose-6-phosphate
FBP	Fructose-1,6-bisphosphate
G3P	Glyceraldhyde-3-phosphate
IPTG	Isopropyl β-D-1-thiogalactopyranoside
KNF	Koshland-Nemethy-Filmer
L.	*Lactococcus*
LAB	Lactic acid bacteria
LB	Lysogeny broth

Lb.	*Lactobacillus*
LbPFK	PFK from *Lactobacillus delbrueckii* subspecies *bulgaricus*
LDH	Lactate dehydrogenase
MOPS	3-[N-Morpholino] Propanesulfonic acid
MWC	Monod-Wyman-Changeux
NAD^+	Nicotinamide adenine dinucleotide, oxidized form
NADH	Nicotinamide adenine dinucleotide, reduced form
$NADP^+$	Nicotinamide adenine dinucleotide phosphate, oxidized form
NADPH	Nicotinamide adenine dinucleotide phosphate, reduced form
n_H	Hill coefficient
PAGE	Polyacrylamide Gel Electrophoresis
PDB	Protein Data Bank
PEP	Phospho(enol)pyruvate
PFK	Phosphofructokianse
PFKs1	Residues 52-61 of LbPFK substituted by 52-61 of TtPFK
PFKs2	Residues 206-218 of LbPFK substituted by 206-218 of TtPFK
PFKs1s2	Combination of PFKs1 and PFKs2
P_i	Inorganic phosphate
pI	Isoelectric point
PG	Phosphoglycolate
PKP	Phosphoketolase pathway
PMF	Proton motive force

PP_i	Pyro-phosphate
PP_i-PFK	Pyro-phosphate dependent PFK
PTS	PEP-dependent phosphotransferase system
PYK	Pyruvate kinase
S.	*Streptococcus*
SDS	Sodium Dodecyl Sulfate
TIM	Triose-phosphate isomerase
Tris	Tris [Hyroxymethyl] aminomethane
TtPFK	PFK from *Thermus thermophilus*
[A]	Concentration of substrate
[E]	Concentration of free enzyme
[X]	Concentration of effector, MgADP
[Y]	Concentration of effector, PEP
[EA]	Concentration of enzyme-substrate complex
[XE]	Concentration of enzyme-effector complex
[XEA]	Concentration of ternary complex
$K_{ia}°$	Dissociation constant for A in the absence of X
K_{ia}^{∞}	Dissociation constant for A in the saturating presence of X
$K_{ix}°$	Dissociation constant for X in the absence of A
K_{ix}^{∞}	Dissociation constant for X is the saturating presence of A
$K_{iy}°$	Dissociation constant for Y in the absence of A
Qax	Coupling constant between substrate and effector X

Qay	Coupling constant between substrate and effector Y
$K_{1/2}$	Concentration of F6P at half-maximal velocity
K_b	Dissociation constant for substrate B
ν	Initial velocity
V_{max}	Maximal velocity
ΔG_a °	Free Energy of F6P binding
ΔG_y °	Free Energy of PEP binding
K_{iy}^{app}	Apparent dissociation constant for effector Y
K_{ix}^{app}	Apparent dissociation constant for effector X
K_i^{PEP}	Dissociation constant for PEP in absence of MgADP
k_{cat}	Catalytic turnover number

TABLE OF CONTENTS

CHAPTER Page

LIST OF FIGURES

FIGURE Page

LIST OF TABLES

CHAPTER I

INTRODUCTION: LACTIC ACID BACTERIAL SUGAR METABOLISM AND THE ROLE OF PHOSPHOFRUCTOKINASE

Phosphofructokinase (PFK) from the lactic acid bacteria (LAB) *Lactobacillus delbrueckii* subspecies *bulgaricus* (*Lb. delbrueckii* subspecies *bulgaricus*), or LbPFK, is a non-allosteric form of PFK. Compared to allosteric forms of PFK from *E. coli* (EcPFK) and *Bacillus stearothermophilus* (BsPFK) LbPFK is similar in both sequence and overall structure. Only the residues within the allosteric site are significantly different. These differences might explain the weak binding for the allosteric ligands, the inhibitor phospho(enol)pyruvate (PEP) and the activator MgADP. In order to get a better understanding of the lack of allosteric regulation of PFK in *Lb. delbrueckii* subspecies *bulgaricus*, a review of sugar metabolism in LAB is given below.

Sugar Transport in Lactic Acid Bacteria

LAB are a heterogeneous group of microorganisms that have one thing in common; they produce lactic acid as the end product of carbohydrate fermentation (*1*). They are gram-positive bacteria that can be found in the shape of rods or cocci and share many biochemical, physiological and genetic characteristics. These bacteria as a whole are acid-tolerant, catalase-negative, non-spore forming, facultative anaerobes with low GC content in their DNA. In addition, LAB are heterotrophic chemoorganotrophs, that

---

This dissertation follows the style of *Biochemistry*.

is they use pre-formed organic carbon for both a source of carbon and energy. There are two pathways of fermentation in LAB, homofermentation and heterofermentation. In homofermentation, lactic acid is produced from 90% of the sugar metabolized but in heterofermentation, acetic acid, ethanol and carbon dioxide are produced in addition to lactic acid. LAB generally possess one pathway or the other but examples of certain species being able to switch between the two exist (*2*).

These bacteria are mostly found in nutrient-rich environments including dairy products, meat products, vegetables, plants and cereals as well as the gastrointestinal and genitourinary tracts of animals and humans. The specific environment that they inhabit plays a huge role in their overall metabolism and genetic make-up (*1, 2*). It is the specific genetic make-up which classifies them into twelve distinct genera. Eight of these twelve (*Lactobacillus, Lactococcus, Leuconostoc, Oenococcus, Pediococcus, Streptococcus, Tetragenococcus* and *Enterococcus*) are used directly in the fermentation of food. These eight can further be divided based on the fermentation pathways they utilize. *Lactococcus, Pediococcus, Streptococcus, Tetragenococcus* and *Enterococcus* are all homo-fermenters, while *Leuconostoc* and *Oenococus* are hetero-fermenters. The genera *Lactobacillus* is different in that it contains both homo- and hetero-fermenters (*2*).

LAB are found in various types of nutrient-rich environments and the environments in which these bacteria thrive influence their overall metabolism. LAB cannot obtain energy by oxidative or respiratory processes because of a lack in cytochrome or electron transport protein (*2*). Therefore, these bacteria must get their

energy from the production of ATP via substrate phosphorylation reactions. The type of pathway used to ferment sugars is dependent on the type of fermentation utilized by the bacteria (Figure 1-1). In the case of homofermentation, glycolysis is used to form pyruvate which is then converted into lactate via lactate dehydrogenase (LDH). This pathway yields two moles of ATP per mole of hexose, that is used as an energy source, and one mole of NADH which must be re-oxidized by LDH in order to keep the [NADH]/[NAD^+] ratio balanced. An example of homofermentation is *Lb. delbrueckii* subspecies *bulgaricus* that is involved in the fermentation of yogurt along with *Streptococcus thermophilus* (*S. thermophilus*). *Lb. delbrueckii* subspecies *bulgaricus* exhibits very simple metabolism only metabolizing lactose, fructose, glucose and mannose. *Lb. delbrueckii* subspecies *bulgaricus* cannot metabolize galactose, formed from the hydrolysis of lactose. Galactose is instead used to uptake more lactose into the cell and thus favors the exclusive use of glycolysis (*3*).

LAB that make use of heterofermentation use the phosphoketolase pathway (PKP) to metabolize hexoses. The main difference between the PKP and glycolysis is the presence of aldolase. Aldolase catalyzes the cleavage of fructose-1,6-bisphosphate (FBP) to form glyceraldehyde-3-phosphate (G3P) and dihydroxyacetone-phosphate (DHAP). Triose-phosphate isomerase (TIM) converts all the DHAP to G3P that then continues through the second half of glycolysis to produce pyruvate and 2 moles of ATP. In the PKP pathway, aldolase is absent and phosphoketolase is used to form G3P that will eventually become lactate and acetyl phosphate which can produce either acetate or ethanol. In order to keep the [NADH]/[NAD^+] ratio balanced, alcohol dehydrogenase

and acetaldehyde dehydrogenase reoxidize the 2 moles of NADH which are made in the first half of the PKP. Some examples of hetero-fermenters include *Leuconostoc lactis* (dairy fermentation), *Lactococcus mesenteroides* subspecies *cremoris* (vegetable fermentation) and *Lb. sanfranciscensis* (making of sourdough bread) (*2*).

One of the major ways by which LAB regulate sugar metabolism is through the uptake and release of carbon sources. There are three main systems used by these bacteria to transport sugars across the outer membrane; the PEP-dependent phosphotransferase system (PTS), symport systems and ATP-binding cassette (ABC) systems. The PTS is the primary way that sugars are transported and is used for highly metabolized sugars such as glucose (*4*). Sugars that are used when glucose is low or absent are mostly transported using either a symport or ABC transport system. The ABC transport system also known as the binding-lipoprotein-dependent transport system in gram positive bacteria is made up of three molecular components. These components include two integral membrane proteins which function as permeases and are made up of 6 transmembrane segments, two peripheral membrane proteins that hydrolyze ATP and a periplasmic or lipoprotein substrate binding protein. Even though these transport systems can be used for sugars they are mostly used to transport amino acids, peptides and osmoprotectants (*2, 5*).

In symport systems, a membrane permease will bind the sugar substrate along with an ion and transport the sugar using an ion gradient. The most common ion gradient in bacteria is the proton motive force (PMF), but some symport systems have been shown to use sodium ion gradients for transport. Some of the sugars utilized by

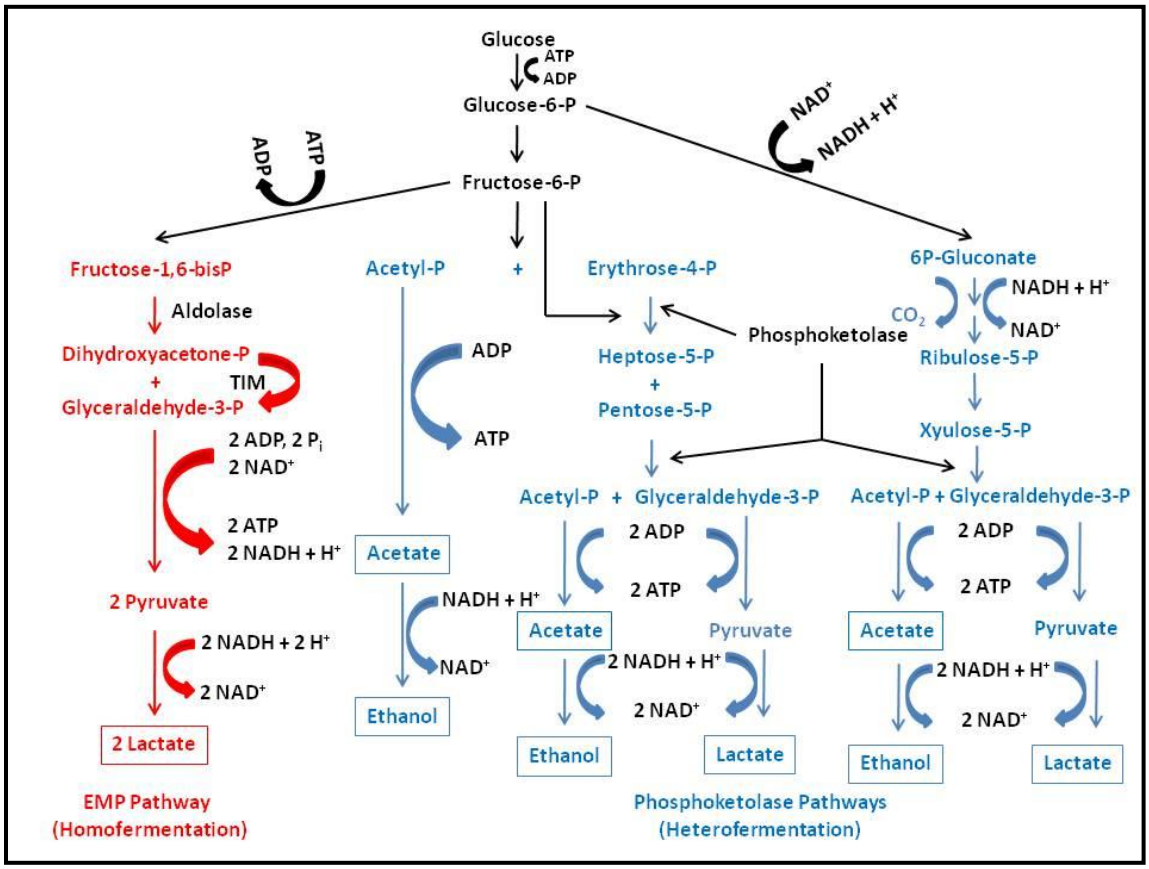

Figure 1-1. Schematic of major pathways involved in hexose fermentation in lactic acid bacteria. The major pathways utilized in hexose fermentation are highlighted, glycolysis (red) and the two phosphoketolase pathways (blue). The main products of fermentation are boxed and the enzymes which make the two distinct are shown in black. TIM = triose-phosphate isomerase. Many steps in both pathways are left out for simplicity. This figure was adapted from (*2*).

symport systems in LAB are lactose, galactose, and xylose (*2*). In the case of lactose, when a symport system is used for its transport, lactose is imported and then hydrolyzed to glucose and galactose (*6, 7*). The glucose is then phosphorylated to form glucose-6-phosphate, which proceeds through glycolysis (Figure 1-1). Then, in most LAB, the galactose is converted into glucose-6-phosphate via the Leloir pathway (*8*). However as mentioned earlier, in *S. thermophilus* and *Lb. delbrueckii* subspecies *bulgaricus* the galactose cannot be fermented and this is due to low expression of enzymes involved in the Leloir pathway.

The main transport system for highly metabolized sugars is the PTS. This system is found across the bacterial kingdom and consists of three main protein components, EI, HPr and EII. EI and HPr are both intracellular proteins and are found in all PTS systems. EII can act as a complex containing multiple proteins or one single protein with multiple domains. EII is also where the substrate specificity is located and is organized in one to two integral membrane domains and two intracellular, hydrophilic domains. The transport in this system occurs through an in-line associative phosphorylation mechanism (Figure 1-2). The first reaction is the phosphorylation of the EI protein by PEP forming P~EI and pyruvate. The steps that follow include the phosphoryl transfer from EI to HPr, HPr to EIIA, EIIA to EIIBC and finally from EIIBC to the sugar substrate. The phosphorylated sugar can then enter either glycolysis or the PKP for fermentation. Each of these phosphoryl transfers occur via a direct interaction between the proteins. The residues involved in these interactions as well as those

involved in phosphorylation have been widely studied (*4*). In LAB, PTS sugar transport provides a very efficient means for the regulation of sugar metabolism.

The way in which the PTS system regulates sugar metabolism is via carbon catabolite repression (CCR). CCR is defined as the ability of certain sugars within the growth conditions to effect the gene expression or the activity of enzymes within the cell involved in the catabolism of other sugars (*4*). CCR is different between gram-negative and gram-positive bacteria depending on the presence/absence of certain proteins. In gram-negative bacteria, the main regulatory protein is EIIA which regulates sugar transport by means of its phosphorylation state. In gram-positive bacteria it is HPr that regulates sugar transport via its phosphorylation state. Each of these proteins allows for the transport of a PTS sugar to affect the transport of a non-PTS sugar.

In gram-negative bacteria, the phosphorylation of EIIA via HPr regulates sugar transport. In an environment where a highly metabolized sugar such as glucose is present, the PTS system is activated and EIIA is phosphorylated by HPr that in turn phosphorylates EIIB. EIIB then subsequently phosphorylates the sugar (Figure 1-2). Unphosphorylated EIIA can then bind and inhibit various enzymes including the lactose permease, melibiose permease, ATP-hydrolyzing component of the maltose transport system and glycerol kinase (*9-14*). These enzymes are involved in the transport of non-PTS sugars and the binding of unphosphorylated EIIA prevents the induction of the genes involved in the uptake and metabolism of these non-PTS sugars in a process known as inducer exclusion. When bacteria are put into a less enriched environment, the PTS system is not needed but is replaced by other transport systems. EIIA stays

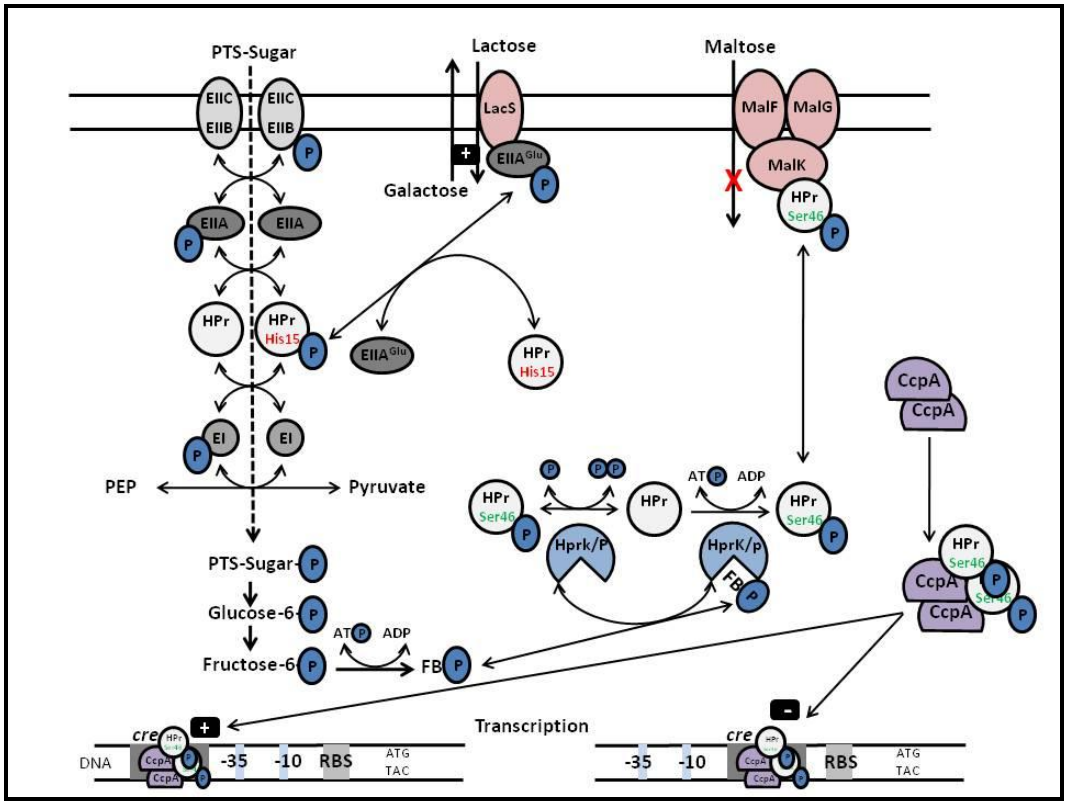

Figure 1-2. Regulation of sugar transport and metabolism in lactic acid bacteria. Highlighted are three transport systems for uptake of PTS-sugars, lactose and maltose. For PTS sugars, the transfer of phosphate from PEP to EI, EI to HPr, HPr to EIIA, and finally EIIA to EIIBC, allows the sugar to enter the cell and become phosphorylated. The sugar then enters glycolysis forming FBP as one of the intermediates. FBP can affect the activity of HPrK/P (HPr kinase/phosphatase) which can either phosphorylate or dephosphorylate HPr are serine 46. Phosphorylation at this position can cause HPr to bind CcpA and this complex can bind to the *cre* element of DNA and effect transcription. Depending on the location of the *cre* element, in reference to the promoter regions which are indicated by the -10 or -35, depends on whether binding of the CcpA/HPr complex causes activation or repression of transcription. P-Ser-HPr can also interact with non-PTS transport systems such as the maltose transporter by binding to its intracellular components. HPr phosphorylation at His15 at the active site can also regulate non-PTS lactose uptake through the phosphorylation of the EIIA involved in glucose uptake ($EIIA^{Glc}$). The $EIIA^{Glc}$ will interact with the LacS membrane protein and stimulate the exchange of lactose for galactose. This figure was adapted from (*4*).

phosphorylated thus relieving the inhibition of the enzymes mentioned above along with the activation of adenylate cyclase. When EIIA is phosphorylated it can directly bind to and activate adenylate cyclase thus forming cAMP. cAMP can then bind to the cAMP binding protein (Crp) that interacts with DNA recognition sites and affects transcription of certain genes. Genes affected by the binding of cAMP/Crp include adenylate cyclase, Crp, EIIA as well as an *E. coli* repressor Mlc, that binds to EIIBC and therefore affects PTS transport. Binding of cAMP/Crp represses the transcription of adenylate cyclase but activates the transcription of genes for Crp, EIIA and Mlc. Increasing the concentration of EIIA, Crp and Mlc would allow for the cell to be prepared in the case where it is once again put into a nutrient rich environment. Overall this regulation helps the bacteria to survive in multiple types of environments, from nutrient-rich to nutrient-depleted.

The presence of metabolites can also affect sugar transport in gram-negative bacteria. The concentrations of PEP and pyruvate affect the phosphorylation state of EIIA and the ratio of PEP to pyruvate changes when cells are grown in different environments. In the absence of glucose, the PEP/pyruvate ratio is between 3-10 but adding glucose to the media causes the ratio decrease to 0.12 in 15 sec (*15*). The drop in the PEP/pyruvate ratio indicates that the PTS system is being utilized in the presence of glucose. The amount of phosphorylated EIIA is dependent on the PEP/pyruvate ratio in that the lower the ratio the lower the amount of phosphorylated EIIA, another indication that the PTS system is being utilized. This decrease in the amount of phosphorylated

EIIA would increase the inhibition of the enzymes involved in the transport of non-PTS proteins thus slowing down the uptake of the non-PTS sugars.

In the case of gram-positive bacteria that have low-GC content DNA, the gene for adenylate cyclase is absent and HPr acts as the protein by which the regulation of sugar transport occurs (*4*). In this type of regulation, it is not only important to consider the phosphorylation state of HPr but also the specific amino acid residue of HPr that is phosphorylated. Under normal PTS transport, HPr is phosphorylated by EI at the active site H15. This phosphorylation is dependent on the presence of PEP thus is often referred to as PEP-dependent phosphorylation of HPr. The phosphate group can then be transferred to EIIA where it will eventually be transferred to the PTS sugar or under non-PTS conditions; the unphosphorylated form of EIIA can bind to other proteins and block/inhibit the transport of non-PTS sugars. The latter is seen in the case of the LacS transporter that is involved in the uptake of lactose via the simultaneous release of galactose (*16-18*). Unphosphorylated EIIA can also interact and inhibit glycerol kinase to slow down the uptake of glycerol in the cell (*19, 20*).

The other amino acid of HPr that can be phosphorylated is S46. S46 is considered the regulatory site since S-46 has no involvement with phosphoryl transfer in the PTS and when HPr is phosphorylated at this position most of the regulation occurs. The phosphorylation of HPr at S46 involves an enzyme with dual activities. The enzyme HPrK/P can act as a kinase as well as a phosphorylase. As with most kinases, HPrK is ATP-dependent so the phosphorylation of HPf by HPrK is known as ATP-dependent phosphorylation. The phosphorylase activity is interesting in that it involves

an inorganic phosphate (P_i) and produces pyro-phosphate (PP_i) (*21*). The P_i can bind to the same site as the β-phosphate of ATP and acts as a nucleophile to attack the P~S-HPr to produce PPi. This mechanism is known as phospho-phosphorolysis. The process of phosphorylation of HPr at S46 is known as inducer expulsion. Inducer expulsion is due to the accumulation of certain sugar phosphates in the cell that become dephosphorylated and expelled as soon as the bacteria are exposed to a nutrient rich environment. Phosphorylation of HPr at S46 affects the phosphorylated of HPr at H15 and vice versa (*22-25*) . HPr phosphorylation is one of the ways that sugar metabolism is controlled in LAB.

As with gram-negative bacteria and EIIA, phosphorylated HPr can affect the transcription of certain genes. When phosphorylated at S46, HPr can interact with the catabolite control protein A (CcpA), and this complex can then interact with a catabolite response element (*cre*) on DNA and affect transcription. *Cre* is located in the promoter region or at the 5' end of many catabolite-repressed transcription units. The location of *cre* in reference to the promoter can lead to activation or repression of transcription of the downstream gene target. If *cre* is located within a promoter, then binding of the HPr/CcpA complex will block the binding of the RNA polymerase and thus repress transcription. If it binds upstream of the start site then it allows transcription of the specific gene to occur. An example of this regulation is the binding of PepRI, whose transcriptional regulation is similar to CcpA in *Lb. delbrueckii s*ubspecies *bulgaricus (26)*. PepRI specifically interacts with the *cre* element upstream of the start site of pepQ which encodes for a dipeptidase involved in hydrolyzing X-Pro dipeptides. PepRI can

also bind to the *cre* element of its own gene *pepRI* and cause auto-regulation which is regulated by the presence of glucose.

The phosphorylation of HPr at S46 is also regulated by the concentration of fructose-1,6-bisphosphate (FBP), an intermediate in glycolysis, ATP and P_i. The metabolite control of HPr at S46 involves the antagonistic activities of the HPrK/P. In some LAB, such as *B. subtilis*, FBP can activate the kinase activity of HprK/P but this effect is less pronounced in the enzyme from *Lb. casei* (*27, 28*) . When grown in the presence of glucose, a highly metabolized sugar, the concentration of both FBP and PP_i increase. FBP activates the ATP-dependent phosphorylation of HPr but inhibits phosphorylation by pyrophosphate. The activation of HPrK would favor PTS transport over other sugar transport system. When the concentration of FBP decreases, the concentration of Pi increases and the increase in Pi would stimulate the dephosphorylation of HPr. Dephosphorylation of HPr that occurs in the presence of less metabolized sugar such as succinate, would in turn stimulate non-PTS sugar transport. Regulation by PPi is not well understood but the regulation of HPr allows for the survival of the bacteria in numerous types of environments (*21*).

Regulation of Glycolysis in LAB

As mentioned above, one of the pathways which is vital in the breakdown and regulation of sugar metabolism is glycolysis. As shown in Figure 1-2, once sugars are imported into the cell they become phosphorylated, enter into glycolysis in the form of glucose-6-phosphate and eventually become pyruvate. During homofermentation the

pyruvate is then converted into the final product of fermentation, lactate, via LDH. There are several steps within this process that are regulated and in bacteria include PFK, pyruvate kinase (PYK) as well as LDH. Regulation of these enzymes can be at the gene level, protein level or both. In the LAB *S. mutans* there is an additional location of regulation in glycolysis using the non-phosphorylation, $NADP^+$-dependent G3P dehydrogenase, which converts G3P to 3-phosphoglycerate bypassing phosphoglycerate kinase allowing for no net ATP production in glycolysis as well as the production of NADPH (*29*). There is also evidence in *Lactococcus lactis* (*L. lactis*) of mixed inhibition of glyceraldehyde-3-phosphate dehydrogenase by ATP, ADP and AMP (*30*). PFK, PYK and LDH are vital in the metabolism of sugars for the majority of bacterial species.

In most bacteria, PFK, PYK and LDH are allosterically regulated by various ligands. Regulation of these enzymes differs between the various species of LAB. In the case of LDH, which catalyzes the conversion from pyruvate to lactate with the concomitant conversion of NADH to NAD^+, FBP acts as an allosteric activator (*31*). LDH can be found in various forms that differ in both their regulation as well as the product formed from the reaction. In some bacteria there is a single LDH that can form both enantiomers of lactate, while some bacteria contain a single LDH which forms a specific enantiomer of lactate. LDHs that only form one enantiomer of lactate are normally coupled to a lactate racemase allowing for the formation of the second enantiomer of lactate (*32*). There is also a third situation where the cell contains both types of LDH without needing a racemase. For example, *Lb. casei* contains both types

of LDH with D-LDH having very low activity and L-LDH being allosterically activated by FBP and irreversible. Along with allosterically activated LDHs, there are examples of non-allosteric versions of the enzyme within LAB. LDH from *Lb. plantarum* and *Lb. acidophilus* are both non-allosteric versions of the allosteric enzyme found within *Lb. casei* and *Lb. curvatus* (*31*). Upon comparing the non-allosteric forms with the allosteric forms, it was found that they shared the common quaternary structure of a homotetramer along with similar pI values. The main differences were the amino acid composition at both the N- and C-termini as well as the overall isoleucine content. The allosteric site for FBP in LAB is thought to be the anion site of the non-allosteric vertebrate enzymes based on sequence comparisons and this site has minor differences when comparing the allosteric and non-allosteric forms of the LAB LDHs (*33-35*).

PYK, another enzyme important in the regulation of glycolysis in bacteria, catalyzes the irreversible phosphoryl transfer from PEP to ADP forming ATP and pyruvate. In eukaryotes there are two forms of PYK which differ based on the allosteric activation by FBP (*36*). Two forms of PYK are also found in *E.coli*, one allosterically activated by FBP and the second activated by AMP and several mono-phosphate sugars (*37, 38*). In the LAB *L. lactis*, PYK was found to be allosterically activated by FBP, inhibited by P_i and to be important in the regulation of glycolysis (*39*). When LAB are grown in the presence of a highly metabolized sugar such as glucose, FBP concentrations increase allowing for the activation of PYK. However once the cells were put in a glucose-deficient environment, the levels of 2-phosphoglycerate, 3-phosphoglycerate and PEP increase and are linked to the increase in P_i which will inhibit

PYK (*40*). The regulation of PYK in the homofermentative LAB *Lb. bulgaricus* is different from PYK in *L. lactis* since FBP acts as an inhibitor rather than an activator. The strong activators are AMP as well as glucose-6-phosphate and ribose-5-phosphate, which are similar to the activators known for PYK from *Bacillus stearothermophilus* (*38, 41*). The difference in the regulation between *Lb. bulgaricus* and *L. lactis* PYK may be due to the differences in the promiscuity of sugar metabolism in each LAB.

The third enzyme which is important in glycolytic regulation in bacteria is PFK which catalyzes the phosphoryl transfer from MgATP to fructose-6-phosphate (F6P) forming MgADP and FBP. In *E.coli*, there are two forms of PFK present in the cell. PFK-1is allosterically regulated by two ligands, the inhibitor PEP and the activator MgADP. But as with LDH there are examples of non-allosteric and allosteric PFKs within LAB. In the 1970s, several PFKs originating from LAB were analyzed for their ability to bind various allosteric effectors (*42, 43*). Doelle concluded that PFK from *Lb. casei* and *Lb. plantarum* were non-allosteric enzymes as they showed no effect with ATP, ADP, citrate or NH_4^+, which are known to either effect the yeast or mammalian enzyme. This study however was not performed with pure enzyme, but *Lb. plantarum* was later studied again in a comparison with PFK from *Lb. acidophilus*. In this later study, pure enzyme was used and both PFKs were analyzed against the effectors FBP, NH_4^+, citrate, PEP, 5'-AMP as well as ADP. PFK from *Lb. plantarum* was not regulated by any of the above effectors except $NH4^+$ which increased the maximal velocity (V_{max}) of the enzyme 20%. However since this was the only effect seen among the various allosteric effectors, it was concluded to be a non-allosteric PFK. In contrast, PFK from

Lb. acidophilus was activated by FBP and inhibited by ADP. Both of these affected the V_{max} of the enzyme with FBP also having an inhibitory effect on the binding of F6P. The inhibition by FBP and ADP could be simply due to product inhibition but the authors concluded that PFK from *Lb. acidophilus* is an allosteric PFK (*42*).

In the early 1980s the PFK from *S. thermophilus* was purified and studied and it was determined to be non-allosteric based on the inability of FBP, PEP, and ADP to affect the activity of the enzyme (*44*). The PFK from *S. thermophilus* is however more stable at higher temperatures compared to PFK from *Lb. plantarum*. Then in the early 1990s, LbPFK was studied in detail by Jean-Renaud Garel (*45, 46*). From these studies, it was concluded that LbPFK was a non-allosteric PFK due to the lack of inhibition by citrate and PEP or activation by the ADP or GDP. Although there appears to be a lack in allosteric regulation of these important glycolytic enzymes there is evidence of regulation at the gene level.

In *E. coli*, PFK-2 is different in both structure and allosteric regulation compared to PFK-1 (*47-50*). Structurally, PFK-1 is a homotetramer while PFK-2 is a homodimer. Both show inhibition by MgATP but through different mechanisms. MgATP inhibition in PFK-1 is though the binding of MgATP to one active site inhibits the binding of F6P to another active site (*51, 52*). MgATP inhibition of PFK-2 is different as binding of MgATP causes a structural change from dimers to tetramers that forms an additional binding site for MgATP (*48*). In 2008, a crystal structure of PFK-2 in its tetrameric form was solved with two MgATP molecules bound to each monomer. One of the MgATP molecules was located where the phosphoryl donor would bind with the other at

another site which was proposed to be an effector site (*53*). Then in 2010, another structure was determined with F6P bound to the active site and upon comparing this structure to the MgATP-bound structure a model for MgATP inhibition was proposed (*54*). It was proposed that upon binding of MgATP a conformation change occurs which induces a negative interplay between the binding of MgATP to the allosteric site and the F6P bound at the active site. This negative coupling is accompanied by changes in both the $K_{1/2}$ for F6P as well as in the catalytic turnover, k_{cat}. In PFK-1, MgATP inhibits the binding of F6P in addition to changing the homotropic coupling between the F6P binding sites (*51*).

Interestingly, a second PFK has been identified in two different strains of *Lb. delbrueckii* subspecies *bulgaricus* (*55, 56*). *Lb. delbrueckii* subspecies *bulgaricus* is the only LAB so far to have acquired a second PFK and the role of this enzyme is unknown. It is proposed that many LAB acquire addition genes from either horizontal gene transfer or gene duplication (*57*). Some examples of genes for which a second gene has been acquired in LAB are genes for various proteins involved in sugar metabolism such as enolase, L-LDH, and proteins from the PTS (*58*). These genes can be acquired from the most recent ancestor or from a distant ancestor so the role of the proteins is difficult to determine.

In determining the potential identity of this second PFK from *Lb. delbrueckii* subspecies *bulgaricus* a sequence alignment was performed with PFK-2 from *E. coli*, PFK-1 from *Lb. delbrueckii* subspecies *bulgaricus* and *E. coli* as well as a pyrophosphate-dependent PFK (PP_i-PFK) from *Thermoproteus tenax* which is an

anaerobic, hyperthermophilic archaeon (*59*). PFK-2 from *Lb. delbrueckii* subspecies *bulgaricus* showed approximately 30% sequence identity to PFK-1 from both *Lb. delbrueckii* subspecies *bulgaricus* and *E. coli*, 30% identity to PP_i-PFK from *Thermoproteus tenax* and only 12% identity to PFK-2 from *E. coli*. PFK-2 from *Lb. delbrueckii* subspecies *bulgaricus* contains 359 amino acids compared to the 319 from *Lb. delbrueckii* subspecies bulgaricus PFK-1, 309 from *E. coli* PFK-2 and 337 from *Thermoproteus tenax* PP_i-PFK. From the sequence comparison it is difficult to identify which PFK this second PFK from *Lb. delbrueckii* subspecies *bulgaricus* would be more closely related to but is unlikely to be a homolog of PFK-2 from *E.coli* due to the lack of sequence identity. Further work is needed to identify the role of this second PFK in sugar metabolism of *Lb. delbrueckii* subspecies *bulgaricus*.

Transcriptional Regulation of PFK, PYK and LDH in LAB

As mentioned earlier, there is strong transcriptional regulation within LAB via the metabolism of sugars transported by the PTS system. In addition to the gene for PepRI in *Lb. delbrueckii* subspecies *bulgaricus*, the transcription of genes for PFK, PYK and LDH have been shown to be regulated via the transport of PTS sugars (*60-64*). In *L. lactis*, the genes for PFK, PYK and LDH form one multicistronic operon called the *las* operon (*65*). This is novel and is not seen in gram-negative bacteria such as *E. coli*, where these genes are unlinked. Within the *las* operon is a strong codon bias, and in *E. coli* a strong correlation between the degree of codon bias and the level of gene expression has been demonstrated where the most highly expressed genes exhibit the

greatest degree of codon bias (*66*). So the strong codon bias of the *las* operon would indicate that these genes are strongly expressed. The promoter region of the *las* operon contains a *cre* element that allows for the regulation by CcpA, which can bind to the *cre* element and either activate or repress transcription. For the *las* operon it was shown that the transcription of *pfk*, *pyk* and *ldh* was diminished when CcpA was absent from the cell (*62*). This indicates that CcpA acts as a transcriptional activator for the *las* operon and would allow for the regulation of these genes thereby linking glycolytic regulation with sugar transport via the PTS system.

The genes for PFK and PYK are also known to form a single operon in other LAB such as *Lb. delbrueckii* subspecies *bulgaricus* (*67*), *Lb. casei* (*64*), *S. thermophilus* (*61*) and *S. bovis* (*60*). Unlike *L. lactis* however these operons do not contain the gene *ldh* and therefore the expression of *ldh* is separate from those of *pfk* and *pyk*. Within these homofermentative LAB there is evidence of regulation of transcription of the *pfk-pyk* operon by CcpA. In *Lb. casei* it has been shown that CcpA represses the transcription of *pfk-pyk*, which is opposite of the CcpA regulation in *L. lactis*. The expression of pfk-pyk is also greater in the presence of PTS sugars such as glucose and lactose compared to non-PTS sugars such as ribose. The opposite regulation of *pfk-pyk* expression by PTS sugars and CcpA would provide a way for the cell to control glycolytic flux in bacteria that have limited regulation at the protein level. In *S. bovis*, the co-transcription of pfk-pyk was regulation by both the presence of PTS sugars and CcpA. However, the effect of CcpA on the transcription was positive which is similar to that of *L. lactis* but opposite of *Lb. casei*. The difference between the transcriptional

regulation of these genes within LAB may involve the differences in the microenvironments which these bacteria thrive along with the differences in the metabolic pathways which they utilize. Also the regulation of glycolysis at the gene level may be in place of the limited control of these enzymes at the protein level in LAB.

Allosteric Regulation of LbPFK

Although it is important to understand sugar metabolism and its regulation in LAB, the main focus of this dissertation is to understand the molecular basis for the lack of allosteric regulation in LbPFK. As mentioned above, PFK from most bacteria is allosterically regulated but is not the case for PFK from several LAB. Allostery is the phenomenon in which the binding of the substrate (K-type effect) or maximal rate of enzyme turnover (V-type effect) of an enzyme is affected by the binding of a ligand to a site other than the active site of that enzyme. There are many examples of allosteric enzymes other than PFK, for example, the first allosteric enzymes studied were aspartate transcarbamoylase and threonine deaminase, and from these studies came two separate models to explain the allosteric phenomena (*68, 69*). The MWC and KNF models are two-state models in which the enzyme can adopt two different states, the active or relaxed R-state and the inhibited or tense T-state (*70, 71*). In the MWC model there is a preexisting equilibrium between the two states, and the enzyme can only be found in one of the two forms. The KNF model is different in that it does not invoke a pre-existing equilibrium between the two states, but rather a conformational change occurs within the enzyme to each subunit as the allosteric ligand binds. The KNF model allows for both

positive and negative cooperativity to be explained, something not considered in the MWC model. However, both of these models are too simple to explain the allosteric phenomena of PFK (*72, 73*).

The approach we have taken in studying the allosteric regulation of PFK involves thermodynamic linkage analysis. In this analysis, a single substrate-single modifier scheme is applied to describe the thermodynamic relationships between the binding of the effector (X) and the binding of the substrate (A) to the enzyme (E) (Figure 1-3) (*74*). In the absence of catalysis, Figure 1-3 can be simplified to two ligands binding to a single enzyme at different sites, and the dissociation constants can be defined as below (*75, 76*):

$$K_{ia}^{\circ} = \frac{[E][A]}{[EA]} = \frac{k_2}{k_1} \tag{1-1}$$

$$K_{ix}^{\circ} = \frac{[E][X]}{[XE]} = \frac{k_6}{k_5} \tag{1-2}$$

$$K_{ia}^{\infty} = \frac{[XE][A]}{[XEA]} = \frac{k_8}{k_7} \tag{1-3}$$

$$K_{ix}^{\infty} = \frac{[EA][X]}{[XEA]} = \frac{k_{12}}{k_{11}} \tag{1-4}$$

where K_{ia}° and K_{ix}° are the dissociation constants for the substrate and the effector in the absence of the other ligand, respectively. K_{ia}^{∞} and K_{ix}^{∞} are the dissociation constants for the substrate and effector in the saturating presence of the other ligand. Based on the definition of the various dissociation constants, the relationship between the dissociation constants for the substrate and effector is given by equation 1-5.

$$K_{ia}^{\circ} \times K_{ix}^{\infty} = K_{ix}^{\circ} \times K_{ia}^{\infty} \tag{1-5}$$

A simple rearrangement of equation 1-5 gives the ratios in equation 1-6, which define the coupling constant Q_{ax} which describes the coupling between the substrate and the effector.

$$Q_{ax} = \frac{K_{ia}^{\circ}}{K_{ia}^{\infty}} = \frac{K_{ix}^{\circ}}{K_{ix}^{\infty}} \tag{1-6}$$

Based on the above definition, the coupling constant Q_{ax} is in itself an equilibrium constant which defines the disproportionation equilibrium below (*77*).

$$EA + EX \leftrightarrow XEA + E \tag{1-7}$$

Through the use of Q_{ax} it is possible to determine the nature of the allosteric response as well as the magnitude of the response. For example, if $Q_{ax} > 1$ the allosteric effector is an activator but if $Q_{ax} < 1$ the allosteric effector is an inhibitor. If $Q_{ax} = 1$ there is no allosteric response to the effector. Through this analysis it is possible to fully describe the thermodynamics parameters of the allosteric system being studied. Since the allosteric response of PFK is solely a K-type effect, it is possible to study this response by analyzing the effect the allosteric ligand has on the binding of the substrate, F6P in this manner. By measuring the change in the Michaelis constant for F6P as a function of X, the data can be plotted on a log-log scale and fit to the following equation to determine the important variables needed to fully describe the thermodynamic properties of the enzyme (Figure 1-4) (*77*).

$$K_{1/2} = K_{ia}^{\circ}\left(\frac{K_{ix}^{\circ} + [X]}{K_{ix}^{\circ} + Q_{ax}[X]}\right) \tag{1-8}$$

where $K_{1/2}$ is the concentration of F6P at half-maximal velocity.

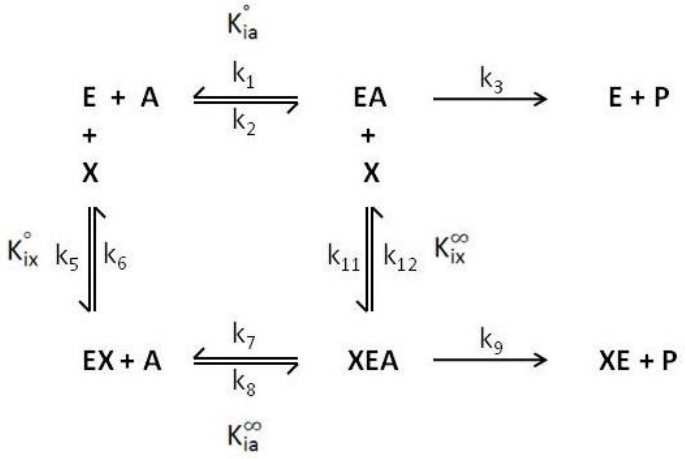

Figure 1-3. Single substrate-single modifier scheme. Above describes the thermodynamic linkage between the substrate (A) and the allosteric effector (X). E denotes enzyme, P denotes product, small *k*'s are rate constants and large *K*'s are dissociation constants defined in the text.

In the case of LbPFK, where saturation with PEP could not be obtained and therefore a Q_{ax} could not be determined (assumes Qax =0 or infinite coupling), the following equation derived from equation 1-8 can be used to determine the dissociation constants for F6P and PEP.

$$K_{1/2} = K_{ia}^{\circ}\left(1 + \frac{[X]}{K_{ix}^{\circ}}\right) \quad (1\text{-}9)$$

K_{ia}° and K_{ix}° can then be compared between various PFKs in order to better understand the basis of the differences in the binding of ligands and allosteric regulation exhibited by the various bacterial PFKs (*78*). This analysis has been used to study EcPFK and BsPFK in great detail and both of these PFKs exhibit strong inhibition by PEP with EcPFK also exhibiting strong activation by MgADP (*72, 79, 80*). More previous studies on the allosteric PFK from the extremely thermophilic, gram-positive *Thermus thermophilus* (TtPFK) indicates that TtPFK is also inhibited by PEP, although not as strongly as EcPFK and BsPFK, and shows slight activation by MgADP. Figure 1-5 shows a comparison of the binding and allosteric inhibition by PEP between these three PFKs along with the non-allosteric LbPFK. It is clear that the four PFKs differ not only in their ability to bind the inhibitor PEP but also in the extent of inhibition which is exhibited by PEP. Of the four, TtPFK exhibits the tightest binding affinity for PEP at 3μM with BsPFK exhibiting the strongest inhibition by PEP (Q_{ay} = 0.001 ± 0.001) (*78, 81*). LbPFK stands out as having very weak PEP binding, approximately 27 mM, with inhibition only evident at very high concentrations of PEP (*82*). Due to these differences the sequences between the allosteric EcPFK, BsPFK and TtPFK and the non-allosteric LbPFK were compared.

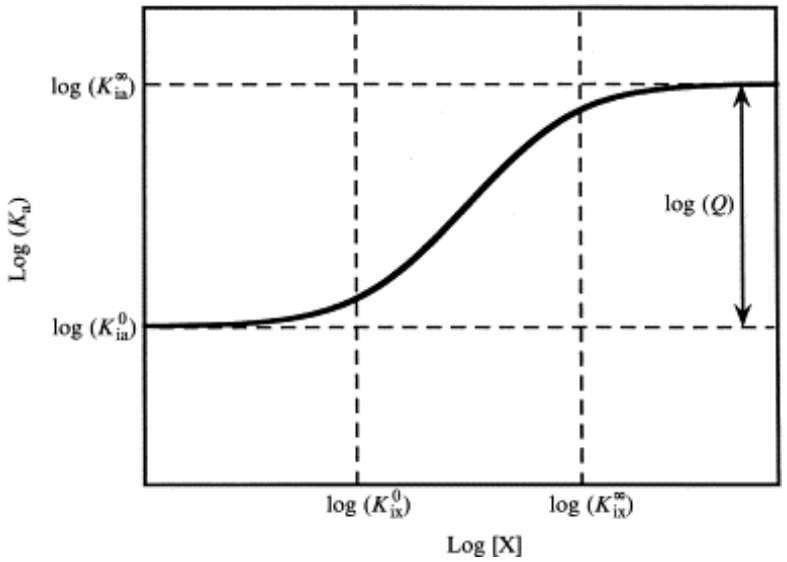

Figure 1-4. Dependence of the dissociation constant for A as a function of X. The equation describing this curve is equation 1-8 in the text.

Figure 1-6 shows the sequence alignment between LbPFK, TtPFK, BsPFK and EcPFK. Upon inspection, it is clear that the overall sequence is well conserved with residues in the 230s and 240s along with the C-terminus being the least conserved. When comparing the four, LbPFK having 47% identity with 66% similarity to EcPFK, 56% identity with 74% similarity and 46% identity with 60% similarity. Another small region that is well conserved between the allosteric PFKs but not in LbPFK contains residues 211-214, which includes 3 positively charged residues in the allosteric PFKs and only one in LbPFK. The first crystal structure of LbPFK was determined at 1.86 Å resolution in 2005 and when residues 211-214 are mapped onto the structure, these residues are found within the allosteric binding site. When this structure is compared to those of EcPFK and BsPFK, the allosteric site is the least conserved region within the enzyme (*83, 84*). The allosteric site contains residues 55 and 59 and residue 55 is not well conserved. Residue 59 is also not conserved with an H present in LbPFK, with the other allosteric PFKs having a D or N. These differences within LbPFK could potentially explain the weak binding affinity for the inhibitor PEP and therefore the lack of allosteric inhibition.

In this study, the molecular basis for the weak PEP binding and lack of allosteric inhibition in LbPFK was examined using crystallography and site-directed mutagenesis. Chapter III introduces the phosphate-bound and substrate-bound structures of LbPFK that will allow for comparisons of the bound active site to F6P-bound EcPFK and BsPFK. Chapter IV introduces the mutations D12A, T156A and H160A which are

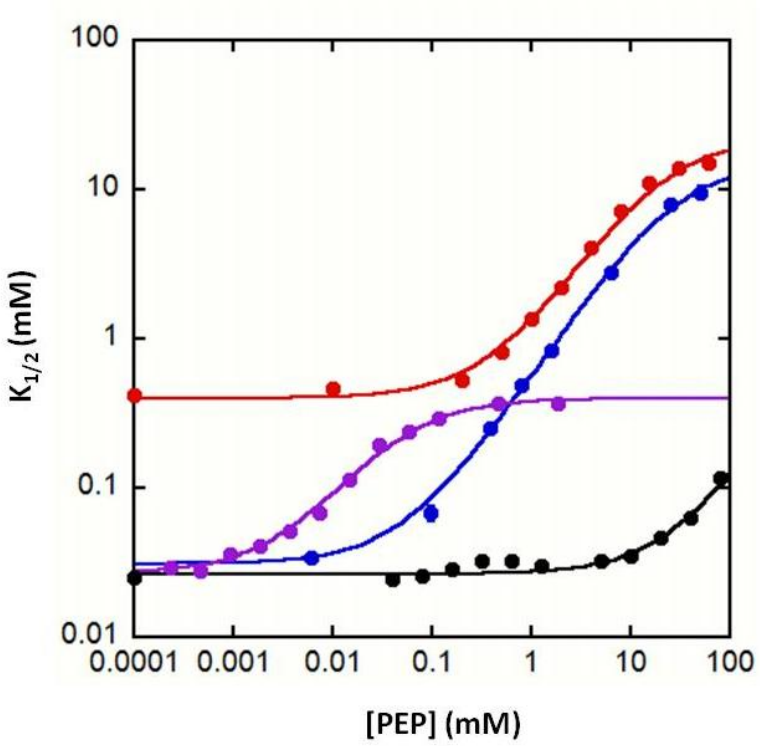

Figure 1-5: Dependence of $K_{1/2}$ for F6P as a function of PEP concentration for LbPFK (black), EcPFK (red), BsPFK (blue) and TtPFK (purple). The $K_{1/2}$ for F6P was measured at various concentrations of PEP and replotted. EcPFK, BsPFK ad TtPFK data were fit to equation 1-8, while LbPFK was fit to equation 1-9. Data for EcPFK from (*72*), BsPFK (*85*) and TtPFK (*78*).

Figure 1-6. Amino acid sequence alignment between LbPFK, BsPFK, EcPFK and TtPFK. The amino acid sequences were aligned using MacVectorTM 7.0. The regions discussed within this dissertation are highlighted by colored boxes with the allosteric site residues in blue and the active site interface residues in red. The numbering of the amino acid residues in the figure is according to the EcPFK sequence but in the text is according to the LbPFK sequence.

located along the active site interface and D12A appears to play a role in the binding of PEP to the allosteric site 15 Å away. The crystal structure of D12A is also introduced and shows no major structural changes when compared to wild-type LbPFK. D12A has also been studied in BsPFK and a comparison between D12A LbPFK and D12A BsPFK will be discussed. Chapter V will discuss the mutagenesis within the allosteric binding site of LbPFK where single as well as long cassette mutations were made in attempt to enhance the binding for PEP to the allosteric site. Finally, chapter VI will introduce a mutant of LbPFK which contains both allosteric site mutants and D12A. This mutant enhanced binding for PEP 25-fold compared to wild-type LbPFK and allowed for the measurement of inhibition by PEP for the first time in a non-allosteric PFK.

CHAPTER II

GENERAL MATERIALS AND METHODS

Materials

All chemical reagents used in buffers, protein purifications, and enzymatic assays were of analytical grade and were purchased from Sigma-Aldrich (St. Louis, MO) or Fisher Scientific (Fair Lawn, NJ). Creatine kinase, the sodium salt of ATP and the ammonium sulfate suspension of glycerol-3-phosphate dehydrogenase were purchased from Roche (Indianapolis, IN). The ammonium sulfate suspensions of aldolase and triosephosphate isomerase, and the sodium salts of phosphocreatine and PEP were purchased from Sigma-Aldrich. The coupling enzymes were extensively dialyzed against 50 mM MOPS-KOH, pH 7.0, 100 mM KCl, 5 mM $MgCl_2$, and 0.1 mM EDTA before use. The sodium salt of F6P was purchased from Sigma-Aldrich or USB Corporation (Cleveland, OH). NADH and DTT were purchased from Research Products International (Mt. Prospect, IL). Mimetic Blue 1 resin used in protein purifications was purchased from Promatic BioSciences (Rockville, Maryland), respectively. Site-directed mutagenesis was performed using the QuikChange Site-Directed Mutagenesis System from Stratagene (La Jolla, CA). Oligonucleotides were synthesized and purchased from Integrated DNA Technologies, Inc (Coralville, IA). DNA modifying enzymes and dNTPs were purchased from Stratagene (Cedar Creek, TX), New England Biolabs (Ipswich, MA), or Promega (Madison, WI). BCA Assay reagents were purchased from Pierce. Deionized distilled water was used throughout.

Methods

Protein Purification for WT LbPFK

MRL277 cells containing pKK223-3/PFK were grown in LB broth in the presence on 0.1 mg/mL ampicillin at 37 °C to an optical density of 0.6 and then induced with 0.5 mM IPTG (Isopropyl β-D-1-thiogalactopyranoside) and allowed to grow at 37 °C for an additional 5 hours. Cells were harvested and stored at -80 °C. The harvested cells were then resuspended in Buffer A (50 mM Tris-HCl pH 7.5, 0.1 mM EDTA), sonicated and centrifuged for 1 hour at 8,000 x g at 4 °C. Next, the cell lysate was treated with DNase I for 20 minutes at 37 °C and centrifuged again for 1 hour at 8,000 x g at 4 °C. The resulting cell lysate was loaded onto a pre-equilibrated Mimetic Blue I column, the column washed with at least 5 column volumes of Buffer A and eluted with a 0-2 M NaCl gradient in the same buffer. The PFK eluted at approximately 1 M NaCl. Fractions containing PFK activity were pooled, dialyzed against Buffer B (50 mM Tris-HCl pH 7.5, 0.1 M EDTA, 5 mM $MgCl_2$) and concentrated. Protein concentration was determined using the BCA protein assay and the purity was assessed with SDS-PAGE.

Kinetic Analysis

Standard conditions for the PFK assay were pH 8.0 and 25 °C. The PFK reaction was measured by coupling the production of fructose-1,6-bisphosphate to the oxidation of NADH and followed at 340 nm. The reaction was initiated by adding 6 µl of PFK into a 600 µl reaction buffer containing V_{max} Buffer (50 mM EPPS pH 8.0, 10 mM $MgCl_2$, 10 mM NH_4Cl, 0.1 mM EDTA), 2 mM DTT, 250 µg of aldolase, 50 µg of

glycerol-3-phosphate dehydrogenase, 25 µg triose-phosphate isomerase, 15 mM ATP and 5 mM F6P. 40 µg/mL creatine kinase and 4 mM phosphocreatine were added to the reaction buffer for the regeneration of MgATP from the production of MgADP. F6P, MgATP, and PEP concentrations were varied as indicated. MgATP was added as a solution of equal molar $MgCl_2$ and ATP. The rate of the reaction was measured by the decrease in absorbance at 340 nm as a function of time. One unit of enzyme activity is defined as the amount of enzyme needed to produce 1 µmol of fructose-1,6-bisphosphate per minute.

Data Analysis

Steady-state rates as a function of F6P concentration were fit to the following equation (*86*):

$$\nu = \frac{V_{max}[A]^{n_H}}{K_{1/2}^{n_H} + [A]^{n_H}} \quad (2\text{-}1)$$

where ν equals the steady-state rate of turnover, V_{max} represents the maximal activity, [A] equals the concentration of F6P, $K_{1/2}$ is the concentration of F6P which results in half-maximal activity and n_H is the Hill coefficient. When determining the kinetic parameters for MgATP, where the n_H is 1, the following equation was used (*87*)**:**

$$\nu = \frac{V_{max}[A]}{K_a + [A]} \quad (2\text{-}2)$$

To quantify the allosteric response of PFK to PEP in the case of allosteric inhibition, the $K_{1/2}$ for F6P was measured at various concentrations of PEP and the results were fit to the following equation (*74*):

$$K_{1/2} = K_{ia}^{\circ} \left[\frac{K_{iy}^{\circ} + [Y]}{K_{iy}^{\circ} + Q_{ay}[Y]} \right] \quad (2\text{-}3)$$

where Y is PEP, $K_{ia}°$ is the dissociation constant for F6P is the absence of PEP, $K_{iy}°$ is the dissociation for PEP in the absence of F6P, and Q_{ay} is the coupling constant between PEP and F6P. The coupling constant describes both the magnitude and nature of the allosteric effect (*74, 88*). When Q_{ay} is greater than 1 the allosteric ligand is an activator and when it is less than 1 then the allosteric ligand is an inhibitor. When Q_{ay} is equal to 1 there is no allosteric response upon binding of the allosteric ligand. When the binding of PEP is weak, as is seen in LbPFK, and saturation of PEP at the allosteric site cannot be achieved, the data are instead fit to the competitive inhibition equation (*89*), which corresponds to equation 2-3 when $Q_{ay} = 0$.

$$K_{1/2} = K_{ia}^{\circ} \left(1 + \frac{[Y]}{K_{iy}^{\circ}} \right) \quad (2\text{-}4)$$

The free energy of binding for various ligands was determined using the following equation:

$$\Delta G^{\circ} = -RT \ln \frac{1}{K_{ia}^{\circ}} \quad (2\text{-}5)$$

where ΔG° is the free energy of ligand binding, R is the gas constant in kcal/mol, and T is the temperature in Kelvin. In the case of other ligands the appropriate dissociation constant was substituted for $K_{ia}°$.

When measuring the binding affinity for MgADP to the allosteric site, a competition experiment was performed in which the apparent K_i for PEP (K_{iy}^{app}) was measured at various concentrations of MgADP. K_{iy}^{app} was then plotted as a function of

[MgADP] and the data were fit to the following equation to determine the K_i for MgADP (K_{ix}^{app}):

$$K_{iy}^{app} = K_i^{PEP}\left(1 + \frac{[MgADP]}{K_{ix}^{app}}\right) \quad (2\text{-}6)$$

where K_i^{PEP} is the dissociation constant for PEP in the absence of MgADP. All data analysis was performed using nonlinear least-squares fitting analysis of Kaleidagraph 3.51 (Synergy).

Site-directed Mutagenesis

PFK from *Lactobacillus delbrueckii* subspecies *bulgaricus* B107 was cloned into the plasmid pK223-3 and was kindly provided by Danone Vitapole SA, France (*46*). Mutagenesis was performed following the protocol outlined in the Quikchange Site-Directed Mutagenesis System from Stratagene. For all LbPFK mutants, two complementary oligos were designed which targeted the sequence surrounding the codon for the amino acid which was mutated. The template oligos for each of the LbPFK variants is presented in the appropriate chapter. The mutant plasmids were finally expressed in the E. coli strain MRL277, which has both the pfk1 and pfk2 genes deleted (*90*).

CHAPTER III

PHOSPHATE AND SUBSTRATE-BOUND STRUCTURES OF THE NON-ALLOSTERIC PHOSPHOFRUCTOKINASE FROM *Lactobacillus delbrueckii* SUBSPECIES *bulgaricus*

In most bacteria, phosphofructokinase (PFK) is allosterically regulated by two K-type effectors, phosphoenolpyruvate (PEP) which acts as an inhibitor and MgADP which acts as an activator. PFK regulation is important in the overall regulation of glycolysis since PFK catalyzes the first committed step where it performs a phosphoryl transfer from MgATP to fructose-6-phosphate (F6P) to form fructose-1,6-bisphosphate (FBP) and MgADP. To better understand the regulation of bacterial PFK many studies have been performed on two highly regulated bacterial PFKs, those from *E. coli* (EcPFK) and *Bacillus stearothermophilus* (BsPFK) (*91, 92*). There has also been extensive work done on the structures of EcPFK and BsPFK with six total structures submitted to the Protein Data Bank (PDB). EcPFK and BsPFK are very similar sharing 55% identity in amino acid sequence, and they are both homotetramers with molecular masses of 140 kDa (*93*). Both homotetramers are formed as a dimer-of-dimers with four active sites and four allosteric sites. These sites lie along respective dimer-dimer interfaces each containing amino acids from two adjacent monomers making it necessary for PFK to be a tetramer for catalytic activity and allosteric regulation (*94*).

Of the six structures in the PDB two are of EcPFK and the other four are of BsPFK. The two from EcPFK are of the apoenzyme (accession code 2PFK) and the

product-bound enzyme with FBP and MgADP bound to the four active site and MgADP bound to all four allosteric sites (accession code 1PFK) (*83, 95*). Comparison of these two structures shows that the overall secondary, tertiary and quaternary structures are almost identical. The four structures from BsPFK have either phosphate bound (accession code 3PFK), substrate-bound (accession code 4PFK), or inhibitor-bound (accession code 6PFK). A mutant BsPFK structure with substrate-bound (accession code 1MTO) (*84, 94, 96*) is also available. The substrate-bound form has the substrate F6P bound to all four active sites with the product MgADP bound to both the four active sites and the four allosteric sites. The inhibitor-bound structure contains the inhibitor analog phosphoglycolate (PG) to all four allosteric sites. It was later determined that PG inhibits BsPFK in a manner similar, but not identical, to the true inhibitor PEP (*79*). The final BsPFK structure contains the mutations W179Y, Y164W and has both F6P and MgADP bound to the four active sites and MgADP bound to all four allosteric sites (*96*). This structure is very similar to the substrate-bound form of wild-type BsPFK. By comparing the substrate-bound form to the inhibitor-bound form, Schirmer and Evans proposed a model for the allosteric control of BsPFK (*84*). This model conforms to the two-state model proposed by Monod, Wyman and Changeax (MWC) in which the enzyme is found in one of two states, the active, relaxed R-state or the inhibited, tense T-state (*70, 84*). The allosteric behavior of EcPFK was thought to conform to the MWC model as well (*91*).

The seventh PFK structure belongs to PFK from *Lactobacillus delbrueckii* subspecies *bulgaricus* (LbPFK, accession code 1ZXX) (*82*). LbPFK, unlike that of

EcPFK and BsPFK, has very weak binding affinity for the allosteric ligands PEP and MgADP (approximately 27 mM) and is therefore considered a non-allosteric form of PFK (*82, 97*). LbPFK is similar to EcPFK and BsPFK in amino acid sequence having 57% identity to BsPFK and 47% identity to EcPFK. The structure of LbPFK contains sulfate bound to all four active sites and all four allosteric sites. Upon comparison to the substrate-bound forms of BsPFK and EcPFK, the overall structure of LbPFK is similar with the only major differences found within the allosteric binding site (*82*).

Here, two new crystal structures of LbPFK are presented. The first structure contains phosphate bound at the four active sites along with the four allosteric sites and was solved to 1.83 Å resolution. The second has the substrate F6P bound within the four active sites along with phosphate bound to the four active sites and four allosteric sites and was solved to 2.2 Å resolution. In each of the structures an additional phosphate is bound to the surface of the enzyme and this is thought to be an artifact of the crystallization. There are also ions bound to each, with a chloride ion bound within the four active sites of the phosphate-bound structure and a magnesium anion bound within the four active sites of the substrate-bound structure. These are most likely due to the fact that the storage conditions for LbPFK contain $MgCl_2$. These are the first crystal structures of LbPFK with substrate bound and phosphate bound, and they allow for further comparisons to be made between LbPFK and the more allosterically responsive enzymes EcPFK and BsPFK.

Materials and Methods

Materials

The crystallization reagents were purchased from Hampton Research (Aliso Viejo, CA).

Crystallization and Data Collection for LbPFK Structures

LbPFK was crystallized using the hanging drop vapor diffusion method (*98*) at 16 °C. For phosphate-bound LbPFK, crystallization was achieved in a 5 µL drop with 2µL solvent (0.1 M Tris-HCl pH 8.5, 2.0 M ammonium phosphate monobasic) and 3 µL protein (stock concentration of LbPFK was 7.6 mg/mL in 50mM Tris-HCl, pH 7.5, 1mM EDTA and 10mM $MgCl_2$). For substrate-bound LbPFK, crystallization was achieved in a 5 µl drop with 2µl solvent (0.1 M Tris-HCl pH 8.5, 2.0 M ammonium phosphate monobasic) and 3 µl protein (stock concentration of LbPFK was 9.6 mg/mL in 50mM Tris-HCl, pH 7.5, 1mM EDTA, 10mM $MgCl_2$ and 2.5mM F6P). Within 24 hours, diamond shaped crystal for both LbPFK proteins were formed. For data collection, crystals were cryoprotected by brief soaking in 30% ethylene-glycol and then flash-frozen in a liquid N_2 stream at 100 K. Diffraction data for the LbPFK-phosphate bound crystal was collected on APS beamLine 23-ID using the MAR CCD detector (MarMosaic from Marresearch – Charged Coupled Device) (Rayonix LLC, Evanston, IL). Diffraction data for Lb-PFK-F6P were collected to resolution 2.2 Å on a Raxis IV++ detector in lab (Rigaku). The HKL2000 program package (HKL Research, Inc., Charlottesville, VA) (*99*) was used for integration and scaling. Crystals belong to the

space group $P6_222$ with unit cell parameters with one molecule in the asymmetric unit. Data collection details are summarized in Table 3-1.

Structure Determination and Refinement for LbPFK Structures

The molecular replacement program PHASER (University of Cambridge, UK) (*100*) was used to solve the structures of LbPFK using the sulfate-bound crystal structure of LbPFK (1ZXX) (*82*) with waters and ions removed as a model. Rigid body refinement followed by simulated annealing refinement at 5000 K was carried out using Phenix (Python-based Hierarchical Environment for Integrated Xtallography, Berkeley, CA) (*101*). Subsequently, refinement was carried out in alternating cycles of manual model building in COOT (Crystallographic Object-Orientated Toolkit, Oxford, UK) (*102*) followed by refinement as implemented in Phenix until R-factors converged. Water molecules were added in the difference electron density maps at positions corresponding to peaks (>3.0σ) and with appropriate hydrogen bonding geometry. The stereochemical quality of the final model for the LbPFK proteins was verified by Molprobity (Duke University, Durham, NC) (*103*).

Results

Structural Characteristics of Phosphate-bound LbPFK

The phosphate-bound LbPFK crystals belong to the space group $P6_222$ with unit cell parameters a=135.0 Å, b=135.0 Å and c=77.7 Å and a hexagonal shape. The asymmetric unit contains a single monomer and the final structure was refined to R-

factor/R-free values of 22.29%/26.91% and has a 1.83 Å resolution. This structure has the highest resolution of LbPFK structures solved to date. Each monomer contains 319 residues, 214 water molecules, 12 phosphates and four magnesium ions. The details of the final refinement parameters are shown in Table 3-1.

Figure 3-1A shows the overall structure of the phosphate-bound LbPFK from two alternate views. There are three phosphate molecules bound per subunit, one in the active site, one in the allosteric site and one on the surface of the enzyme. The one in the active site forms potential hydrogen bonds with R252, R243, H249 and a H_20 molecule. When compared to the substrate-bound structure of BsPFK this phosphate appears to be positioned in the same area as the phosphate of F6P. The phosphate in the allosteric site could potentially interact with several residues including R21, R25 and R154 along with H215, which are all conserved between LbPFK, EcPFK and BsPFK. The surface phosphate is positioned to interact with R194 and K312. Since these residues are not involved in binding of either the substrates or effectors, the binding of this phosphate is most likely due to the crystallization conditions.

Characteristics of Substrate-bound LbPFK

The substrate-bound LbPFK crystals belong to the space group $P6_222$ with unit cell parameters *a*=134.5 Å, *b*=134.5 Å and *c*=77.7 Å and a hexagonal shape. The asymmetric unit containing a single monomer and the final structure was refined to R-factor/R-free values of 19.86%/23.25% and has a 2.20 Å resolution. Each monomer contains 319 residues, 138 H2O molecules, 12 phosphates, four F6P molecules and

Table 3-1. Data collection and refinement statistics for LbPFK strucures[a]

Data set	phosphate-bound LbPFK	Substrate-bound LbPFK
Unit cell (Å)	*a*=135.0	*a*=134.5
	b=135.0	*b*=134.5
	c=77.7	*c*=77.7
Space group	$P6_222$	$P6_222$
Monomers per asymmetric unit	1	1
Resolution (Å)	68-1.83	47-2.2
Redundancy	13.54(2.01)	21.3(21.1)
Observations	34,307	21,557
Observations (Test set)	1,432	1,106
Completeness (%)	92.7(40.1)	100(100)
$\boldsymbol{R_{merge}}$	0.089(0.549)	0.069(0.450)
$\boldsymbol{I/I\sigma}$	12.1(1.4)	74.3(11.6)
Refinement		
Resolution (Å)	68-1.83	47-2.2
$\boldsymbol{R_{cryst}}$ **(%)**	22.29	19.86
$\boldsymbol{R_{free}}$ **(%)**	26.91	23.25
Number of protein atoms/number of waters	2380/214	2372/138
Number of ligands (including ions)	19	32
Average *B* factor (Å^2)	36.8	54.3
rmsd bond length (Å)	0.004	0.007
rmsd bond angles (°)	0.566	0.964
Ramachandran statistics		
most favored	97.79%	98.11%
Allowed	2.21%	1.89%

[a] For details of the crystallization and structure determination, see text. Values in parentheses are for high resolution shells. $R_{merge} = \Sigma_h\Sigma i|I_{hi} - \langle I_{hi}\rangle|\backslash\Sigma_h\Sigma_i I_{hi}$ where I_{hi} is the *i*th observation of the reflection *h*, where $\langle I_h\rangle$ is the mean intensity of reflection *h*. $R_{cryst} = \Sigma_h|F_o| - |F_c|/|F_o|$. R_{free} was calculated with a fraction (5%) of randomly selected reflections excluded from refinement. rmsd, root-mean-square deviations from ideal geometry.

four chloride ions. The details of the final refinement parameters are shown in Table 3-1.

Figure 3-1B shows two views of the overall structure of the substrate-bound structure of LbPFK. This structure contains F6P in all four active sites along with a phosphate as well as a phosphate bound to the allosteric site and on the surface of the protein. The location of the phosphate in the allosteric site and on the surface of the enzyme is similar to that seen in the phosphate-bound LbPFK structure. The main difference between the structures is the position of the phosphate within the active site. The F6P is bound in a similar way as in the substrate-bound BsPFK structure (Figure 3-2). It interacts with R127, R171, R243 and R252 as well as G170, E222 and H249. Upon the addition of F6P to the active site, the free phosphate moves to a new position where is now interacts with R162 but still keeps its interaction with R252. When compared to the substrate-bound BsPFK structure, the free phosphate is positioned between where F6P and MgADP would potentially bind. This could mean that the free phosphate is bound close to where the γ-phosphate of MgATP would be bound and then transferred to F6P to form FBP during catalysis.

Active Site Comparison

Figure 3-2 shows a close-up of the active site for BsPFK (3-2A) and LbPFK (3-2B). In both cases a comparison was made between the phosphate-bound structures and the substrate-bound structures. For BsPFK, it appears that the only major difference between the two structures is the position of R171. This R moves towards the F6P

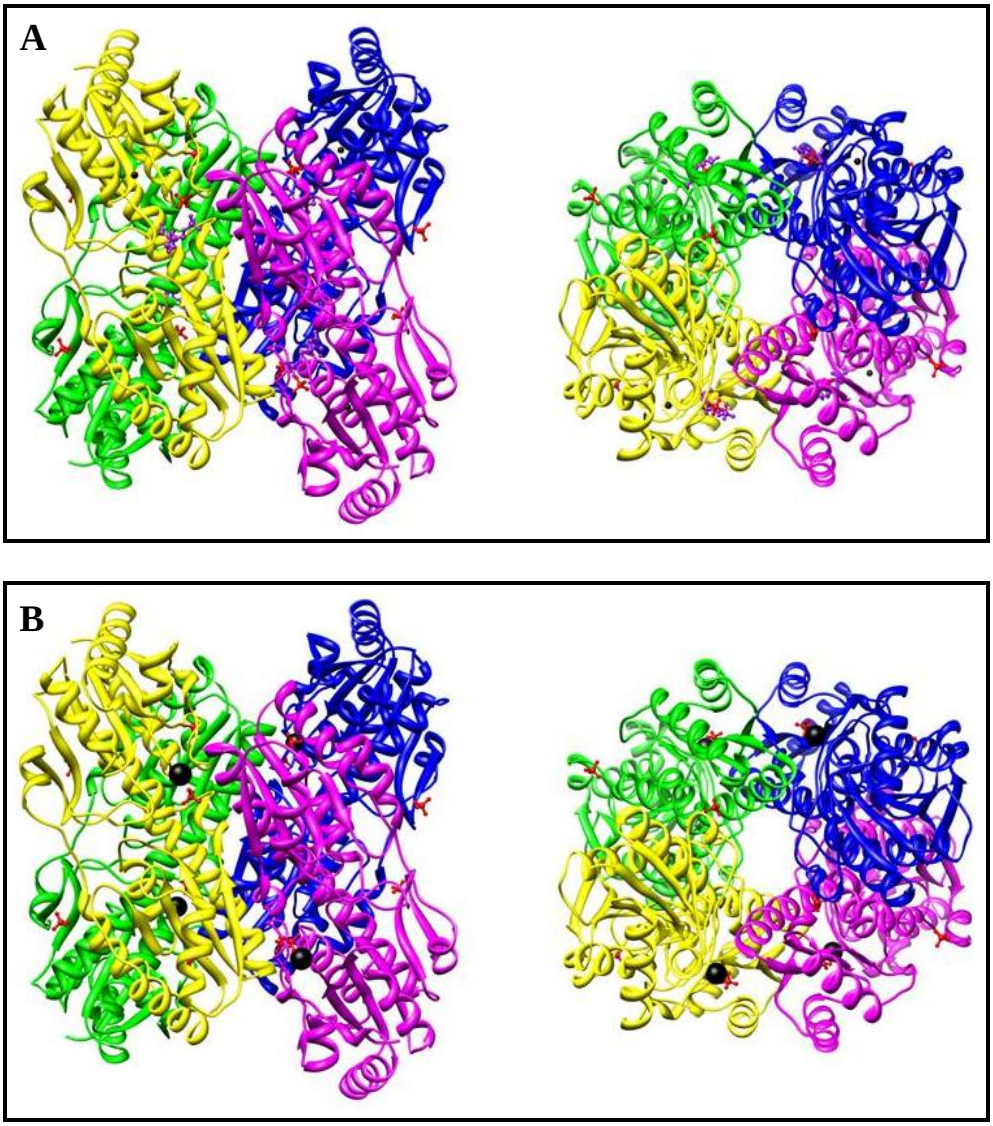

Figure 3-1. Phosphate-bound and substrate-bound LbPFK structures. Subunit A colored yellow, subunit B colored pink, subunit C colored blue and subunit D colored green, phosphates colored red, F6P colored purple and ions colored black. View showing the substrate binding interface between subunit A and B on the right and alternate view with a 90 ° rotation along the horizontal axis on the left for (A) Phosphate-bound structure with calcium ion bound and (B) Substrate-bound structure with magnesium ion bound.

molecule putting the NH1 3.0 Å from the OH of the F6P molecule. In the absence of F6P, this arginine is facing out of the active site and only interacts with the solvent surrounding the enzyme. There is also a minor shift in E241, which causes a break in the potential hydrogen bond with R162 (which is present in the phosphate structure but absent when F6P is bound). However, this change does not affect the interaction between R162 and either PO_4 or F6P, as these hydrogen bonds remain intact.

As with BsPFK, the only major difference in the location of the residues within the active site is the movement of R171. Again, it moves towards the bound F6P to form a potential hydrogen bond with the OH of the ring. All the other residues are not greatly displaced. There are however differences when comparing the actual amino acids between the active sites of BsPFK and LbPFK. In BsPFK, as mentioned before, E241 interacts with R162 in the phosphate-bound structure but this interaction is absent in LbPFK since there is now a D at 241. The shortening of the chain doesn't allow for the hydrogen bond with R162. R162 instead interacts with the free phosphate when F6P is bound and does not form any interaction in the presence of only phosphate.

Allosteric Site Comparison

The allosteric site was the area that contains the largest differences in comparing the non-allosteric LbPFK to the allosteric BsPFK and EcPFK. To keep things simple, only a comparison between LbPFK and BsPFK is presented. When comparing the allosteric sites between the substrate-bound and the phosphate-bound structures of both BsPFK and LbPFK, only a few differences appear within the allosteric site of BsPFK

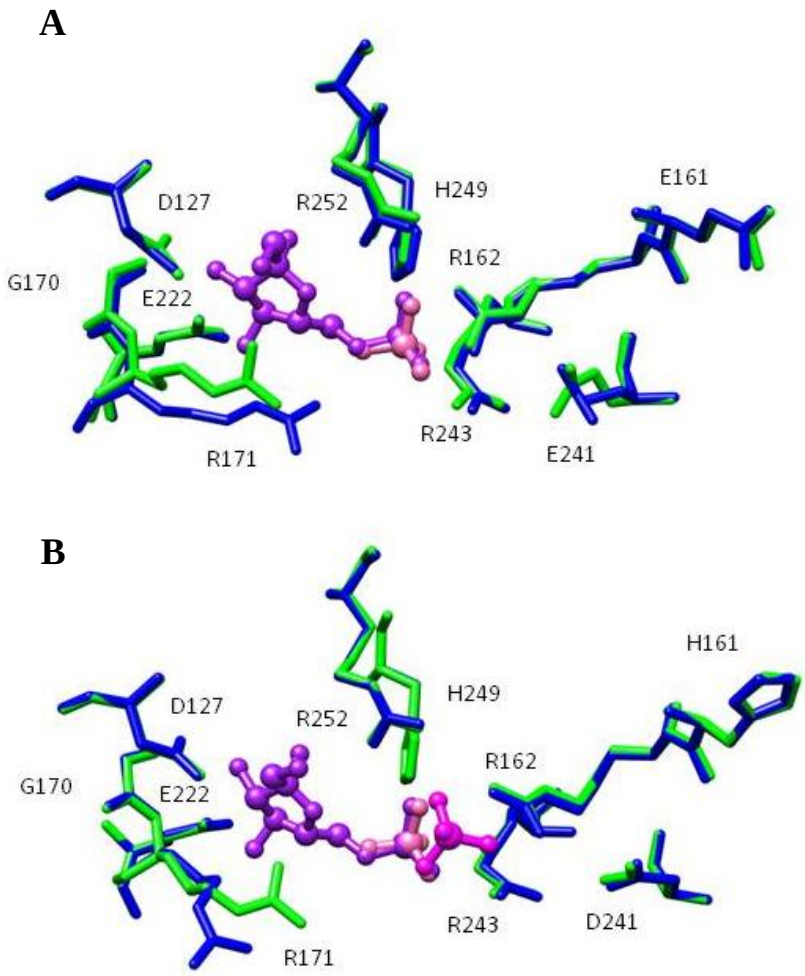

Figure 3-2. Active site comparison between phosphate-bound and substrate-bound forms of (A) BsPFK and (B) LbPFK. Phosphate-bound structures in blue with substrate-bound structures in green with F6P highlighted in purple and free phosphates highlighted in pink, light pink for phosphate-bound structure and dark pink for phosphate bound in substrate-bound structure LbPFK. Amino acid residues are labeled with three-letter abbreviations and numbers. Amino acid residues 161, 162, 241 and 243 are from one monomer with 127, 170, 171, 222, 249 and 252 belonging to the monomer across the active site interface.

(Figure 3-3A) and no major changes appear in LbPFK (Figure 3-2A). In the substrate-bound structure of BsPFK, MgADP is bound to the allosteric site. Figure 3-3A shows a comparison between the allosteric sites of the substrate-bound and phosphate-bound BsPFK. Of the many residues which come in contact with the ligands, the region containing residues 213-215 appears to change positions the most. In both LbPFK and BsPFK, there is a K at position 213 and an H at position 215. However, residue 214 is quite different, with BsPFK having a K and LbPFK having a D (Figure 3-3C).

In the phosphate-bound structure, K214 forms a hydrogen bond with the carbonyl oxygen of H206 but when MgADP binds to the allosteric site, K214 moves inward towards MgADP and forms a new hydrogen bond with the carbonyl oxygen of G212. The movement of K214 occurs at the same time as the movement of K213 and H215 which also move closer to MgADP causing K213 to hydrogen bond with both MgADP and H215. These movements appear to be important for the positioning of MgADP in the allosteric binding site.

D214 in LbPFK interacts with several other residues within the allosteric binding site. D214 forms hydrogen bonds with H59, two water molecules, H215 and Y69 which is located in the adjacent monomer. The hydrogen bond between 214 and 59 would not occur in BsPFK since K214 and D59 are not in close enough contact in either the phosphate-bound structure (16 Å) or the substrate-bound structure (11 Å). As can be seen in figure 3-3C, along with residues 214 and 59 there are other differences within the allosteric binding site including residue 55. In BsPFK there is a glycine at position 55 while LbPFK has a glutamate. These differences could help explain the weak binding

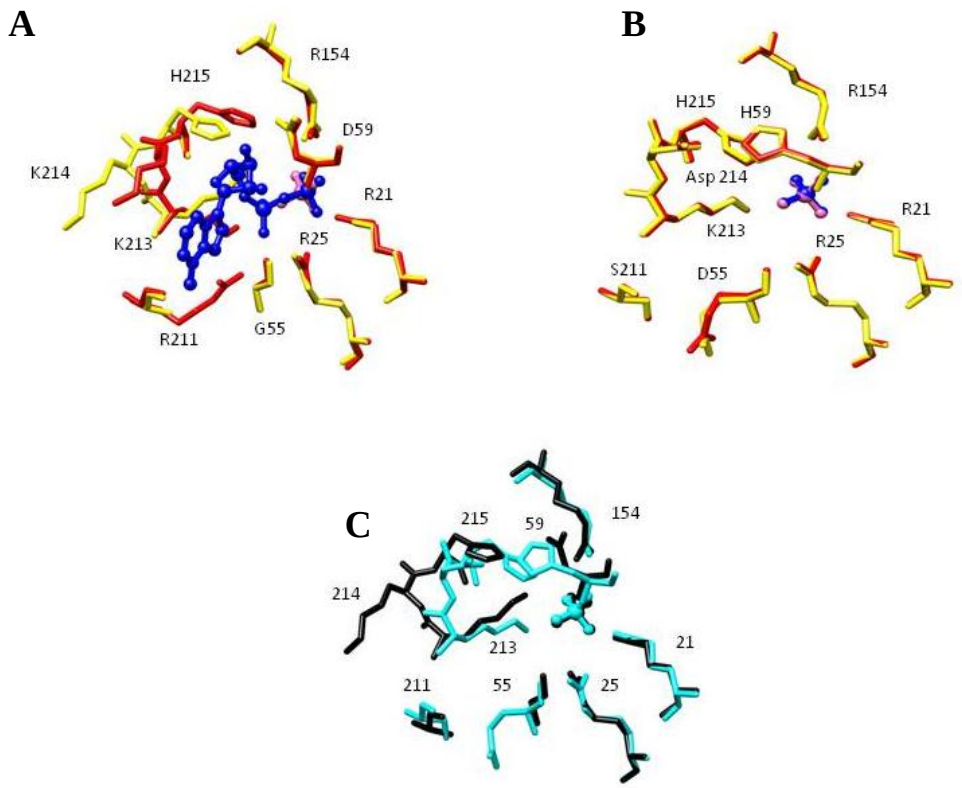

Figure 3-3. Allosteric site comparison between various BsPFK and LbPFK structures. (A) phosphate-bound BsPFK (yellow) vs. substrate-bound BsPFK (red) with MgADP (blue) and PO_4 (pink). (B) Phosphate-bound (yellow) LbPFK vs. substrate-bound (red) LbPFK with PO_4 (pink) and PO_4 bound with F6P (blue). (C) Phosphate-bound BsPFK (black) vs. phosphate-bound LbPFK (cyan) with bound PO_4 highlighted. Individual residues which form potential interactions with various ligands labeled.

affinity for effector ligands seen in LbPFK.

B-factor Comparison between LbPFK Structures

The B-factor, or temperature factor, in crystal structures is thought to be a measurement of how much an atom oscillates or vibrates around the position specified by the model. Through the refinement process the B-factor is computed for each of the main-chain and side-chain atoms and from these values it is possible to gain some insight into the dynamics of the protein. A small value for the B-factor indicates less movement compared to a high value which would indicate more movement (*104*). Figure 3-4 shows the B-factor comparison between the phosphate-bound and substrate-bound structures of LbPFK. From the comparison of the tetramers it is clear that the over-all structure becomes much more rigid upon binding of F6P to the four active sites (Figure 3-4A). Upon closer inspection of the dimer-dimer interfaces, it is clear that both interfaces increase in their rigidity especially along with active site interface (Figure 3-4B). The allosteric site interface also becomes more rigid but is still more flexible compared to the active site interface for both LbPFK structures (Figure 3-4C). Some of these differences could be due to the differences in the resolution of the two structures but overall suggest a more rigid structure when the substrate F6P is bound.

Since the B-factor can also help in determining the validity of the model in the final structure, care must be taken when comparing B-factors between two structures with different resolutions (*104*). The phosphate-bound and sulfate-bound structures are different in resolution, 1.83 Å and 2.2 Å respectively, which indicate that both are high

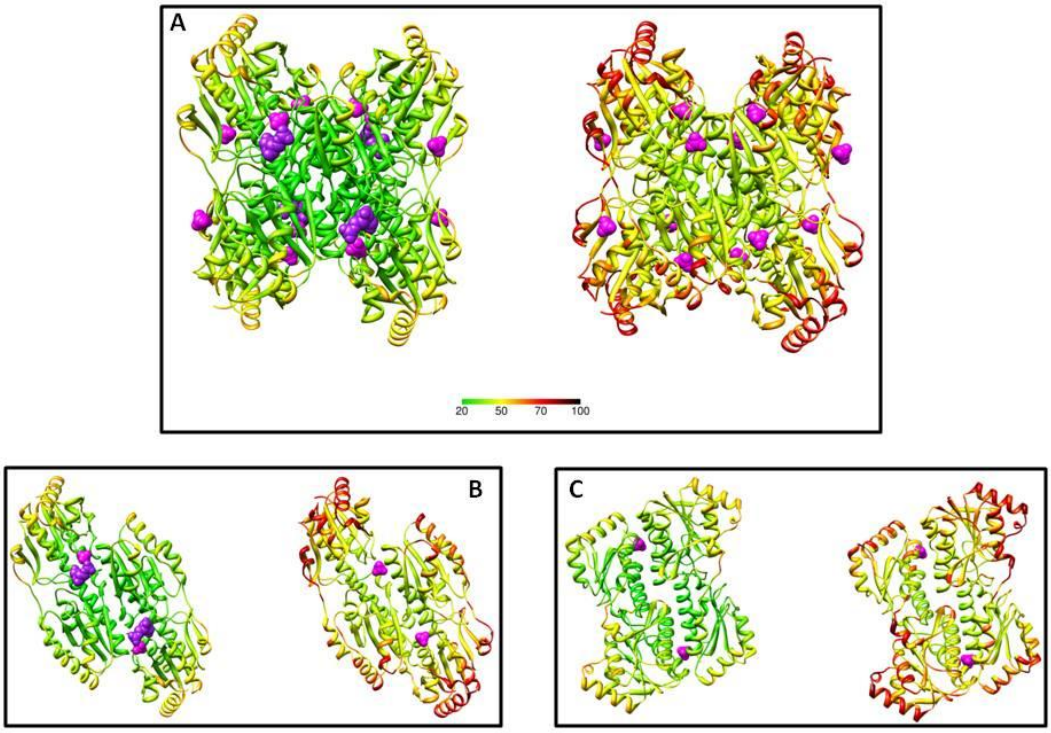

Figure 3-4. B-factor comparison of LbPFK structures with substrate-bound (left) and phosphate-bound (right). (A) Comparison of LbPFK tetramers. (B) Comparison of LbPFK dimers focusing along active site interface. (C) Comparison of LbPFK dimers focusing along allosteric site interface. Bound ligands are depicted as space filled molecules with F6P in purple and $P0_4$ in pink.

resolution structures. Therefore, the comparison of B-factors between these two structures will likely give insight into the differences in the overall rigidity of the structures.

Discussion

For many years the regulation of prokaryotic PFKs has been studied using crystal structures (*82-85, 94, 95*). From these studies several models have been proposed concerning the allosteric regulation of BsPFK and EcPFK and the possible reason for the weak binding for the allosteric ligands seen in LbPFK. In BsPFK, it was proposed that the transition between the active, R-state and the inhibited, T-state was due to a quaternary shift along the active site interface accompanied by binding of PG (*84*). This quaternary shift was also accompanied by several secondary-structural changes one of which involved residues within the allosteric binding site. A more recent study had shown that this quaternary shift is actually move important for the binding of the inhibitor, PEP, than the actual allosteric inhibition (*85*). In that study, several new crystal structures were determined including the apoenzyme of BsPFK and the PEP-bound D12A BsPFK. Comparative analysis of these structures with the other structures of BsPFK allowed for further insight into the allosteric mechanism of BsPFK.

When comparing the apoenzyme of BsPFK to the substrate-bound and the PG-bound BsPFK structures determined that only the PG-bound structure had undergone the quaternary shift and that significant differences in the B-factors for the amino-acid side-chains were evident. B-factor analysis has been used in numerous crystal structure

comparisons to show what happens upon ligand binding as well as to indicate differences in protein stability between the same proteins from thermophilic and mesophilic organisms (*105, 106*). In the comparison of BsPFK structures, it was found that the substrate-bound structure was the most flexible and the PG-bound was the most rigid, with the apoenzyme being somewhere in between. Also, the active site interface was determined to be more flexible than the allosteric site interface which would allow for the quaternary shift to occur along the active site interface. The only exception was the region containing residues 156-162 which is more rigid in the substrate-bound structure compared to the other two structures. This region has been implicated to be involved in the quaternary shift since the helix containing 156-162 changes secondary structure upon binding of the inhibitor PEP as well as several residues being involved in important hydrogen bonds across the active site interface (*85*). This shows how the comparison of B-factors can shed some light on the role of certain regions within the protein in the binding of ligands.

When comparing the B-factors for each of the two LbPFK structures, it is clear that the substrate-bound structure is much more rigid overall than the phosphate-bound structure. In each structure the interior of the enzyme is more rigid than the exterior with several of the solvent exposed helices being the most flexible. By looking at the PFK dimers, each split along the opposite dimer-dimer interface, it is also evident that the active site interface is more rigid than the allosteric site interface. Increased flexibility along the active site interface is opposite of what was seen in BsPFK and could be an explanation for the weak binding affinity for the effector ligands in LbPFK. Since both

LbPFK structures were crystallized under similar conditions and have the same crystal contacts, the differences in the B-factors for the main-chain are most likely due to binding of the various ligands. Therefore, since the only difference in the ligand binding between the two is the presence of F6P in the active site and the movement of the phosphate within the active site, it may be that the binding of F6P is causing the over-all structure to become more rigid. This could potentially lock the enzyme in a catalytically favorable structure where only the two substrates F6P and MgATP could bind and the reaction take place.

This lock in structure along with the non-conservation of the allosteric site between LbPFK and the allosteric PFKs could explain its weak binding for both allosteric ligands. Having a very rigid active site interface might inhibit the quaternary shift from occurring and therefore make it even harder for the allosteric ligands to bind. Therefore, it is necessary to look at both the active site interface as well as the allosteric binding site when attempting to make mutations which would enhance binding for either PEP or MgADP. It would also be of interest to solve the crystal structures for any mutants which enhance binding for the allosteric ligands and compare the B-factors for those structures to the ones presented here to test these predictions.

CHAPTER IV

THE EFFECT OF CONSERVED RESIDUES ON THE BINDING OF AN ALLOSTERIC LIGAND FROM A DISTANCE

Phosphofructokinase (PFK) is an allosterically regulated, glycolytic enzyme which catalyzes the phosphoryl transfer from MgATP to fructose-6-phosphate (F6P) to form MgADP and fructose-1,6-bisphosphate. In bacteria, PFK is usually allosterically regulated by two ligands, phospho(enol)pyruvate (PEP) which acts as an inhibitor and MgADP which acts as an activator. Both ligands bind to the same allosteric site, but exert opposite effects. PFK is structurally a homotetramer with four active sites and four allosteric sites. It is assembled as a dimer of dimers, and the binding sites lie along respective dimer-dimer interfaces. The structures of both PFK from *E. coli* (EcPFK) and *Bacillus stearothermophilus* (BsPFK) have been determined with various ligands bound (*83, 84, 94, 95*). From these structures, there has been a model proposed to explain the structural basis for allosteric regulation (*84*). In this model, the substrate-bound structure of BsPFK with MgADP and F6P bound to the active site as well as MgADP bound to the allosteric site is contrasted to the inhibitor-bound structure of BsPFK with phosphoglycolate (PG) bound to the allosteric site. It was proposed that the inhibition exerted by PG was accompanied by a 7° shift along the active site interface. Along with the large quaternary change, several changes in secondary structure occur including the movement of a loop located in the allosteric site. This model has been used extensively in the literature to explain the allosteric inhibition of PFK.

In the model proposed by Schirmer and Evans, one of the secondary changes which occurs upon the 7° shift, also referred to as the quaternary shift, involves an α-helix and loop containing the amino acid residues 155-162 and the surrounding residues. Several of these residues are involved in hydrogen bonds across the active site interface and upon the quaternary shift, this hydrogen bonding pattern is changed. The residues which are involved in these hydrogen bonds are T156, S159 and H160. All of these form a hydrogen bond with D12 across the active site interface. D12 also hydrogen bonds within the same subunit with R252, which in turn interacts with the substrate F6P in the active site. Upon binding of PG, this hydrogen bonding pattern is interrupted and a new hydrogen bond is formed between D12 and T158 as well as a salt bridge between R72 and E241. These changes in hydrogen bonds are proposed to be involved in the inhibition of PFK by the inhibitor PEP even though the allosteric binding site is 15 Å away.

Several of the residues involved in the quaternary shift are 100% conserved when comparing 150 bacterial ATP-dependent PFK sequences. These include D12, T156 and R252. S159 and H160 are also highly conserved. T156, S159 and H160 were all mutated in EcPFK to the corresponding residues in BsPFK or rabbit muscle PFK (both the C-terminal and N-terminal regions) and exhibited various effects on both substrate and effector binding affinities (*107*). In the case of H160, when mutated to an N, there was a decrease in the binding affinity for F6P as well as for PEP, which as mentioned previously is located far away from the allosteric binding site. T156, when changed to either a G or S, exhibited weaker binding affinity for F6P and surprisingly activation in

the case of PEP (*107*). Activation by T156E/S is similar to that seen when E187, which is located within the allosteric site, is mutated to an A (*108*). The activation by PEP was proposed by Kundrot and Evans to involve the residues within the region between T156 and the allosteric binding site (*107*). Finally, when S159 was mutated to an N, the effects were similar for the binding of F6P as seen with H160N and T156G/S as well as the effect on PEP binding being weaker as with H160N. The effects were explained due to the structural changes seen between the shift from substrate-bound to inhibitor-bound in BsPFK, but shows the need for a model in which intermediate states are allowed.

Even though all of these residues form hydrogen bonds with D12, it wasn't until more recently that the effect upon mutating D12 would have on the properties of bacterial PFK was studied. D12A was first introduced in BsPFK in combination with R252A and this showed a weakening in the binding for the substrate F6P as well as enhanced binding for PEP (*73*). A more extensive study of D12A in BsPFK found that this mutation weakened F6P binding 50-fold, increased the binding affinity for PEP by 100-fold but had little to no effect on the extent of inhibition seen with PEP when compared to wild-type BsPFK (*85*). A structure of D12A BsPFK was also solved to 2.0 Å resolution with the inhibitor PEP bound to the allosteric site, which is the first time a structure of PFK has been solved with the physiological inhibitor bound. This structure is quite similar to that of the PG-bound BsPFK structure solved by Evans and colleagues and exhibits the same structural changes seen upon the quaternary shift. T156A was also introduced in BsPFK and has similar properties as seen in D12A, but not to the same degree. A PEP bound structure of T156A was also solved in BsPFK and this structure,

as with D12A, shows the characteristics of the quaternary shift (*85*). These results suggest that the quaternary shift is most likely involved in the binding of PEP but not in its ability to inhibit PFK.

Unlike EcPFK and BsPFK, PFK from the lactic acid bacteria *Lactobacillus delbrueckii* subspecies *bulgaricus* (LbPFK) has weak binding for both allosteric ligands, and both ligands inhibit at high concentrations (*82*). The structure of LbPFK was recently solved to 1.83 Å resolution with phosphate bound to all eight sites and comparison between this structure and those of BsPFK and EcPFK show high over-all conservation in structure (see Chapter III). The hydrogen bonding pattern between D12 and the residues across the active site interface, T156 and H160 is also present in the LbPFK structure. It is unclear if there is a potential hydrogen bond between D12 and S159 in LbPFK. D12 also interacts with R252 within the same subunit, as seen in BsPFK.

To investigate the role of this hydrogen bonding network in LbPFK, D12, T156 and H160 were mutated to A. H161, which is an E in BsPFK and a Q in EcPFK, was also mutated to A. H161 could potentially take the place of H160 in the H160A variant, therefore the single H161A variant was created as well as the combination variant H160A/H161A. All of these mutants, with the exception of H161A, showed diminished binding for the substrate F6P. D12A also exhibited a 7-fold enhancement in MgATP binding compared to LbPFK. D12A was the only mutant to show enhancement in PEP binding and therefore was analyzed for MgADP binding. MgADP binds 9-fold tighter to D12A compared to wild-type. MgADP continues to act as an inhibitor even though

MgADP acts as an activator in other allosteric PFKs such as EcPFK. D12A LbPFK was crystallized and solved to 2.3 Å resolution. Sulfate was bound to all eight sites and when compared to the sulfate bound wild-type LbPFK structure, no major structural changes are observed. The change in PEP binding and structure is small compared to that seen in BsPFK, and may be due to the other differences within the enzymes such as the lack in conservation at the allosteric site.

Methods

Site-directed Mutagenesis

The strategy employed for site-directed mutagenesis is similar to that discussed in Chapter II. Below are the template strands for the oligonucleotides used in combination with the complementary strand in the creation of D12A, T156A, H160A, H161A and H160A/H161A. For the creation of H160A/H161A, an additional oligonucleotide was needed to introduce H161A into the plasmid pK223-3 that already contained the mutated H160A LbPFK gene. Figure 4-1 shows the oligonucleotides used with the codon that was changed in the mutagenesis reaction underlined.

Protein Purification for D12A

D12A LbPFK was purified following the protocol for LbPFK in Chapter II with the following exceptions. The buffer used throughout the purification contained 1mM F6P and the cell lysate was applied to a 100 mL pre-equilibrated Mimetic-Blue A column and washed at 4°C. Also, the protein eluted from the column during the wash

D12A: ACT GGC GGT GCC GCC CCT GGT ATG

T156A: C GAC AAG ATC CGT GAC ACT GCT TTC TAG CCA CC

H160A: AC ACT GCT TCT AGC GCC CAC CGC GTC TTC ATT G

H161A: C ACT GCT TCT AGC CAC GCC CGC GTC TTC ATT GTC

H161A for H160A: CT GCT TCT AGC GCC GCC CGC GTC TTC ATT G

Figure 4-1. Template strands used for site-directed mutagenesis to create the active site mutations in LbPFK. For each LbPFK variant (bolded), the DNA sequence for the template strand is shown and was used along with the complementary strand to introduce the change in the DNA sequence.

and the fractions containing PFK activity were pooled and 5mM $MgCl_2$ added to the sample.

Protein Purification for H160A, H161A and H160A/H161A

H160A LbPFK was purified following the protocol for LbPFK in Chapter II with the exceptions of having 1mM F6P in buffers throughout the purification and a 0-1M NaCl gradient applied to the Mimetic BlueA column. H160A LbPFK was stored at 4°C in Buffer A (50mM Tris-HCl pH 7.5, 0.1 mM EDTA), 1mM F6P and 10% glycerol.

H161A LbPFK was purified as described for LbPFK in Chapter II with the exceptions being the presence of 1mM F6P in the buffers throughout the purification, and after eluting from the Mimetic-Blue A column with a 0-2M NaCl gradient, fractions containing PFK were pooled and dialyzed into Buffer A + 1mM F6P. Following dialysis the sample was applied to an anion-exchange MonoQ column, washed with Buffer A + 1mM F6P and eluted with a 0-1M NaCl gradient in Buffer A + 1mM F6P. The fractions containing PFK activity were pooled and dialyzed into Buffer B (Buffer A + 5mM $MgCl_2$) + 1mM F6P.

H160A/H161A was purified with the following exceptions. After eluting from the Mimetic- Blue A column, the fractions containing PFK were pooled and dialyzed into Buffer A. The sample was then applied to two anion-exchange MonQ columns, the first at pH 7.5 followed by a second at pH 6.0. In both cases the column was eluted with a 0-0.7M NaCl gradient in Buffer A, the fractions containing PFK pooled and then

dialyzed into the appropriate buffer. The final sample was dialyzed into Buffer B and stored at 4°C.

Protein Purification for T156A

6L of LB containing ampicillin were inoculated with an overnight culture of cells containing the plasmid pK223-3 that contained the T156A LbPFK gene (2 mL of the overnight were used to inoculate each 1.5L sample). Samples were grown at 37°C to an OD_{600}=1.4, cooled to 15°C and allowed to grow at 15°C for 24 hours. Cells were harvested and the pellet stored at -80°C. The purification was performed following the protocol for LbPFK in Chapter II with the following exceptions. All buffers throughout the purification contained 1mM F6P and the majority of the PFK eluted off the Mimetic-Blue A column during the wash step. All fractions containing PFK activity were pooled and concentrated to a final volume of 20 mL with polyethylene glycol (PEG). 50% ammonium sulfate was then added to the sample and the sample incubated for 30 minutes on ice with constant stirring. The sample was dialyzed into Buffer A to remove ammonium sulfate and concentrated to 4 mL with PEG. The sample was then applied to a S200 gel-filtration column at 4°C at a rate of 0.2 mL/min and 1 mL fractions collected. All fractions containing PFK activity were pooled, dialyzed into Buffer B and stored at 4°C.

Crystallization and Data Collection for D12A LbPFK

D12A LbPFK was crystallized using the hanging drop vapor diffusion method (*98*) at 16 °C. Crystallization was achieved in a 6 μL drop with 2μL solvent (0.1 M sodium acetate trihydrate pH 4.6, 2.0 M ammonium sulfate) and 4 μL protein (stock concentration of LbPFK was 13.3 mg/mL in 50mM Tris-HCl, pH 7.5, 1mM EDTA and 1mM F6P). Within 24 hours, diamond shaped crystals were formed. For data collection, crystals were cryoprotected by brief soaking in 30% ethylene-glycol and then flash-frozen in a liquid N_2 stream at 100 K. Diffration data were collected to a resolution 2.3 Å on a home-source Raxis IV++ detector (Rigaku). The HKL2000 program package (HKL Research, Inc., Charlottesville, VA) (*99*) was used for integration and scaling. Crystals belong to the space group $P6_222$ with unit cell parameters containing one molecule in the asymmetric unit. Data collection details are summarized in Table 4-1.

Structural Determination and Refinement of D12A LbPFK

The molecular replacement program PHASER (University of Cambridge, UK) (*100*) was used to solve the structure of D12A LbPFK using the sulfate-bound crystal structure of LbPFK (1ZXX) (*82*) with waters and ions removed as a model. Rigid body refinement followed by stimulated annealing refinement at 5000 K was carried out using Phenix (Python-based Hierarchical Environmnet for Integrated Xtallography, Berkeley, CA) (*101*). Subsequently, refinement was carried out in alternating cycles of manual model building in COOT (Crystallographic Object-Orientated Toolkit, Oxford, UK)

Table 4-1. Data collection and refinement statistics for D12A LbPFK structure[a]

Data set	D12A LbPFK
Unit cell (Å)	*a*=135.4
	b=135.4
	c=77.7
Space group	$P6_222$
Monomers per asymmetric unit	1
Resolution (Å)	50-2.3
Redundancy	30.2(29.8)
Observations	20,143
Observations (Test set)	977
Completeness (%)	99.7(96.9)
R_{merge}	0.082(0.576)
$I/I\sigma$	83.92(9.03)
Refinement	
Resolution (Å)	50-2.3
R_{cryst} **(%)**	17.48
R_{free} **(%)**	21.41
Number of protein atoms/number of waters	2388/157
Number of ligands (including ions)	15
rmsd bond length (Å)	0.007
rmsd bond angles (°)	0.927
Ramachandran statistics	
most favored	98.42%
Allowed	1.58%

[a] For details of the crystallization and structure determination, see text. Values in parentheses are for high resolution shells. $R_{merge} = \Sigma_h \Sigma i|I_{hi} - \langle I_{hi}\rangle|\backslash\Sigma_h\Sigma_i I_{hi}$ where I_{hi} is the ith observation of the reflection h, where $\langle I_h\rangle$ is the mean intensity of reflection h. $R_{cryst} = \Sigma_h|F_o| - |F_c|/|F_o|$. R_{free} was calculated with a fraction (5%) of randomly selected reflections excluded from refinement. rmsd, root-mean-square deviations from ideal geometry.

(*102*) followed by refinement as implemented in Phenix until R-factors converged. Water molecules were added in the difference electron density maps at positions corresponding to peaks (>3.0σ) and with appropriate hydrogen bonding geometry. The stereochemical quality of the final model for the LbPFK proteins was verified by Molprobity (Duke University, Durham, NC) (*103*).

Results

Steady-state Kinetics of D12A LbPFK

Weak binding of the allosteric ligands, PEP and MgADP, to the allosteric site of LbPFK has been previously thought to be due to the lack of conservation of amino acids within the allosteric binding site (*82*). The role of these non-conserved residues in the binding of both PEP and MgADP is discussed in Chapter 5 of this dissertation. Another region which has been identified to have a role in PEP binding in BsPFK is the area surrounding the 100% conserved D12 (*73, 85*). D12 is located along the dimer-dimer interface that contains the four active sites and is located approximately 6 Å from the active site. D12 interacts with R252 that in turn interacts with the substrate F6P. Upon changing D12 to an A (D12A), the binding affinity for PEP in BsPFK increases 100-fold compared to wild-type and a nearly 7° quaternary shift along the active site interface is induced (*85*). Since D12A enhances the affinity of BsPFK for PEP, this mutation was introduced into LbPFK.

The steady-state kinetics parameters were measured for D12A LbPFK and compared to the wild-type enzyme. Figure 4-2 shows titration curves for F6P and

MgATP comparing D12A to LbPFK. Due to an 8-fold decrease in the overall specific activity upon introducing D12A, the rates shown in Figure 4-2 are normalized. It is evident from the shifting of the titration curve right that the binding affinity for F6P is diminished (Figure 4-2A) while the titration curve for MgATP (Figure 4-2B) is shifted to the left, indicating an enhancement in binding for D12A compared to wild-type. Both changes are approximately 7-fold (Table 4-2) and could be explained by the proximity of D12 to the active site.

D12A not only effects binding of both substrates to the active site but also the binding affinity for the allosteric ligands PEP and MgADP to the allosteric site. Since PEP and MgADP are K-type allosteric effectors, i.e. binding of these ligands to the allosteric site affects the binding of the substrate F6P to the active site, the binding affinity for F6P was measured at various concentrations of either PEP or MgADP. Figure 4-3 shows the effect for both PEP and MgADP on F6P binding for D12A LbPFK. Binding for both PEP and MgADP were enhanced, 9-fold and 11-fold respectively, compared to WT LbPFK as well as allosteric inhibition being exhibited in both cases (Table 4-2). Since saturation of either allosteric ligand could not be reached in these experiments, the allosteric response could not be quantitated, i.e. Q_{ay} and Q_{ax} could not be determined. Q_{ay} and Q_{ax} are the coupling constants which describe both the nature of the allosteric effector as well as the magnitude of the allosteric effect (*88*). The inhibition of F6P binding exhibited by MgADP is most likely due to an allosteric effect and not to product inhibition since all the experiments were performed in the saturating presence of MgATP. MgATP is also present in equal molar concentrations with

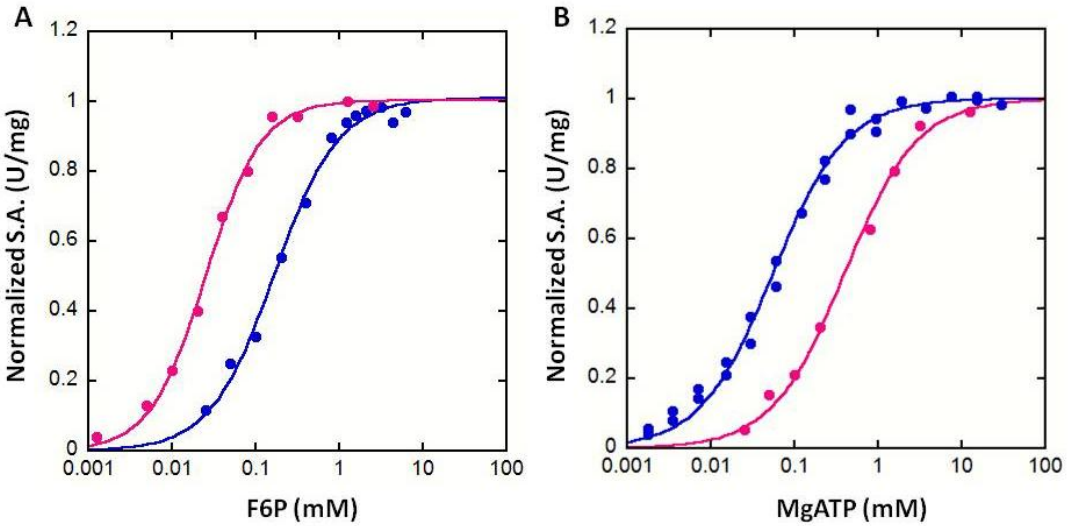

Figure 4-2. Substrate titration curves for wild-type LbPFK and D12A LbPFK at 25°C, pH 8.0. (A) F6P titration curves for LbPFK (pink) and D12A LbPFK (blue). The experiment was performed with [MgATP] = 15 mM for LbPFK and 3mM for D12A LbPFK. (B) MgATP titration curves for LbPFK (pink) and D12A LbPFK (blue). Experiment was performed with [F6P] = 3mM for LbPFK and 5mM for D12A LbPFK. In both experiments, the specific activity was normalized for each PFK to the appropriate $V_{max,}$ 250 U/mg for LbPFK and 28 U/mg for D12A LbPFK.

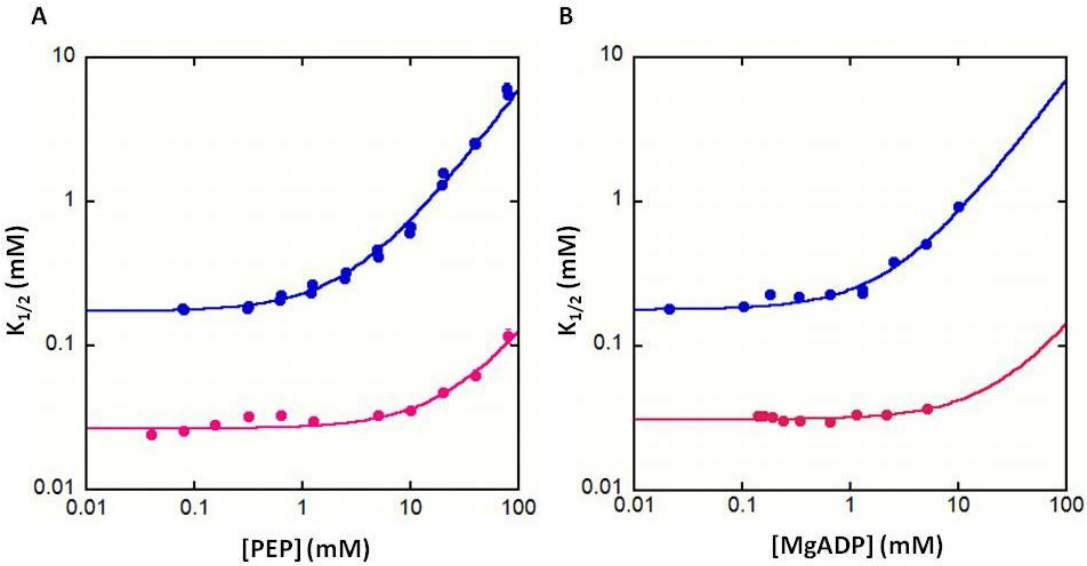

Figure 4-3. Binding and allosteric response of PEP and MgADP for wild-type and D12A LbPFK at 25°C, pH 8.0. The $K_{1/2}$ for F6P was measured at various concentrations of (A) PEP or (B) MgADP for LbPFK (pink) and D12A LbPFK (blue). Each measurement was determined at [MgATP] = 15 mM for LbPFK and [MgATP] = 3mM for D12A LbPFK. All data were fit to equation 2-4 to determine values given in Table 4-1. MgADP Data for LbPFK are from (*82*).

Table 4-2. Steady state kinetic parameters for wild-type and D12A LbPFK at 25°C, pH 8.0

PFK	S.A. (U/mg)[a]	K_b (mM)[b]	$K_{ia}{}^{oc}$	$K_{iy}{}^{oc}$	$K_{ix}{}^{oc}$
Wild-type	250	0.34 ± 0.4	0.025 ± 0.001	27 ± 2	28 ± 8[d]
D12A	28	0.049 ± 0.003	0.17 ± 0.02	3.0 ± 0.1	2.6 ± 0.2

[a] S.A. = specific activity. [b] K_a for MgATP was determined for WT LbPFK at [F6P]=3mM and D12A LbPFK at [F6P] = 5mM. [c] Values were determined at [MgATP] = 15mM for WT LbPFK and 3mM for D12A LbPFK. [d] (*82*)

MgADP in the experiment making the chances of MgADP binding to the active site highly unlikely.

Steady-state Kinetics for T156A, H160A, H161A and H160A/H161A

Along with the interaction with R252, D12 also forms potential hydrogen bonds across the active site interface with two residues, T156 and H160. In LbPFK there is also an H at position 161 which is an E in BsPFK and a N in EcPFK. H161A does not come in contact with D12 in LbPFK but in the absence of H160 might interact with D12 LbPFK. Breaking of the D12-T156 interaction has been proposed to be involved in the effects of D12A (*85*). Therefore T156A and H160A, as well as H161A, were introduced into LbPFK. The double mutant H160A/H161A was also created to completely remove the histidine from across the interface from D12. These mutants were analyzed for substrate binding as well as binding for the inhibitor PEP.

Table 4-3 gives the steady-state kinetic parameters for T156A, H160A, H161A and H160A/H161A LbPFK. The specific activity for H160A and H161A were determined and when compared to LbPFK showed 2.5 and 1.3-fold decreases, respectively. The specific activity for T156A and H160A/H161A was not determined because of the low protein expression for both mutants which caused each to only be purified to approximately 50% purity. Low levels of purity would cause an inaccurate value for specific activity to be determined. However, the kinetic assay used in measuring the steady state kinetic parameters is accurate enough that the low level of purity should not skew the results.

Binding affinities for both F6P and MgATP were determined for the mutant H160A with MgATP binding being the same as wild-type, while F6P binding was diminished 11-fold. Similar effects on F6P binding were seen with T156A and H160A/H161A, and these effects could all be attributed to the close proximity of these residues to the active site. H161A showed a small effect on F6P binding, diminishing F6P binding 1.9-fold. Therefore, the 10-fold decrease in F6P binding exhibited by H160A/H161A is due more by the H160A mutation than the H161A mutation. Due to the similarity in MgATP binding for the active site interface variants, the same concentration of MgATP was used for all the variants when analyzing the binding affinity for both F6P as well as PEP.

Figure 4-4 shows the analysis to determine the binding affinity for PEP to these active site interface mutants. Upon mutating any of the residues across the active site interface from D12, no enhancement in PEP binding was observed (Table 4-3). H160A/H161A actually showed a slightly negative effect on PEP binding compared to native enzyme. Lack of enhancement in PEP binding suggests that the breaking of the interaction between D12 and T156 and H160 does not contribute to the effect of D12A. Due to the lack of change in PEP binding, these mutants were not analyzed for binding to the allosteric ligand MgADP.

Structural Analysis of D12A LbPFK

In hopes of better understanding the change in binding of the allosteric ligands to D12A LbPFK, the crystal structure of D12A LbPFK was determined to 2.3 Å

Table 4-3. Steady state kinetic parameters for active site interface mutants of LbPFK at 25°C, pH 8.0

LbPFK	S.A. (U/mg)[a,b]	K_b (mM)[c]	$K_{ia}°$ (mM)[d]	$K_{iy}°$ (mM)[d]
T156A	N.D.	N.D.	0.390 ± 0.01	30 ± 7
H160A	100	0.33 ± 0.03	0.330 ± 0.002	20 ± 4
H161A	200	N.D.	0.047 ± 0.002	28 ± 3
H160A/H161A	N.D.	N.D.	0.250 ± 0.007	37 ± 5
WT	250	0.34 ± 0.4	0.025 ± 0.001	27 ± 2

[a] S.A. = Specific Acitivity, [b] N.D. = not determined. Purity of T156A LbPFK and H160A/H161A LbPFK were low so an accurate specific activity for either was not determined. [c] K_b for MgATP was determined at [F6P] = 3mM for WT LbPFK and LbPFK mutants. [d] Determined for WT and all mutants at [MgATP] = 15mM.

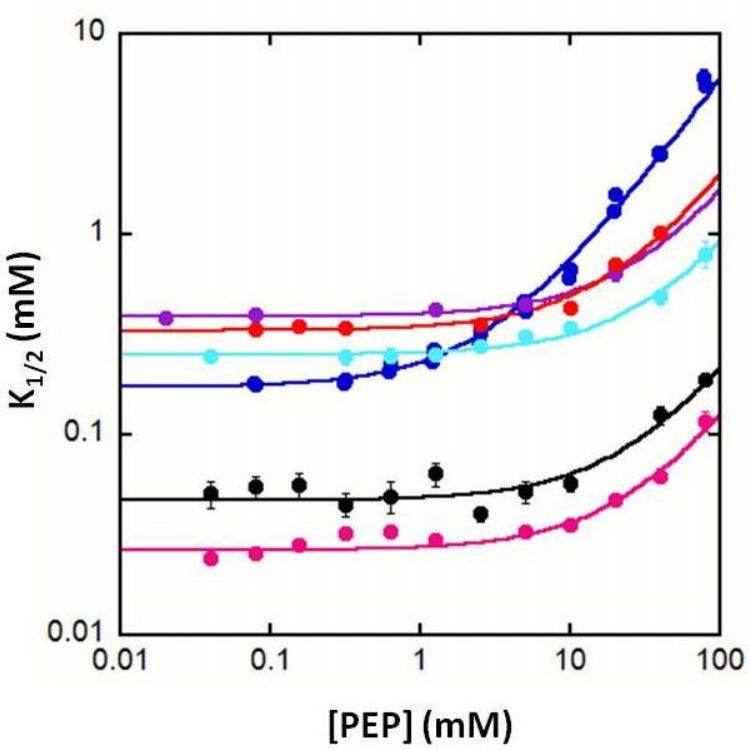

Figure 4-4. Binding and allosteric response of PEP for active site interface variants compared to wild-type LbPFK at 25°C, pH 8.0. The $K_{1/2}$ for F6P was measured at various concentrations of PEP for LbPFK (pink), D12A (blue), T156A (purple), H160A (red), H161A (black) and H160A/H161A (cyan). Each measurement was determined at [MgATP] = 15 mM for LbPFK and variants of LbPFK except for 3mM for D12A LbPFK. All data were fit to equation 2-4 to determine values given in Table 4-2.

resolution. The D12A LbPFK crystals belong to the space group $P6_222$ with unit cell parameters *a*=135.4 Å, *b*=135.4 Å and *c*=77.7 Å with a hexagonal shape. The asymmetric unit contains a single monomer and the final structure was refined to R-factor/R-free values of 17.48%/21.41%. Each monomer contains 319 residues, 157 water molecules and 12 sulfate ions. The details of the final refinement parameters are shown in Table 4-1.

Figure 4-5A shows the overall structure of the tetrameric form of D12A LbPFK looking along the dimer-dimer interface where the active sites are located. Each monomer contains 3 sulfate ions with one bound to the active site, one bound to the allosteric site and one bound to the surface. The sulfate bound to the surface of each monomer is likely a result of the crystallization conditions that contained 2.0M ammonium sulfate. The sulfates bound to each of the binding sites are in a similar position as the sulfates bound to the wild-type LbPFK structure (*82*). A close-up of the region around residue 12 is shown in Figure 4-5B. A12 is highlighted in red and belongs to the yellow monomer with T156, H160 and H161 highlighted in cyan belonging to the pink monomer. R252, also highlighted in cyan, interacts with F6P in the active site. Sulfate, shown in black, binds to the active site of D12A LbPFK in an orientation similar to that of the phosphate of F6P in BsPFK (*84*). Due to proximity of residue 12 to the active site and the effect of D12A on the binding of the two substrates, a comparison was made between the active site residues of D12A to LbPFK (Figure 4-6).

Residues within the active site that are involved in F6P binding are highlighted in Figure 4-6A. The location of the sulfate bound in the active site is also indicated. When

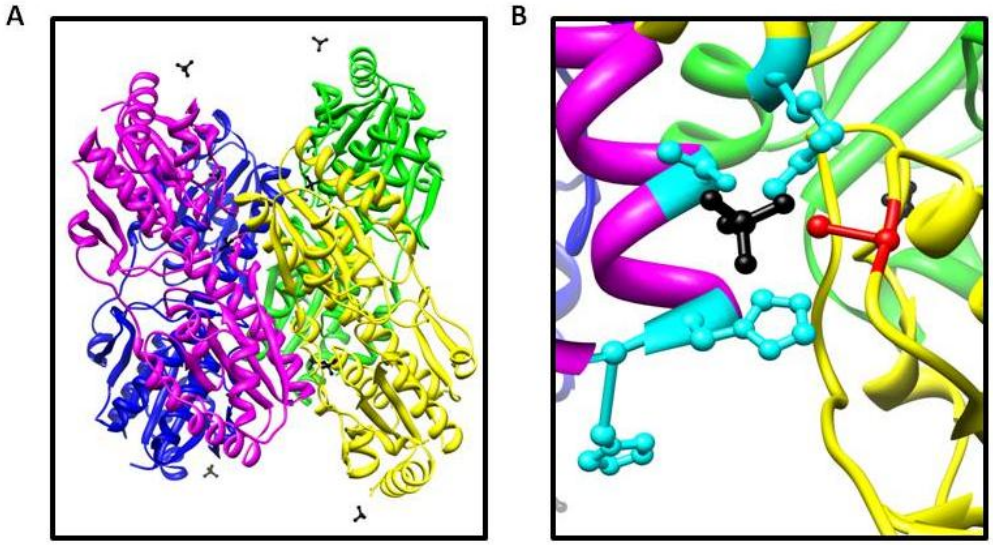

Figure 4-5. Crystal structure of D12A LbPFK to 2.2 Å resolution. (A) Tetramer of D12A with monomers colored pink, yellow, blue and green with sulfate (black) bound to all four active sites, all four allosteric sites and on the surface of each monomer. (B) Close-up of region around residue 12 highlighting sulfate bound to the active site (black), A12 (red) with T156, H160, H161 and R252 (cyan).

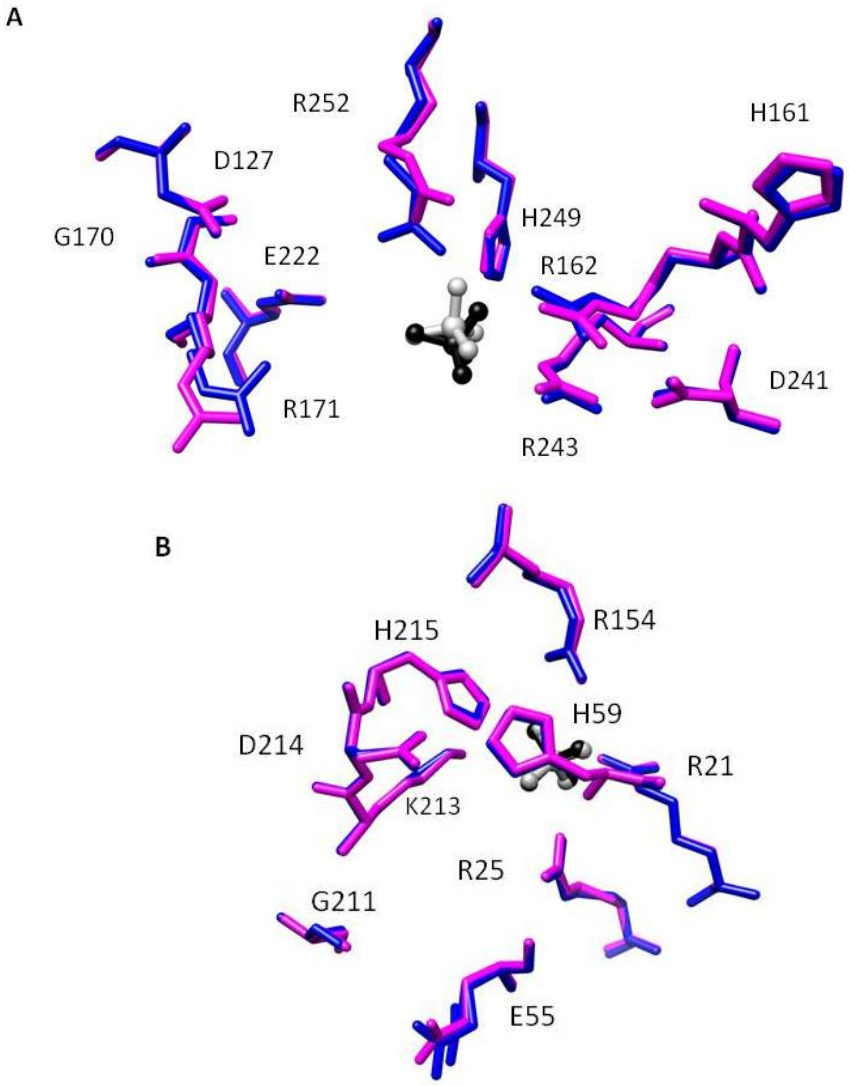

Figure 4-6. Active and allosteric site comparison between sulfate-bound wild-type and D12A LbPFK structures. (A) Active site and (B) allosteric site comparison between wild-type (pink) and D12A (blue) LbPFK. Highlighted are bound sulfates (black for D12A, grey for wild-type) with each residue labeled with the three-letter abbreviation and number. RMSD between the two structures equals 0.169.

comparing D12A to LbPFK there are not many changes that occur within the active site. R252, R171 and R162 are the only residues that show any change in position upon the D12A mutation, but even these changes are minor. There is also a slight change in the position of the sulfate within the active site but this could be due to the slight shift in the residues mentioned above. Comparison of the amino acids involved in the binding of MgATP, based on binding of MgADP to BsPFK, show no change between the two crystal structures (*84*). Lack of changes within the binding site indicates that the effects on both F6P and MgATP binding are not easily explained by changes within the structures of the active and allosteric sites of the enzyme.A comparison of the allosteric binding site between D12A and LbPFK was also performed and no major changes in the residues within the allosteric site were observed. This lack of change within the allosteric site in unlike what is seen in BsPFK upon mutation of D12A in which several residues change position in order to better interact with the allosteric ligand (*85*). Differences between LbPFK and BsPFK are most likely due to lack of conservation in the allosteric binding site.

In BsPFK, upon binding of the inhibitor-analog PG, the helix containing T156 and H160 unwinds (*84*). The unwinding of this helix causing T156 and H160 to move away from D12 causing any interactions between these residues to be broken. D12A would also break these interactions indicating that the enhanced PEP binding in BsPFK could be due partially to the unwinding of this helix. Figure 4-7 shows the regions surrounding residues 12 in both wild-type and D12A LbPFK. When comparing the two structures the helix containing T156 and H160 stays intact and the distances between

these residues and residue 12 do not change dramatically. Only the distance between residue 12 and R252 changes which could potentially affect the binding of F6P. Overall, the relative lack of structural changes could be the reason that D12A only exhibits a 9-fold change in PEP binding compared to the 100-fold effect seen in BsPFK (*85*).

Discussion

Allosteric regulation of bacterial PFK has been explained by several different models. One of the structural models indicates that a quaternary shift occurs along the active site interface upon binding of the inhibitor-analog PG (*84*). This quaternary shift is accompanied by several small secondary structural changes including the unwinding of a helix, which contains T156 and H160, along the active site interface across the interface from D12. In the allosteric binding site, a loop containing residues 211-215 moves in concurrence with the quaternary shift upon binding of PG. Allosteric inhibition by PEP was therefore thought to occur via this structural mechanism. More recent studies have shown that mutating D12 to an alanine enhances PEP binding 100-fold in BsPFK without changing the extent by which PEP inhibits (*85*). Structural studies of D12A BsPFK indicate that upon the D12A mutation, the helix which contains T156 and H160 unwinds in a similar fashion as what was seen upon binding of PG. These studies suggest that breaking the interactions between D12 and the residues across the active site interface are important for PEP binding to the allosteric site. LbPFK, unlike BsPFK and EcPFK, has very weak binding affinity for both the allosteric ligands PEP and MgADP. Overall the structure of LbPFK is similar to that of BsPFK and

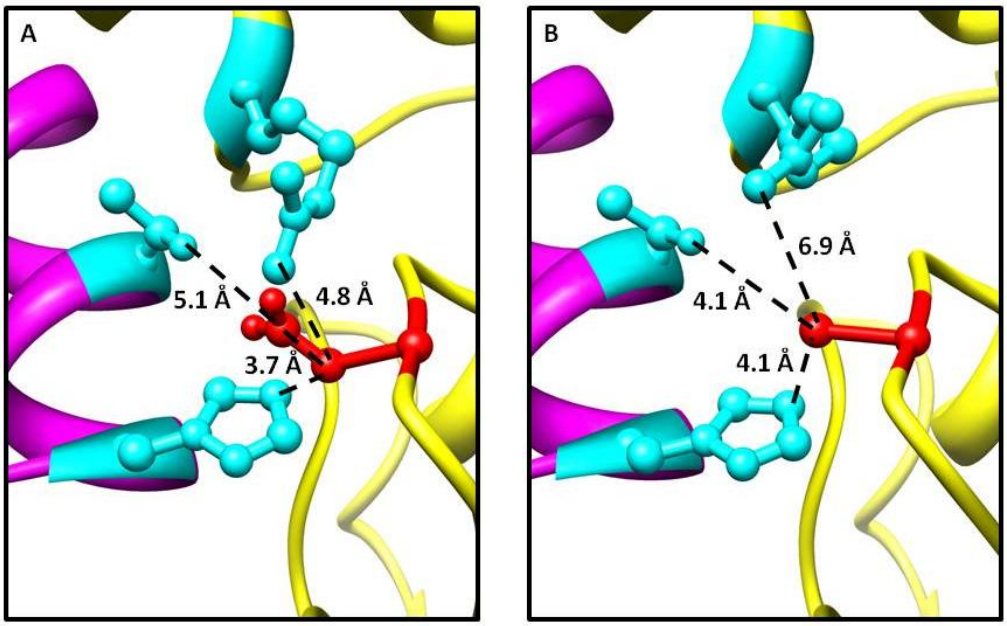

Figure 4-7. Comparison of distances between T156, H160 and R252 with residue 12 in wild-type and D12A LbPFK. Enhancement of active site interface between the pink and yellow monomers. Distances between T156, H160 and R252 and residue 12 were measured in (A) wild-type LbPFK and (B) D12A LbPFK structures. Highlighted are residues 12 (red), R252, T156 and H160 (cyan).

EcPFK with the exception of the allosteric binding site (*82-84*).

Since mutating D12 in BsPFK enhanced binding affinity for PEP, the same mutation was introduced into LbPFK. D12A LbPFK exhibited weaker binding for F6P with enhanced binding for MgATP to the active site as well as PEP and MgADP binding to the allosteric site. Since D12 interacts with R252, an active site residue which interacts with the phosphate of F6P, diminishing F6P binding upon introducing D12A is most likely due to the breaking of the interaction between D12 and R252. Breaking of this bound could reposition R252 to not interact with F6P as strongly and comparing the position of R252 in the structure of D12A LbPFK to wild-type LbPFK, it is clear that R252 does move away from the bound sulfate in the active site. This sulfate is bound where the phosphate of F6P would be bound so it serves as a point of comparison in the LbPFK structures. The effect of MgATP binding is harder to rationalize structurally since none of the residues which would interact with MgATP change position upon the introduction of D12A into LbPFK. Enhancement in MgATP binding could however be explained by the antagonistic relationship between F6P and MgATP binding. When one is diminished the other is enhanced.

In LbPFK, like BsPFK, D12A did enhance the binding of the allosteric inhibitor PEP though not to the same extent. D12A LbPFK only showed a 9-fold enhancement compared to the 100-fold enhancement seen in BsPFK (*85*). The smaller enhancement is likely related to the lack of structural changes in D12A LbPFK compared to LbPFK which are present when comparing D12A BsPFK to BsPFK. As mentioned earlier, D12A BsPFK causes a major shift to occur along the active site interface which is

accompanied by the unwinding to a helix that contains T156 and H160. In D12A LbPFK the helix containing T156 and H160 remains intact, and the distances between the residues and residue 12 do not change. It is therefore unlikely that the breaking of these interactions causes the enhanced binding of PEP to the allosteric site in LbPFK.

In order to further understand the role in the interactions between D12 and T156 and H160 across the active site interface, T156A and H160A were introduced into LbPFK. Both of these showed weaker F6P binding similar to D12A but did not show any enhancement in PEP binding. LbPFK contains an H at position 161 which could take the place of H160 in the event that it is missing, so H161A as well as H160A/H161A were introduced and neither mutant showed enhanced PEP binding compared to LbPFK. H161A did not affect F6P binding to the same extent as the other mutation and H160A/H161A had a similar binding affinity for F6P as that of H160A indicating that H160A plays the role in the decrease in F6P binding for the double mutant. These mutations further support the hypothesis that the breaking of interaction between D12 and T156 or H160 is not involved in the enhancement of PEP binding seen in D12A LbPFK.

The affinity of D12A LbPFK for the allosteric activator MgADP was also determined. As was the case for PEP, D12A showed an enhanced binding for MgADP compared to LbPFK as well as an inhibitory response. In EcPFK MgADP acts as an allosteric activator so it is interesting that MgADP appears to be acting as an allosteric inhibitor in both LbPFK as well as D12A LbPFK. One explanation could be that MgADP acts as a product inhibitor since MgADP is a product of the reaction. Product

inhibition by MgADP is unlikely since throughout the experiment MgATP is saturating at the active site, and since MgATP is also present at equal molar concentrations to MgADP competing with MgADP for binding at the active site. Therefore the inhibition of F6P binding resulting from MgADP binding to the allosteric site is most likely allosteric inhibition. Since there is no change in the position of the allosteric site residues upon mutating D12, it is harder to explain the enhanced binding for PEP and MgADP to this site as well as the inhibitory effect of MgADP.

The effects of D12A are also interesting given the distances between D12 and the four allosteric binding sites which are 15, 20, 33 and 41 Å in LbPFK. With the shortest distance being 15 Å, it is possible that there is a network of residues from D12 to the allosteric binding site in LbPFK that becomes interrupted with the introduction of D12A. In BsPFK, the link appears to involve a large structural change combined with smaller secondary changes in both regions. One residue that appears to link the two sites within the structures is T158 which interacts with the allosteric site residues H215 in the substrate-bound form of BsPFK but moves to interact with D12 in the PG-bound structure. For this reason, T158A was introduced into BsPFK but showed no enhancement in PEP binding as well as a decrease in the extent of inhibition by PEP (*85*). Due to these results and LbPFK having S158 as well as H215, it is unlikely that residue 158 plays as significant a role in LbPFK.

Another possible explanation for the weaker response of D12A in LbPFK compared to BsPFK is the lack of conservation within the allosteric binding site. Since the weak binding for PEP is likely due to the weak conservation of residues within the

allosteric binding site, combining changes there with D12A could potentially cause a more dramatic effect on PEP as well as MgADP binding. Therefore mutations must be made within the allosteric site to determine the potential role of these residues as well as combining these mutations with D12A in hopes of a better understanding of the overall weak binding for allosteric effectors to LbPFK.

CHAPTER V

SINGLE AND LONG CASSETTE MUTATIONS WITHIN THE ALLOSTERIC SITE OF LbPFK

Phosphofructokinase (PFK) catalyzes the first committed step in glycolysis performing a phosphoryl transfer from MgATP to fructose-6-phosphate (F6P) forming MgADP and fructose-1,6-bisphosphate. Structurally, PFK is a homo-tetramer organized as a dimer of dimers. It contains four active sites along one dimer-dimer interface with the allosteric sites along the other dimer-dimer interface. PFK from most bacterial sources is allosterically regulated by two ligands, the inhibitor phospho(enol)pyruvate (PEP) and the activator MgADP. In contrast, the PFK from *Lactobacillus delbrueckii* subspecies *bulgaricus* (LbPFK) exhibits weak binding affinity for the allosteric ligands, approximately 25 mM for PEP and MgADP, as well as inhibition at very high concentrations (*82*). These differences allow LbPFK to be used as a model for understanding the molecular basis for binding of PEP and MgADP as well their allosteric responses.

LbPFK shows high sequence identity to both EcPFK (47% identity with 66% similarity) and BsPFK (56% identity with 74% similarity) and has an overall conservation in structure (Figure 5-1). In 2005, the first structure of LbPFK was solved to 1.86 Å resolution with sulfate bound to all eight binding sites, four being the active sites and four being the allosteric sites (*82*). In EcPFK, several residues were identified to be important for MgADP binding at the allosteric site. These residues include D59,

Figure 5-1. Amino acid sequence alignment of LbPFK, TtPFK, BsPFK and EcPFK. Sequences were aligned using MacVector® 7.0. Highlighted in green are amino acid residues involved in binding to the allosteric site for MgADP in EcPFK and PG in BsPFK with the exception of 211. Highlighted in red are the single mutations made from the residues in LbPFK to the corresponding residue in TtPFK with the large cassette mutations in blue. The numbering of the amino acid residues in the figure is according to the EcPFK sequence but the numbering in the text is according to the LbPFK sequence.

E187 and R21, R25, R54, and R154 (*83*). BsPFK was crystallized with the inhibitor-analog phosphoglycolate (PG) and most of the residues involved in MgADP binding in EcPFK are also involved in PG binding with the addition of R211 and K213 (*84*). Residue 54 is a valine in BsPFK but is an arginine in EcPFK therefore R211 takes the place of the missing positive charge at position 54 in BsPFK.

The allosteric site of LbPFK is similar to EcPFK and BsPFK in that it contains D187, K213 and R21, R25 and R154 (Figure 5-1). However, LbPFK is different at positions 54 and 211, having a S at both positions as well as position 59 where an H replaces a D. Another major difference within the allosteric site of LbPFK compared to EcPFK and BsPFK is the residue at position 214. LbPFK has a D while EcPFK and BsPFK have lysines. In EcPFK, the mutation K214D exhibits diminished binding for MgADP and PEP as well as weaker allosteric responses in both cases (*84, 109*). R25, R211 and K213 were all mutated to glutamates in BsPFK and showed diminished binding for PEP and weakened allosteric inhibition (*73, 110*).

Schirmer and Evans in 1990 identified the involvement of residues 213-215 in the transition of BsPFK from the substrate-bound R-state to the inhibitor-bound T-state (*84*). In that study, the substrate-bound structure of BsPFK with F6P and MgADP bound to the active site as well as MgADP bound to the allosteric site was compared to the inhibitor bound structure with the PEP analog PG bound to the allosteric site (*84*). One of the main structural changes identified between these two structures is a “hinge movement” involving the loop containing residues 213-215 which pivots at residues 212 and 216. In the absence of ligand, the binding site is open but when either effector binds

the loop closes so that the ligand is packed tightly within the site. According to this model, the extent of the hinge movement is dependent on the size of the effector ligand with PG inducing a smaller change than MgADP. Another major change is the conformation of E187 that is coordinated to the Mg ion of MgADP in the substrate-bound BsPFK. Upon binding of PG, E187 is rotated 140° where the side-chain is no longer in contact with the ligand but is sandwiched between an α-helix and a β-sheet. It is possible that the differences in the residues found within these regions of the allosteric binding site of LbPFK inhibit these movements and interactions causing weaker binding affinity for both MgADP and PEP.

TtPFK, another allosterically regulated PFK, is similar in sequence to EcPFK (46% identity with 62% similarity), BsPFK (57% identity with 70% similarity) and LbPFK (46% identity with 60% similarity). It has the highest binding affinity for the allosteric inhibitor PEP of this group of PFKs, with a dissociation constant equal to 3 μM. This is 20-fold tighter than BsPFK and 9,000-fold tighter compared to LbPFK. No crystal structure is available for TtPFK, but a sequence comparison to BsPFK and EcPFK shows that it contains E187, K214 as well as the essential R21, R25, R154, and R211 in order to bind the allosteric ligands. TtPFK shows differences within the allosteric site residues compared to BsPFK and EcPFK with a R at position 55, a N at position 59 and a S at position 215. N59 would not form the interactions between the allosteric ligands and the D59 in EcPFK and BsPFK and the same would be true with S215 compared to H215. R55, which is an E in EcPFK and a G in BsPFK, introduces an extra positive charge in the allosteric binding site facilitating the binding of the

negatively charged MgADP and PEP in TtPFK. R55 when changed to an E, the corresponding residue in LbPFK, diminished the binding for PEP 500-fold compared to wild-type TtPFK (*78*). N59D and S215H were also introduced into TtPFK and both exhibited differences in PEP binding and allosteric inhibition, respectively (*78*).

In this chapter, amino acids in the allosteric site of LbPFK that were not conserved compared to the allosteric PFKs were mutated to the corresponding residues in TtPFK. These residues were changed alone and in combination and characterized for their ability to bind the inhibitor PEP. Single residue changes were made from LbPFK to TtPFK at positions 55, 59, 211, 214, 215 and 216 with no enhancement in PEP binding measured. A combination mutant was designed which included residues 211, 214 and 215, but this mutant was unstable and therefore could not be studied.

Another approach utilized in this study was to introduce long cassettes of mutations into LbPFK substituting the residues in LbPFK for the corresponding residues in TtPFK (Figure 5-1). Regions containing residues 206-218 (substitution 1, PFKs1) as well as 52-61 (substitution 2, PFKs2) were mutated as two single cassettes and mutated simultaneously to form a double cassette variant (PFKs1s2). The double cassette variant contains all the residues involved in binding for MgADP to EcPFK and PG to BsPFK (*83, 84, 111*). This is the first time this approach has been used for the study of PFK in the Reinhart lab.

In a previous study by Byrnes, et. al., a chimeric enzyme was created using BsPFK and EcPFK by fusing the first 122 amino acids of BsPFK with the remaining C-terminal residues of EcPFK (*112*). PEP did bind to this chimeric PFK but no allosteric

inhibition was measured, even though the allosteric binding site was exactly that of EcPFK. Byrnes, et. al. hypothesized that the lack of allosteric inhibition was due to the fact that the structural changes within BsPFK upon PG binding were absent in the chimeric enzyme. Single mutations of residues 55, 59, 211, 214, 215 and 216 as well as large cassette mutations PFKs1 and PFKs2 were introduced into the allosteric binding site with the goal of enhancing PEP binding. None of the single mutants along with the cassettes PFKs1 and PFKs2 enhanced binding for PEP when compared to wild-type LbPFK. However, PFKs1s2 exhibited a 9-fold enhancement in PEP with no change in the binding affinity for MgADP. The results of PFKs1s2 indicate a need for multiple mutations within the allosteric binding site to enhance binding for the inhibitor PEP.

Methods

Site-directed Mutagenesis

The protocol used for site-directed mutagenesis is explained in detail in Chapter II. The template strands for the single variants are shown in Figure 5-2.

RKS LbPFK, which combines the mutations S211R, D214K and G216S, was created by changing each amino acid in a sequential manner. Due to the fact that 211, 214 and 216 are in close proximity to one another, another set of oligos were needed to make sure the new mutation was introduced without disturbing the mutations already present within the gene. Figure 5-2 shows the template strands for the set of oligonucleotides to introduce the mutations D214K and G216S into pKK223-PFK

E55R: GAC ATT TTC CCA TTG GAA AGT CGT GAC GTA GCC CAC TTG ATC

H59N: GT GAA GAC GTA GCC AAC TTG ATC AAT GTT TCC GGT AC

S211R: G CAA GCC CAG GAA CGT GGC AAG GAC CAC GG

D214K: C CAG GAA AGC GGC AAG AAG CAC GGT TTG GTA GTT

H215S: G GAA AGC GGC AAG GAC AGC GGT TTG GTA GTT GTT G

G216S: GAA AGC GGC AAG GAC CAC AGC TTG GTA GTT GTT GC

D214K/G216S for S211R:

C CAG GAA CGT GGC AAG AAG CAC AGC TTG GTA GTT GTT GCT GAA G

PFKs1: GCC AAC CGG CTC GAG GCC TCC CAG AGG CGG GGG AAG AAG AGC TTCC ATC GTG GTT GTT GCT GAA G

PFKs2: GC GAC ATT TTC CCA TTG GGG GTG CGG GAC GTG GCC AAC ATC AAT GTT TTC CGG TAC C

Figure 5-2. Template strands used for site-directed mutagenesis to create the allosteric site mutations in LbPFK. For each LbPFK variant (bolded), the DNA sequence for the template strand is shown and was used along with the complementary strand to introduce the change in the DNA sequence. For E55R, H59N, S211R, D214K, H2215S, G216S and D214K/G216S for S211R, the codon(s) that was changed is underlined. For PFKs1 and PFKs2, the sequence underlined make up the template strand used to delete the sequence from LbPFK and the whole template strand shown above was used to introduce the new sequence from TtPFK into the plasmid containing LbPFK.

containing the S211R mutation.

For the long cassette mutations, two separate mutagenesis reactions were performed. The first one deleted the sequence of DNA from the LbPFK gene and the second introduced the corresponding sequence from TtPFK into the LbPFK gene. In the deletion reaction for PFKs1, an oligo was designed which contained 12 bases upstream of the sequence to be deleted along with 13 bases downstream that when combined formed an oligo 25 bases long. The 25 base oligo along with the complementary strand deleted the DNA sequence corresponding to residues 52-61 from the LbPFK gene. Deletion of PFKs2 involved an oligonucleotide that combined 14 bases upstream with 16 bases downstream of the deletion to form a 30 base oligonucleotide which when paired with the complementary strand deleted the DNA sequence corresponding to residues 206-218 from the LbPFK gene. Then for the insertion reaction, another oligo was designed which contained the DNA sequence to be inserted into the LbPFK gene between the bases which were upstream and downstream of the sequence that had been deleted. Shown below are the template strands for the insertion of the DNA sequence from TtPFK into the LbPFK gene with the underlined bases indicating the DNA sequence used to form the deletion appropriate deletion oligonucleotide. Along with the complementary strand, the oligonucleotides in figure 5-2 were used to create PFKs1 and PFKs2.

Protein Purification of Allosteric Site Mutants

The majority of the mutants, expressed in MRL277, were grown in similar conditions to those for LbPFK with the exception of PFKs1s2. This mutant was grown in LB broth with 0.1 g/mL ampicillin at 37 °C to an optical density of 0.6, cooled to 25 °C, induced with 0.5 mM IPTG and grown at 25 °C for 19 hours. The cells were then harvested and stored at -80 °C.

The majority of the mutants were purified under the same conditions as LbPFK with the exception of D214K, S211R, G216S, PFKs1 and PFKs2. Due to instability of the protein, D214K and S211R were purified in the presence of 1 mM F6P. In the case of G216S and PFKs2, a 0-2.5 M NaCl gradient was needed to elute the mutant proteins off the Mimetic Blue I column.

In the case of D214K, after the Mimetic Blue I column additional steps were needed to obtain a purified sample. After eluting the mutant PFK off the Mimetic Blue 1 column using a 0-1 M NaCl gradient in Buffer A-1 (Buffer A + 1 mM F6P), the fractions containing PFK were dialyzed against Buffer A-1 and then loaded onto a DE52 anion-exchange column, washed with at least 5 column volumes of Buffer A-1 and eluted with a 0-0.5 M NaCl gradient in Buffer A-1. Fractions containing the PFK were then pooled and dialyzed against Buffer A-1, pH 8.0. Finally the sample was loaded onto a MonoQ anion-exchange column at pH 8.0, washed with 2 column volumes of Buffer A-1 and eluted with a 0-1 M NaCl gradient in Buffer A-1. The fractions containing the mutant PFK were pooled and dialyzed into Buffer B-1 (Buffer B + 1 mM F6P), concentrated and stored at 4 °C.

In the case of S211R, after eluting the mutant PFK off the Mimetic Blue 1 column with a 0-1 M NaCl gradient, the pooled fractions were dialyzed into Buffer A-1 pH 8.0, loaded onto a MonoQ anion-exchange column, washed with 2 column volumes of Buffer A-1 and eluted with a 0-1 M NaCl gradient in Buffer A-1. The fractions containing the purified mutant PFK were pooled, dialyzed into Buffer B-1, concentrated and stored at 4 °C.

For PFKs1s2, the purification was performed at 4°C in the presence of 1 mM F6P. The crude lysate was applied to a 100 mL Mimetic Blue A column and washed with 1200 mL Buffer A-1. The majority of the protein eluted off the column after 600-1000 mL of wash buffer had been applied to the column. The fractions sample was adjusted to 8.5, and the sample was applied to a 20 mL pre-equilibrated High-Q anion exchange column. The column was washed with Buffer A-1, pH 8.5 and the protein was eluted with a 0-1M NaCl gradient. The fractions containing PFK activity were pooled, dialyzed into Buffer B-1 and stored at 4 °C. All experiments with this variant PFK were performed with the sample on ice.

Results

Allosteric Site Comparison of Bound PFKs

WT LbPFK has been shown previously to have weak binding affinity for the allosteric ligands PEP and MgADP (*82, 97*). A crystal structure of WT LbPFK was recently determined to 1.83 Å resolution with phosphate groups bound in the four active sites and four allosteric sites (see Chapter III). The determination of this structure has

allowed for structural comparison with other ligand bound allosteric PFKs, which demonstrate tighter affinities for both PEP and MgADP (*83, 84, 113, 114*). PFK is a tetramer which is organized as a dimer of dimers. The active sites lie along one dimer-dimer interface and the allosteric sites span the other dimer-dimer interface. The active sites and allosteric sites share amino acids from two separate monomers making it necessary for the tetramer to be intact for proper binding to both the active and allosteric sites. By overlaying the dimers which are formed along the allosteric site interface from phosphate-bound LbPFK, PEP-bound D12A BsPFK (which is similar in structure to the PG-bound structure of WT BsPFK) and MgADP-bound EcPFK (*83-85*), it is evident that the over-all secondary structure of the dimer is similar between the three (Figure 5-2A). There are slight shifts in some of the secondary structural elements in BsPFK compared to LbPFK or EcPFK, that occur along with the large quaternary shift proposed by Mosser and Reinhart to be involved in binding of PEP to the allosteric site (*85*).

A structural comparison between LbPFK, BsPFK and EcPFK indicates that LbPFK contains several residues which are different to the corresponding residues in BsPFK and EcPFK (Figure 5-3B-D). The conserved residues between the three PFKs compared include R21, R25, R154, K213 and H215. Residue 187 is slightly different with BsPFK and EcPFK having an E and LbPFK having a N. When MgADP is bound to the allosteric site of BsPFK, E187 is in a folded conformation and coordinates with the Mg ion. Once PG binds to the allosteric site, the χ_1 torsion angle rotates 140° causing the side-chain to face away from the ligand (*82*). When mutated to an alanine, E187 actually activates PEP in the presence of MgATP and MgADP has no effect on F6P

binding in EcPFK (*108, 111*). In LbPFK, D187 has a shorter side-chain making the coordination of the Mg ion weaker and therefore weakening the binding affinity for MgADP (*82*).

The major differences seen within the allosteric site include the loop containing residues 211-215 as well as the α-helix containing residues 54-55 that is located across the interface from 211-215. Residues 54 and 55 are not well conserved between the three PFKs with LbPFK having a S at 54 and an E at 55, BsPFK having a V at 54 and a G at 55, and EcPFK having an R at 54 and Y at 55. Y55 shows strong base-packing with the adenosine ring of MgADP in EcPFK and the absence of this interaction could potentially affect the ability of MgADP to bind as tightly in LbPFK. The other residue that is different between LbPFK and the two allosteric PFKs is the histidine at position 59. Both BsPFK and EcPFK have an aspartate at that position that forms a hydrogen bond with the ribose O_3 of ADP and the absence of this hydrogen bond would potentially weaken binding for MgADP (*82*).

Within the loop containing residues 211-215, there are some major differences in LbPFK. The number of positive residues decreases from 4, which is found in both EcPFK and BsPFK, to 2 in LbPFK. In BsPFK, the side-chain of K214 changes positions from pointing away from the allosteric ligand in the substrate-bound form to pointing towards PG in the inhibitor-bound form of BsPFK. K214 also interacts with PEP via a backbone hydrogen bond and any change in the position of the side-chain or interactions

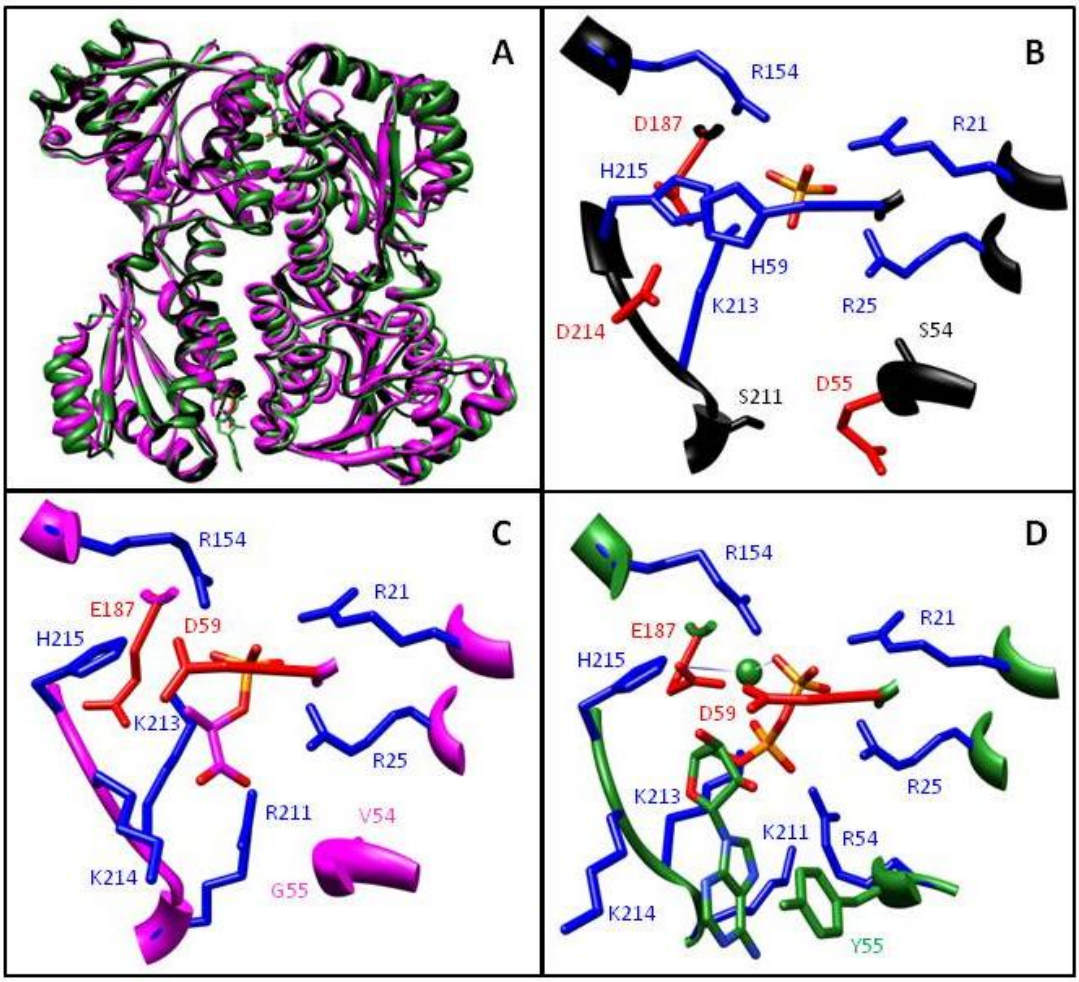

Figure 5-3. Structural comparison between phosphate-bound LbPFK, PEP-bound D12A BsPFK and MgADP-bound EcPFK. (A) Overlay of allosteric interface PFK dimer with phosphate-bound LbPFK in black, PEP-bound D12A BsPFK in pink and MgADP-bound EcPFK in green. Ligands are shown in both sites. Allosteric site with specific residues highlighted from (B) phosphate-bound LbPFK. (C) PEP-bound D12A BsPFK. (D) MgADP-bound EcPFK. Positively charged residues highlighted in blue and negatively charged residues highlighted in red.

between K214 and other residues could have an effect on this backbone interaction. In LbPFK there is an D at position 214 that is opposite in charge to a lysine and has a much shorter side-chain. Any interactions between K214 and other residues would not be present in LbPFK and the interactions between D214 and other residues would be much different. LbPFK is also missing a positive charge at position 211 which is present in both BsPFK and EcPFK. In BsPFK, R211 interacts with both PEP and MgADP and interacts with a water molecule in the absence of any ligand (*85*). A S at this position would interrupt any interaction with either ligand and would therefore have an effect on ligand binding.

Single Mutations within Allosteric Site

E55, H59, S211, D214, H215 and G216 were each changed to the corresponding residue in TtPFK forming the LbPFK mutants E55R, H59N, D214K, H215S and G216S. These modified PFKs were analyzed for their ability to bind F6P and PEP as well as their ability to exhibit allosteric inhibition. The kinetic parameters V_{max} and $K_{1/2}$ were determined for F6P binding for each mutant by fitting initial velocity data to equation 1 (Table 5-1). V_{max} values for almost all of the single mutants were close to that for the wild-type enzyme with the exception being G216S, which has a maximal activity of 1.3 U/mg. The effect of G216S on maximal activity is interesting since the residue is 17 Å from the active site, and the binding for F6P is similar to LbPFK. To compare the binding of F6P between the mutants and the wild-type enzymes, the free energy of binding ($\Delta G_a°$) was calculated using equation 2-5. Figure 5-4B shows that the binding

of F6P to the single allosteric site variants are similar to LbPFK and TtPFK, both approximately -6 kcal/mol, and the mutations do not greatly affect the binding of F6P to the active site. The binding for MgATP was also analyzed since TtPFK has a 58-fold tighter K_b (Michaelis constant) compared to LbPFK (*78*). For all the mutants analyzed, the dissociation constant for MgATP was not altered significantly compared to WT LbPFK (Table 5-1). From these data, it appears that the single mutations introduced in the allosteric binding site have no significant effect on ligand binding to the active site of LbPFK.

To examine the extent of binding and allosteric inhibition for the wild-type enzyme and single mutants, the $K_{1/2}$ for F6P was determined at various concentrations of PEP. Figure 5-4A shows the replot of the $K_{1/2}$ for F6P as a function of PEP, and fitting the data to either equation 2-3, in the case of TtPFK, or equation 2-4 for LbPFK and the LbPFK mutants, yields the dissociation constant for F6P (K_{ia}^0) and PEP (K_{iy}^0) in the absence of the other ligand. When saturation with PEP is evident, then the coupling constant (Q_{ay}) between F6P and PEP can be determined. Q_{ay} describes both the magnitude and the nature of the allosteric response (*88*). The weak binding affinity for PEP in WT LbPFK does not allow for the determination of Q_{ay}, and none of the single allosteric site mutations enhanced binding enough for that value to be determined. As with F6P, the $\Delta G°$ was determined for PEP binding ($\Delta G_y°$) so that a comparison could be made between the wild-type PFKs and the variants. $\Delta G_y°$ is quite different when comparing LbPFK to TtPFK with values of -2.2 ± 0.05 kcal/mol and -7.5 ± 0.02 kcal/mol respectively. The change in $\Delta G_y°$ corresponds to a 9,000-fold difference in

Table 5-1. Steady state kinetic parameters for wild-type and variant PFKs at 25°C, pH 8.0

PFK	S.A.[a] (U/mg)	K_b (mM)[b,c]	K_{ia}° (mM)	K_{iy}° (mM)	Q_{ay}[d]
WT LbPFK	240	0.34 ± 0.04	0.025 ± 0.0001	27 ± 2	N.A.
E55R	280	N.D.	0.043 ± 0.0007	33 ± 3	N.A.
H59N	250	N.D.	0.025 ± 0.0004	38 ± 2	N.A.
S211R	200	0.35 ± 0.02	0.050 ± 0.001	23 ± 1	N.A.
D214K	180	0.37 ± 0.02	0.063 ± 0.001	29 ± 2	N.A.
H215S	200	N.D.	0.029 ± 0.0005	37 ± 3	N.A.
G216S	1.3	0.29 ± 0.02	0.038 ± 0.001	21 ± 2	N.A.
PFKs1	260	0.15 ± 0.01	0.035 ± 0.0006	42 ± 3	N.A.
PFKs2	200	N.D.	0.042 ± 0.0008	32 ± 3	N.A.
PFKs1s2	240	0.27 ± 0.001	0.045 ± 0.001	2.7 ± 0.1	N.A.
WT TtPFK[e]	45	0.0059 ± 0.0005	0.027 ± 0.0006	0.003 ± 0.0001	0.068 ± 0.002

[a] S.A. = specific activity, [b] K_b for MgATP at [F6P] = 5 mM, [c] N.D. = not determined, [d] N.A. = not assessable, [e] (*78*)

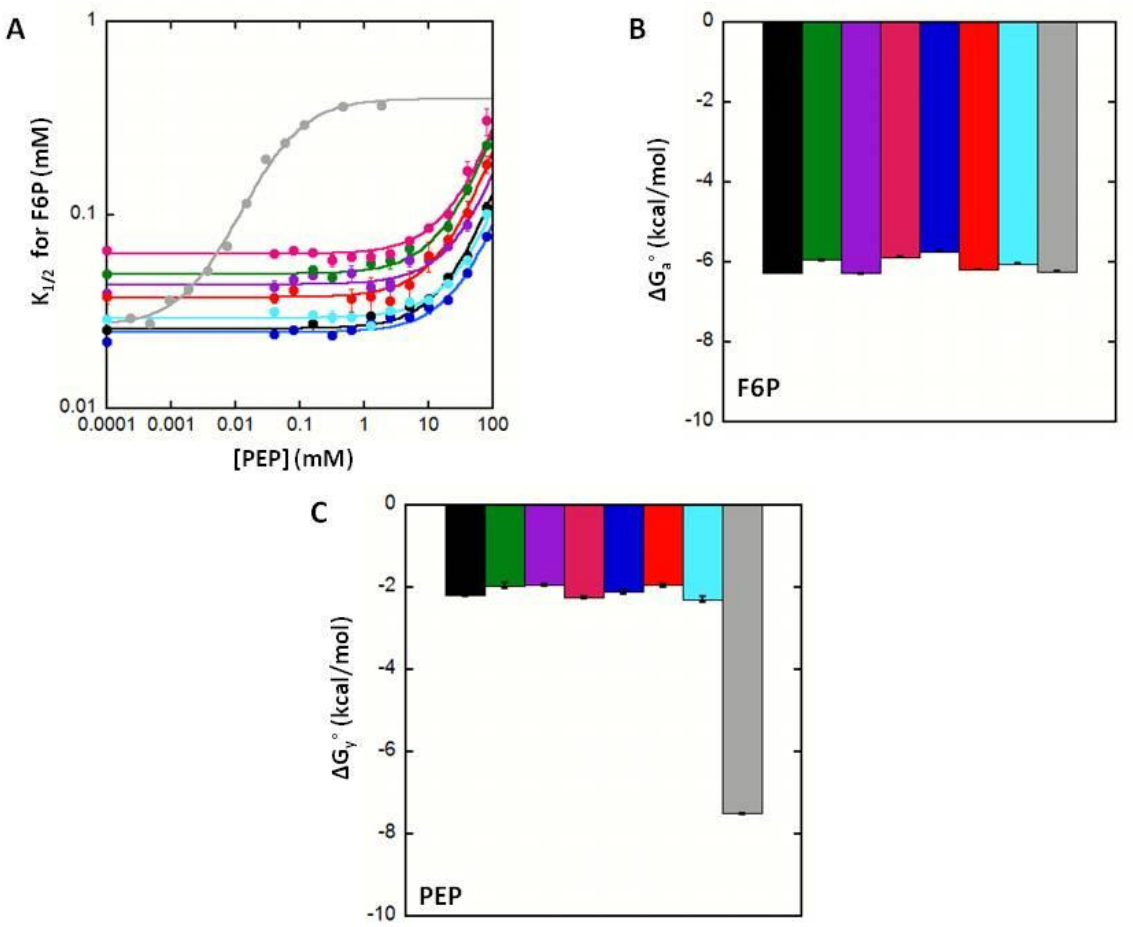

Figure 5-4. Effect of single variants on binding of F6P and PEP in LbPFK at 25°C, pH 8.0. The binding affinity ($K_{1/2}$) for F6P was measured as a function of the allosteric inhibitor PEP. (A) Replot of $K_{1/2}$ for F6P as a function of PEP with LbPFK (black), E55R (green), H59N (purple), S211R (pink), D214K (blue), H215S (red), G216S (cyan) and TtPFK (grey). Data for TtPFK was fit to equation 2-3 to determine the dissociation constant for F6P (K_{ia}^0) and PEP (K_{iy}^0). Since saturation could not be reached with PEP for LbPFK and LbPFK mutants, data were fit to equation 3. To compare the extent of ligand binding, the free energy of binding for (B) F6P ($\Delta G_a°$) and (C) PEP ($\Delta G_y°$) were calculated using equation 2-5. All experiments were performed at 25 °C at [MgATP] = 15 mM.

PEP binding. None of the single mutants enhanced binding affinity for PEP to the allosteric site when compared to WT LbPFK. Several actually had a negative effect on PEP binding with E55R and H59N having the weakest binding at 36 ± 4 mM and 38 ± 2 mM respectively. The mutations at 211, 214, 215 and 216, which are located across the dimer-dimer interface from 55 and 59, all showed similar PEP binding as LbPFK. These data indicated that a single mutation within the allosteric binding site is not sufficient to enhance PEP binding.

Large Allosteric Site Substitutions

Since no large change in PEP binding is seen with the single allosteric site mutations, combination mutations were designed in which several amino acid residues were changed simultaneously. Initially double, triple and even quadruple mutants were designed including various combinations of the residues mentioned above. However most of these mutations were unstable and therefore could not be analyzed (data not shown). In order to circumvent this problem, long cassettes of mutations had to be introduced. Two regions of the allosteric site were chosen, one including residues 55 and 59 and one including residues 211-216. Making these long cassette mutations would keep the secondary structure the same as in LbPFK and lead to improved protein stability. So, PFKs1 and PFKs2 were designed and substituted the residues included between 52-61 and 206-218 in LbPFK to the corresponding residues from TtPFK (Figure 5-1). The changes were easily introduced using the protocol from the Stratagene® Quik-Change Mutagenesis Kit. Only two reactions were needed, the first

of which deleted the DNA sequence from the parent plasmid and a second that replaced the deleted sequence with the new DNA sequence from the TtPFK gene. The two mutants were also combined to form PFKs1s2. These three mutants were analyzed to determine the binding affinity for both substates F6P and MgATP as well as the allosteric inhibitor PEP. PFKs1, PFKs2 and PFKs1s2 had binding constants for F6P ranging from 35 to 45 μuM (Table 5-1). These are approximately 1.5-fold weaker than LbPFK and TtPFK. The K_b (Michaelis constant) for MgATP was 1.6-fold tighter for PFKs1s2 and 3-fold tighter for PFKs1 when compared to LbPFK. The K_a was not determined for PFKs2.

These K_b values are closer to those of LbPFK than those of TtPFK suggesting that these residues are not indirectly involved in the binding of MgATP. The specific activities (S.A.) of the long cassette mutations were also more comparable to LbPFK than to TtPFK, ranging from 200 to 260 U/mg (Table 5-1). Similar substrate binding and S.A. for these mutations compared to LbPFK suggest that the amino acids changed within the allosteric binding site don't exhibit large effects at the active site.

These variants were analyzed for their ability to bind PEP to the allosteric site (Figure 5-5A). As with the single mutants, $\Delta G_a°$ and $\Delta G_y°$ were calculated and used to compare the mutants with both LbPFK and TtPFK. PFKs1 exhibited weaker PEP binding compared to WT LbPFK with a $\Delta G_y°$ value of -1.9 ± 0.04 kcal/mol compared to -2.2 ± 0.04 kcal/mol. The change in $\Delta G_y°$ corresponds to a 1.7-fold decrease in PEP binding. PFKs2 also exhibited a weakened PEP binding. However, when the two mutants were combined to form PFKs1s2, PEP binding was enhanced approximately 10-

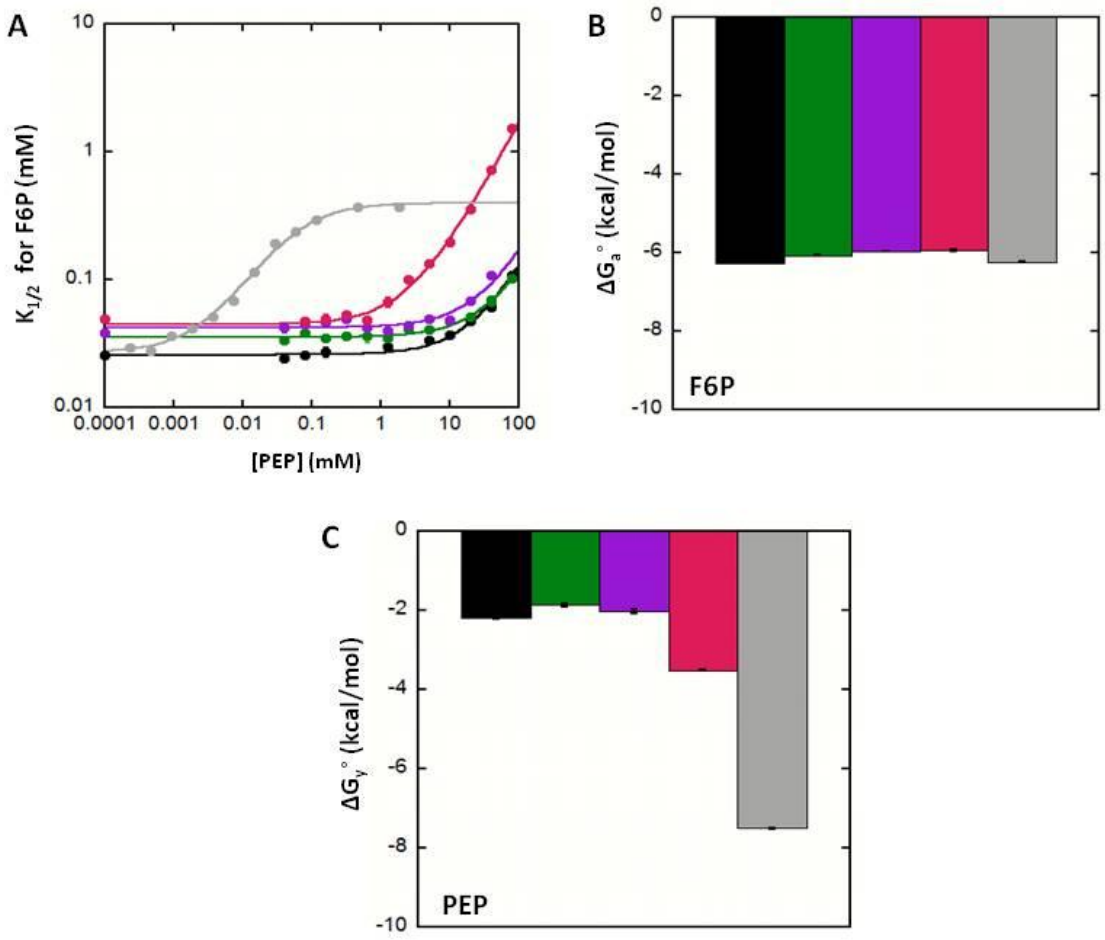

Figure 5-5. Effect of long cassette variants on binding of F6P and PEP in LbPFK at 25°C, pH 8.0. The binding affinity ($K_{1/2}$) for F6P was measured as a function of the allosteric inhibitor PEP. (A) Replot of $K_{1/2}$ for F6P as a function of PEP with LbPFK (black), PFKs1 (green), PFKs2 (purple), PFKs1s2 (pink) and TtPFK (grey). Data for TtPFK was fit to equation 2-3 to determine the dissociation constant for F6P (K_{ia}^0) and PEP (K_{iy}^0). Since saturation could not be reached with PEP for LbPFK and LbPFK variants, data were fit to equation 2-4. To compare the extent of ligand binding, the free energy of binding for (B) F6P ($\Delta G_a°$) and (C) PEP ($\Delta G_y°$) were calculated using equation 2-5. All experiments were performed at 25 °C at [MgATP] = 15 mM.

fold compared to WT LbPFK. This is the first modification introduced within the allosteric binding site to exhibit an increase in the binding affinity for the inhibitor PEP. $\Delta G_y°$ for PFKs1s2 was -3.5 ± 0.02 kcal/mol, a change of 1.3 kcal/mol relative to LbPFK. This $\Delta G_y°$ is still not as great as seen in TtPFK, whose -7.5 ± 0.02 kcal/mol is the greatest of the four bacterial PFKs studied in the Reinhart lab (*78*).

Another interesting characteristic seen with PFKs1s2 is the change in the Hill coefficient (n_H) for F6P upon the binding of PEP to the allosteric site. In LbPFK, the n_H for F6P does not change significantly with increasing concentration of the inhibitor PEP (Figure 5-6). The n_H for F6P also showed no change for the variants PFKs1 and PFKs2. However, in the case of PFKs1s2, as the concentration of PEP is increased the n_H for F6P also increases. In the absence of PEP the n_H is similar to that of LbPFK, around 1.2, but at the highest concentration of PEP, 80 mM, the n_H is close to 4. This dependence of n_H for F6P on the concentration of PEP is also seen in TtPFK and the pattern is similar to that seen with PFKs1s2 (Figure 5-6). The n_H starts out around 1.5 at low concentration of PEP and stops at a value of 2.6 at saturating concentration of PEP in TtPFK. The n_H begins increasing around the concentration of PEP which is equal to the $K_{iy}°$ in both TtPFK and PFKs1s2 and stops changing close to the saturating concentration of PEP. Any further increase in the n_H for PFKs1s2 is unlikely since any number above 4 would be greater than the number of binding sites for F6P in the tetramer. It is also unclear how the n_H would further change at PEP concentrations above 80mM since saturation of PEP could not be reached for PFKs1s2.

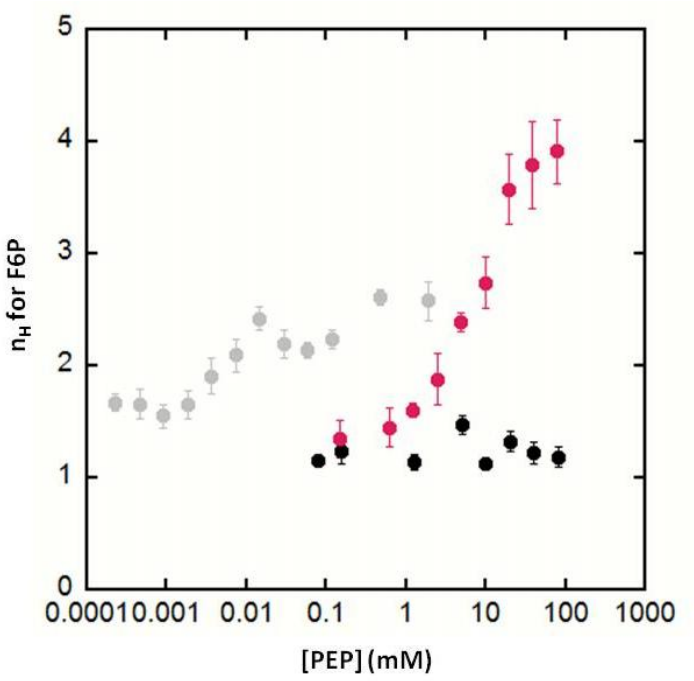

Figure 5-6. Hill coefficient for F6P as a function of PEP concentration at 25°C, pH 8.0. Titration curves for F6P were performed at various concentration of PEP and the data fit to equation 1 to determine the hill coefficient for F6P. A replot of the hill coefficient at each concentration of PEP is shown for LbPFK (black), PFKs1s2 (pink) and TtPFK (grey). All experiments were performed at 25°C, pH 8.0.

Due to the enhanced binding for PEP to the allosteric site of PFKs1s2, the binding affinity for the activator MgADP was also determined. The $K_{1/2}$ for F6P was measured at various concentrations of MgADP and no significant change was observed (data not shown). Therefore a competition experiment was performed in which the binding of PEP was determined at various concentrations of MgADP (Figure 5-7A). From this experiment, the K_{iy}^{app} was determined at each concentration of MgADP and then plotted as a function of concentration of MgADP (Figure 5-7B). From these data, it was determined that the binding affinity for MgADP to the allosteric binding site is 23 ± 3 mM, which is similar to 28 ± 8 mM, exhibited by LbPFK (*82*).

Discussion

The allosteric site of the non-allosteric LbPFK is the only part of the enzyme that is dramatically different when compared to the allosteric enzymes EcPFK, BsPFK and TtPFK. Several key residues identified by Evans to be involved in MgADP and PG binding to BsPFK are not conserved in LbPFK and lack of these residues may cause the allosteric ligands to bind less tight to LbPFK compared to EcPFK, BsPFK and TtPFK (*83, 84*). To test the involvement of these key residues, mutations were made within the allosteric binding site changing amino acid residues from those found in LbPFK to those of TtPFK, which exhibits the tightest binding affinity for PEP of the three allosteric PFKs, BsPFK, EcPFK and TtPFK (*78*). Upon changing the amino acid residues 55, 59, 211, 214, 215 and 216 alone, no change was seen in the binding affinity for PEP. There were also no significant changes in the binding of the substrates F6P and MgATP. This

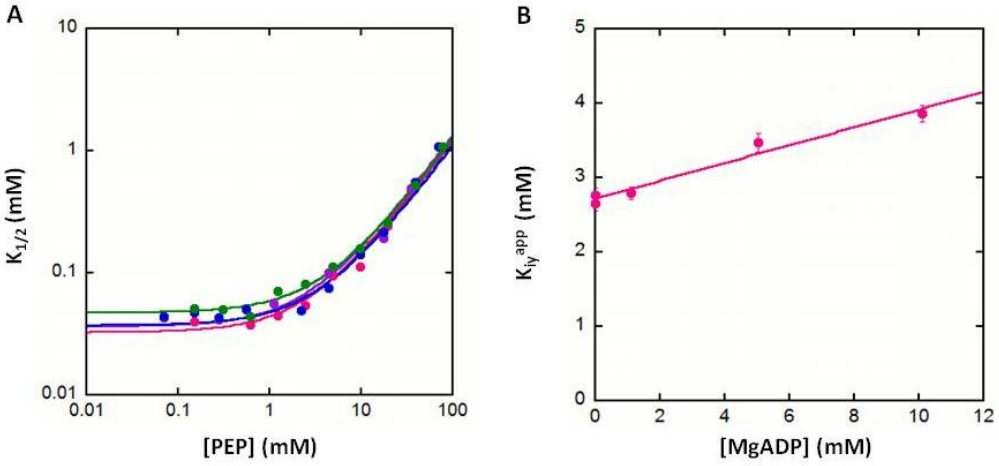

Figure 5-7. PEP/MgADP competition assay for PFKs1s2 at 25°C, pH 8.0. (A) The $K_{1/2}$ for F6P was measured as a function of PEP and the data were fit to equation 3-3 to determine the K_{iy}^{app} for PEP at each [MgADP]. This was performed and plotted from 0 to 10 mM MgADP with 0mM (pink), 1mM (purple), 5mM (blue) and 10mM (green). (B) The K_{iy}^{app} for PEP was plotted as a function of MgADP and fit to equation 2-6 to determine the K_{ix}^{app} for MgADP.

result indicates that more than one amino acid residue change is most likely needed to enhance binding for the inhibitor PEP to the allosteric site.

To test this hypothesis several residues were mutated at the same time. Several of these combination mutants were unstable and a new approach was utilized in which a stretch of amino acid residues was changed simultaneously from the sequence found in LbPFK to that found in TtPFK. The two areas chosen to study were residues 52-61 and 206-218. These sequences encompass the residues chosen in the single mutant study. The two single combination mutants PFKs1 and PFKs2 exhibited similar kinetic properties as LbPFK, most importantly with regard to binding of PEP to the allosteric site. There was an enhancement in the K_m for MgATP along with a weakening in F6P binding at the active site, which is approximately 17 Å away but these changes were very small when compared to LbPFK. The binding of MgATP to the active site of TtPFK is extremely tight compared to LbPFK and according to these results the amino acids within the allosteric site don't seem to be involved in this difference.

The two long cassette variants were combined to form PFKs1s2 which was the only mutant in this study to show any enhancement in PEP binding. The dissociation constant for PEP was decreased by approximately a factor of 10. Even with this enhancement in PEP binding saturation with PEP could not be reached and a coupling constant could not be determined. Not reaching saturation with PEP indicates that the coupling between F6P and PEP is stronger than what is seen in TtPFK. TtPFK has a Q_{ay} of 0.068 ± 0.02, which is the weakest PEP inhibition exhibited by TtPFK, BsPFK or EcPFK (*78*). If the coupling in LbPFK is the same as that seen in TtPFK and based on

the definition of Q_{ay}, the concentration of PEP required to reach maximum saturation would be approximately 40 mM(*74*). In these experiments the highest concentration of PEP used was 80 mM and it is therefore likely that PEP is a better inhibitor in PFKs1s2 than in TtPFK. The enhanced PEP binding in PFKs1s2 also suggests that both sides of the allosteric site must be changed in order for significant PEP binding to occur. These mutations also introduce several positive charges which would be expected to help the negatively charged PEP bind tighter within the allosteric binding site.

From structural studies of BsPFK one of the regions that has been proposed to change position upon the binding of the inhibitor analog PG is a loop which contains residues 213-215 (*84*). In the allosteric BsPFK and EcPFK, all three of these residues are positively charged but one of these charges is missing in LbPFK which may prevent this structural change from occurring. TtPFK contains only two positive charges since residues 215 is a serine. Across the interface are residues 55 and 59 which are also quite different in LbPFK compared to the allosteric PFKs. The role of 55 is not clear since this residues is not well conserved between the four PFKs but 59 are interesting because LbPFK is the only PFK of the four which has a positively charged H in place of either a D or N. In BsPFK, 59 and 215 are close enough to form a potential hydrogen bond when PG is bound, and this would not be possible in LbPFK since both of these residues are histidines. This hydrogen is also not present in TtPFK since there is a N at position 59 and a S at position 215. Since TtPFK has tighter PEP binding than BsPFK, the hydrogen bond may not be involved in PEP binding, but there is evidence that it may be involved in allosteric inhibition (*78*). These two regions are changed in the mutant

PFKs1s2 and having both sides of the allosteric site mutated at the same time might allow for any potential interactions across the interface to remain intact to allow for optimal PEP binding.

Another interesting characteristic of PFKs1s2 that is not seen in LbPFK is the change in n_H as a function of PEP concentration. This phenomenon is called heterotropically induced homotropic cooperativity and occurs when the binding of the effector causes a change in the magnitude of the coupling between the active sites (*88*). The change in the n_H caused by effector binding is best explained using a dimer as an example. Consider a dimer of monomers, each containing one active site and one allosteric site, which allow for both intrasubunit and intersubunit heterotropic couplings (Q_{ay1} and Q_{ay2}). There are also three homotropic couplings to consider; Q_{aa}, $Q_{aa/y}$ and $Q_{aa/yy}$ which occur in the absence of effector, when one allosteric site is occupied or when two allosteric sites are occupied, respectively. The values of any and all of these couplings can determine the effect the heterotropic ligand has on the homotropic coupling (*88*).

In BsPFK, the change in n_H is described as sub-saturating heterotropically induced homotropic cooperativity. In this case, the effect of the allosteric ligand on the cooperativity of the substrate is close to unity when Y = 0 and when Y is saturating and reaches a maximum value at sub-saturating concentrations of Y (*88*). The maximum number for n_H reached is dependent on the magnitude of the heterotropic coupling so that the stronger the coupling, the greater the change in n_H. Sub-saturating heterotropically induced homotropic cooperativity is not seen with TtPFK where n_H

starts out around 1.5 and then begins to increase once PEP binds reaching a maximum value of 2.5 at saturating concentrations of Y (*78*). In this case, the effect on n_H at 0 and saturating PEP are not equal. The effect on n_H by PEP seen in PFKs1s2 could potentially be explained by either mechanism but since saturation with PEP cannot be reached, the actual mechanism is hard to determine. It is clear that the effect of PEP on F6P binding is stronger in PFKs1s2 than in TtPFK in Figure 4-3. Since the allosteric sites are very similar between the mutant and TtPFK these differences may arise from differences found in other regions of the enzyme.

Even though there was an enhancement in the binding affinity for PEP to the allosteric site of PFKs1s2, the same was not true for the activator MgADP. PFKs1s2 binds PEP 8.5-fold tighter than MgADP, which binds with the same affinity as LbPFK (*82*). This difference in binding most likely is due to the lack of the residues needed to properly bind MgADP. In EcPFK, MgADP interacts with several residues including E187, D59, and R21, R25, R54 and R154 (*83*). Of these residues the only one which was modified was 59, which in LbPFK is an H and in PFKs1s2 was changed to a N. In the case of the other residues, PFKs1s2 contains R21, R25 and R154, a V at 54 and a D at 187. The shorter side-chain of aspartate might weaken the interaction between 187 and the Mg ion of MgADP. Therefore, it might be necessary to introduce D187E along with the other residues to enhance MgADP binding to the allosteric site of LbPFK.

Another possible reason for weak binding of MgADP are the differences at positions 59 and 154. In PFKs1s2 there is a N at 59 rather than the aD that is present in EcPFK and BsPFK. The D hydrogen bond with the –OH of the adenosine ring of

MgADP. A N could not form this potential interaction as it would be unable to accept the hydrogen from the oxygen. In EcPFK, R154 forms two potential hydrogen bonds with the β-phosphate of MgADP and these hydrogen bonds would not be present PFKs1s2 due to the V at position 154. However, there is a V at position 54 in BsPFK and MgADP still binds to the allosteric site even without these interactions. Instead, R211 takes the place of V154 in the interactions with MgADP, and PFKs1s2 contains an R211 which could potentially take the place of R154 as is seen in BsPFK (*83*). Not changing these residues in combination with those already mutated in PFKs1s2 might explain the differences seen between binding affinities of PEP and MgADP to the allosteric site.

In conclusion, the multiple amino acid differences within the allosteric binding site of LbPFK and the absence of many positively charged residues are likely involved in the weak binding affinity of the allosteric inhibitor PEP. This is further evident when these residues are mutated simultaneously from the residues in LbPFK to those in TtPFK, which has the tightest PEP binding compared to other allosteric bacterial PFKs studied. Modifying residues 55, 59, 211, 213, 214, 215 and 216 enhanced PEP binding but in order to fully understand how these residues enhanced PEP binding a crystal structure of PFKs1s2 must be solved.

CHAPTER VI

INTRODUCING ALLOSTERIC INHIBITION IN LbPFK BY COMBINING MUTATIONS FROM REMOTE REGIONS

In most bacteria, phosphofructokinase (PFK) is an allosterically regulated enzyme which binds the inhibitor phospho(enol)pyruvate (PEP) and the activator MgADP. However in the bacterium *Lactobacillus delbrueckii* subspecies *bulgaricus*, PFK (LbPFK) exhibits weak binding affinity for both PEP and MgADP and therefore presumably will not be allosterically regulated by these ligands in the cell (*82*). PFK catalyzes the first committed step in glycolysis transferring a phosphoryl group from MgATP to fructose-6-phosphate (F6P) forming fructose-1,6-bisphosphate (FBP) and MgADP. Bacterial PFKs are structured as homotetramers that contain four active sites and four allosteric sites. These sites are located along the dimer-dimer interfaces with the active sites along one dimer-dimer interface and the allosteric sites along the other dimer-dimer interface. For those PFKs that respond, binding of either PEP or MgADP to the allosteric binding site will cause a change in the binding affinity for the substrate F6P at the active site with no change in the catalytic rate, so PEP and MgADP are considered K-type allosteric effectors.

LbPFK shows high sequence identity to three known allosterically regulated PFKs, those from *E. coli* (EcPFK), *Bacillus stearothermophilus* (BsPFK) and *Thermus thermophilus* (TtPFK). LbPFK shows 56% identity to BsPFK, 47% identity to EcPFK and 46% identity to TtPFK. In 2005, the first crystal structure of LbPFK was solved to

1.86 Å resolution and a structural comparison between LbPFK and known structures from EcPFK and BsPFK was performed. This comparison indicates an overall conservation in secondary, tertiary and quaternary structure (*82-84, 94, 95*). The allosteric site residues are not well conserved compared to the other allosterically regulated PFK. The lack of conservation within the allosteric binding site was considered to be a reason for the weak binding for both PEP and MgADP to LbPFK.

Of the three allosterically regulated PFKs, TtPFK exhibits the tightest binding to the inhibitor PEP with a $K_{iy}°$ equal to 3μM (*78*). LbPFK binds PEP 9,000-fold tighter than TtPFK ($K_{iy}°$ = 27mM). For this reason, residues within the allosteric site of LbPFK were changed to the corresponding residues in TtPFK. Since no crystal structure of TtPFK has been solved, BsPFK was used in structure comparisons to identify which residues to target for mutagenesis studies. Residues 55, 59, 211, 214, and 215 were targeted based on the lack on conservation as well as proximity to the allosteric binding site. Several of these residues have also been identified in the literature as being involved in the binding of either PEP or MgADP to the allosteric binding site (*84, 85, 111*). Both individual mutations as well as long cassette mutations were created that contained the stretches of residues 52-61(PFKs1) and 206-218 (PFKs2). It was only when the two large cassette mutations were combined to form PFKs1s2 that PEP binding was enhanced 10-fold compared to LbPFK. The binding of MgADP to PFKs1s2 exhibited no change from wild-type ($K_{ix}°$ = 24mM) which indicates that more mutations within the allosteric site are needed for MgADP to bind to LbPFK with higher affinity.

Another region that has been identified to be important in PEP binding to BsPFK is along the active site interface and involves the 100% conserved residue D12 (*73, 85*). D12 is located 15 Å away from the closest allosteric site, and changing D12 to an alanine (D12A) enhances PEP binding to BsPFK 100-fold compared to wild-type. D12A was also introduced in LbPFK and enhanced binding for PEP 9-fold compared to WT LbPFK (see Chapter IV). In BsPFK the effect of D12A has been correlated to structural changes within PFK upon this mutation that involve both a 7° quaternary shift as well as the unwinding of a helix located along the active site interface across from D12 (*85*). D12A LbPFK was crystallized to 2.4 Å resolution and comparisons to the structure of wild-type LbPFK indicate no major changes between the two structures. Lack of the structural changes upon the D12A mutation in LbPFK compared to those seen in D12A BsPFK may indicate why there is only a 9-fold change in PEP binding compared to the 100-fold seen in BsPFK.

D12A LbPFK exhibited not only enhanced binding of PEP to the allosteric site but enhanced binding of the activator MgADP as well. MgADP binds weakly to LbPFK and causes inhibition as high concentration (≥ 5mM) compared to the activation seen in EcPFK. In D12A LbPFK, MgADP binding is enhanced 9-fold and still appears to act as an inhibitor. The MgADP inhibition might be due to dead end product inhibition since MgADP is a product of the reaction, but since MgATP is saturating throughout the experiment this mechanism is highly unlikely. Therefore, MgADP appears to be acting as an allosteric inhibitor of LbPFK, and this inhibition is more evident in D12A LbPFK due to the enhanced binding for MgADP at the allosteric site.

The lack of conservation within the allosteric site may be a reason for the smaller enhancement in binding of the allosteric ligands exhibited by D12A LbPFK compared to BsPFK. Therefore the large cassette mutations encompassing the allosteric site were combined with D12A in LbPFK in an attempt to further enhance the binding for the allosteric ligands. The combination mutant (PFKs1s2D12A) binds PEP with a dissociation constant equal to 1.3 mM, which is 21-fold tighter than LbPFK. Moreover MgADP exhibits a $K_{ix}°$ equal to 3.4 mM, an 8-fold enhancement compared to LbPFK. PEP binding to PFKs1s2D12A appears to show a nearly additive effect between the two regions since PFKs1s2 exhibits a 10-fold effect and D12A a 9-fold effect. Binding for MgADP seems to be due to the mutation D12A since no further enhancement was measured upon combining the two regions. Therefore, other residues in the allosteric site need to be changed in order for further enhancement in MgADP binding to be observed.

Along with the enhancement in PEP binding in PFKs1s2D12A, allosteric inhibition was quantified for the first time in a variant of LbPFK. A coupling constant (Q_{ay}) equal to 0.007 ± 0.0008 was measured for PFKs1s2D12A, and this value is 2-fold less than that seen in EcPFK (Q_{ay} = 0.016 ± 0.003), 7-fold greater than that in BsPFK (Q_{ay} = 0.001 ± 0.0001) and 9-fold less than that seen in TtPFK (Q_{ay} = 0.068 ± 0.002) (*72, 78, 81*). Therefore, it is evident that through mutations within two distinct and remote regions of LbPFK, binding for the allosteric ligands PEP and MgADP has been enhanced allowing the nature and magnitude of the allosteric inhibition to be quantified for the first time in a variant of LbPFK.

Methods

Site-directed Mutagenesis

The strategy employed for site-directed mutagenesis is similar to that discussed in Chapter II. PFKs1s2D12A was created by using pKK223-3/PFK containing the mutation PFKs1s2 as the parent plasmid and introducing D12A using the oligonucleotide pair presented in Chapter IV.

Purification of Tt/Lb 2 + D12A

PFKs1s2D12A was purified using the protocol for D12A LbPFK with the following exceptions. After pooling fractions with PFK activity off the 100 mL Mimetic-Blue A column, the sample was concentrated to 20 mL with PEG (polyethyleneglycol), dialyzed into Buffer A-1 (20mM Tris-HCl, pH 8.5, 0.1mM EDTA, 1mM F6P) and loaded onto a 20 mL anion-exchange HighQ column at 1mL/min, 4°C. A 0-1mM NaCl gradient was applied to the HighQ column and 1 mL fractions were collected. The fractions containing PFK activity were pooled, dialyzed into Buffer A-1 + 5mM $MgCl_2$ and stored at 4°C. Protein purity was assessed using SDS-Page, and the concentration was determined using the BCA protein assay.

Results

Two distinct regions of LbPFK were targeted for mutagenesis in order to enhance binding for the allosteric inhibitor PEP in LbPFK, the allosteric binding site and the active site interface region surrounding D12A. Within the allosteric binding site, two

large cassettes of mutations were created that contain residues 52-61 and 206-218 and these stretches of residues are located across the interface from one another and make up the allosteric site along with several conserved arginines. Due to the tight binding affinity for PEP to TtPFK, these cassettes of residues were mutated from the residues in LbPFK to the corresponding residues in TtPFK. In LbPFK, 52-61 contains the residues 52-L E S E D V A H L I -61 and was mutated to the residues in TtPFK 52-L G V R D V G N I I -61 to create PFKs1. LbPFK 206-218 contains the residues 206- K Q A Q E S G K D H G L V -218 and was mutated to the TtPFK sequence 206- E A S Q R R G K K S S I V-218 to create PFKs2. When these two cassettes were combined to form PFKs1s2 binding for PEP to the allosteric site was enhanced 10-fold compared to WT LbPFK (Figure 6-3, Table 6-1). However, these mutations had no effect on MgADP binding to the allosteric site. A complete examination for PFKs1s2 is found in Chapter V.

D12A was also introduced into LbPFK and enhanced binding for both PEP and MgADP 9-fold compared to LbPFK. D12 is located along the active site interface, 15 Å from the nearest allosteric binding site yet effects binding to that site from this distance (Figure 6-1). Due to the effects of both D12A and PFKs1s2, the two mutations were combined to form PFKs1s2D12A, and the binding affinities for both the substrates as well as the allosteric ligands were determined. Figure 6-2 shows the titration curves for the substrates F6P and MgATP for PFKs1s2D12A compared to LbPFK as well as PFKs1s2 and D12A. Due to the dramatic differences in specific activity for these mutants, the rates were normalized to the specific activity given in Table 6-1. PFKs1s2D12A has weaker F6P binding but a lower K_b for MgATP binding compared to

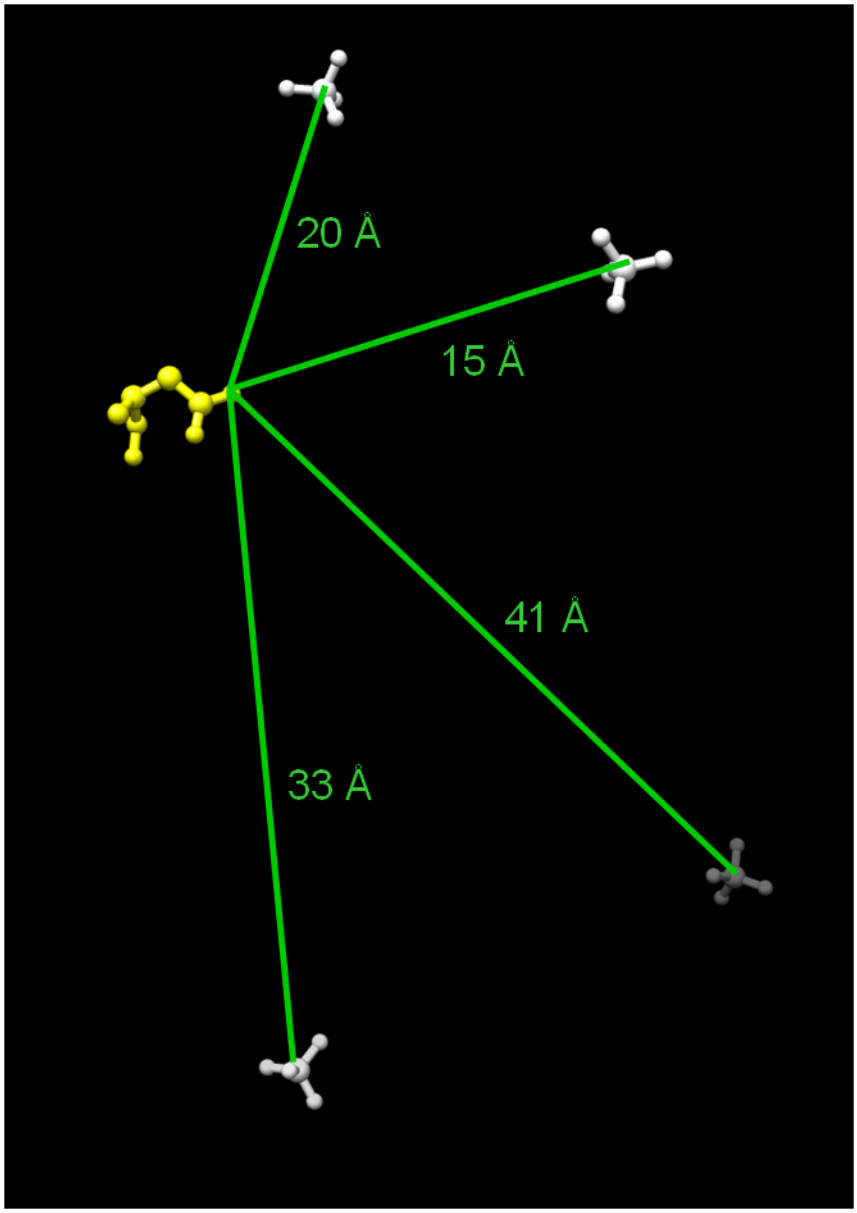

Figure 6-1. Distances between D12 and allosteric site phosphates in LbPFK crystal structure. In the crystal structure for LbPFK, the distances between D12 (yellow) and each of the four phosphates bound to the four allosteric binding sites (white) were measured using UCSF-Chimera®. Each distance is highlighted in green with the distance given in Å.

both wild-type and PFKs1s2, with similar binding affinities as D12A. Therefore the changes in the binding affinities for F6P and MgATP for PFKs1s2D12A are due more to the D12A mutation than to the allosteric site mutations.

To determine the binding affinity for the allosteric ligands, the $K_{1/2}$ for F6P was measured at various concentrations of PEP or MgADP and then plotted as a function of the allosteric ligand concentration (Figure 6-3). PEP binds to PFKs1s2D12A with an affinity of 1.3 mM and MgADP with an affinity of 3.4 mM. Compared to LbPFK, the binding to PFKs1s2D12A is 21-fold tighter for PEP and 8-fold tighter for MgADP. The 21-fold effect on PEP binding exhibited by PFKs1s2D12A is nearly additive given the 10-fold effect of PFKs1s2 and the 9-fold effect of D12A. Enhancing PEP binding 21-fold allowed for a coupling constant, Q_{ay}, to be determined for PEP inhibition (Q_{ay} = 0.007 ± 0.0008). Q_{ay} for PFKs1s2D12A is 2-fold stronger than that of EcPFK (Qay = 0.016 ± 0.003) (*72*). MgADP binding to PFKs1s2D12A is similar to D12A but tighter than both wild-type and PFKs1s2 so the effect on MgADP binding is due to the D12A mutation. MgADP is also an inhibitor of all three variants as well as wild-type, which is opposite the effect seen in other PFKs such as EcPFK and TtPFK (*78, 80*).

Since MgADP is a product of the PFK reaction and to ensure that the binding for MgADP determined from the coupling experiments is to the allosteric site and not to the active site, a competition experiment was performed where the apparent binding affinity for PEP (K_{iy}^{app}) was determined at various concentrations of MgADP. MgATP was at a saturating concentration throughout these experiments as well as phosphocreatine and

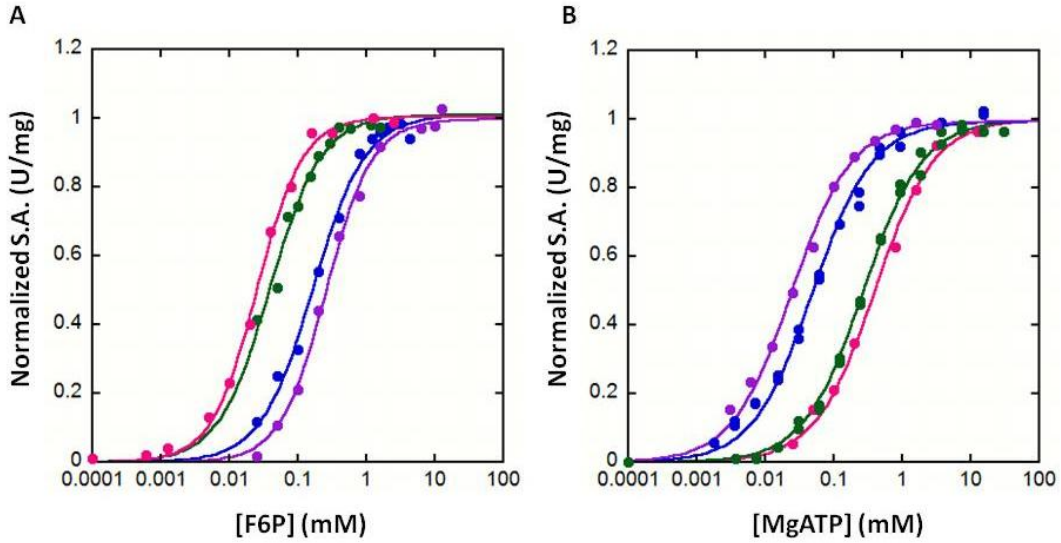

Figure 6-2. Substrate titration curves for wild-type LbPFK vs. LbPFK variants at 25°C, pH 8.0. (A) F6P titration curves for LbPFK (pink), PFKs1s2 (green), D12A (blue) and PFKs1s2D12A (purple). Experiment was performed at [MgATP] = 15 mM for LbPFK, 10mM for PFKs1s2 and 3mM for both D12A and PFKs1s2D12A. All data were fit to equation 2-1. (B) MgATP titration curves for LbPFK (pink), PFKs1s2 (green), D12A (blue) and PFKs1s2D12A (purple). Experiment was performed at [F6P] = 3mM for LbPFK and PFKs1s2 and 5mM for D12A and PFKs1s2D12A. All data were fit to equation 2-2. In both experiments, the specific activity was normalized for each PFK to the appropriate V_{max} from Table 5-2.

Table 6-1. Steady state kinetic paremeters for wild-type and LbPFK variants at 25°C, pH 8.0 .

LbPFK	S.A. (U/mg)[a]	K_b (mM)[b]	$K_{ia}°$ (mM)[c]	$K_{iy}°$ (mM)[c]	$K_{ix}°$ (mM)[c,d]	Q_{ay}[c]
WT	250	0.34 ± 0.4	0.025 ± 0.0001	27 ± 2	28 ± 8	N.A.
PFKs1s2	240	0.27 ± 0.01	0.039 ± 0.003	2.8 ± 0.1	32 ± 6	N.A.
D12A	30	0.049 ± 0.003	0.17 ± 0.02	3.0 ± 0.1	2.6 ± 0.2	N.A.
PFKs1s2D12A	12	0.025 ± 0.002	0.26 ± 0.02	1.3 ± 0.05	3.4 ± 0.2	0.007 ± 0.0008

[a] S.A.= Specific activity. [b] K_b for MgATP was determined at [F6P] = 3mM for WT LbPFK and Tt/Lb 2 and 5mM for D12A and Tt/Lb 2 + D12A. [c] Values were determined at [MgATP] = 15mM for WT LbPFK, 10mM for Tt/Lb 2 and 3mM for D12A and Tt/Lb 2 + D12A. [d] $K_{ix}°$ for LbPFK from (*82*).

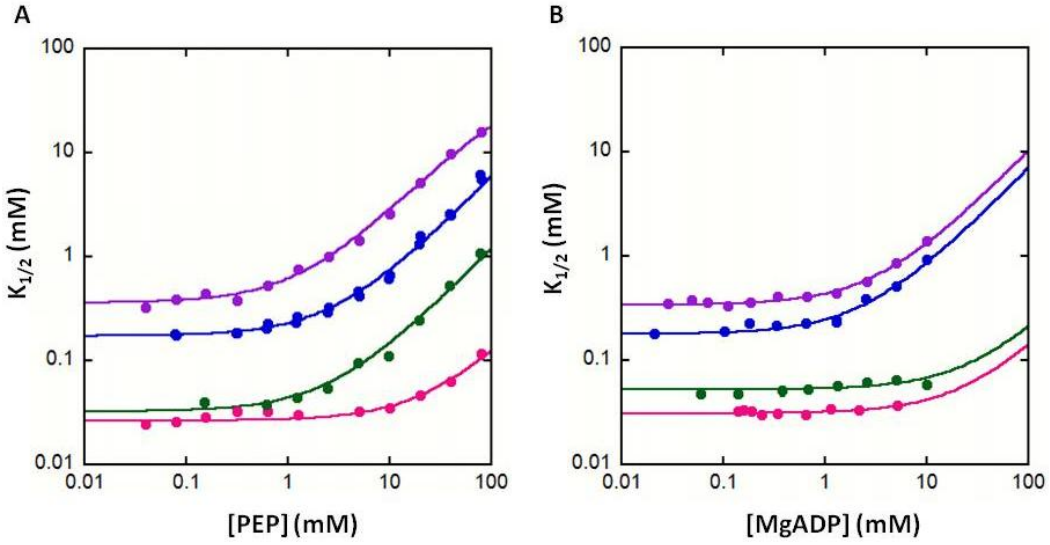

Figure 6-3. Binding and allosteric response of PEP and MgADP for wild-type and LbPFK variants at 25°C, pH 8.0. The $K_{1/2}$ for F6P was measured at various concentrations of (A) PEP or (B) MgADP for LbPFK (pink), PFKs1s2 (green), D12A (blue) and PFKs1s2D12A (purple). Each measurement was determined at [MgATP] = 15 mM for LbPFK, 10mM for PFKs1s2 and 3mM for D12A and PFKs1s2D12A. All data were fit to equation 2-4 except for PFKs1s2D12A PEP binding was fit to equation 2-3 to determine values given in Table 6-1 and 6-2. MgADP data for LbPFK from (*82*).

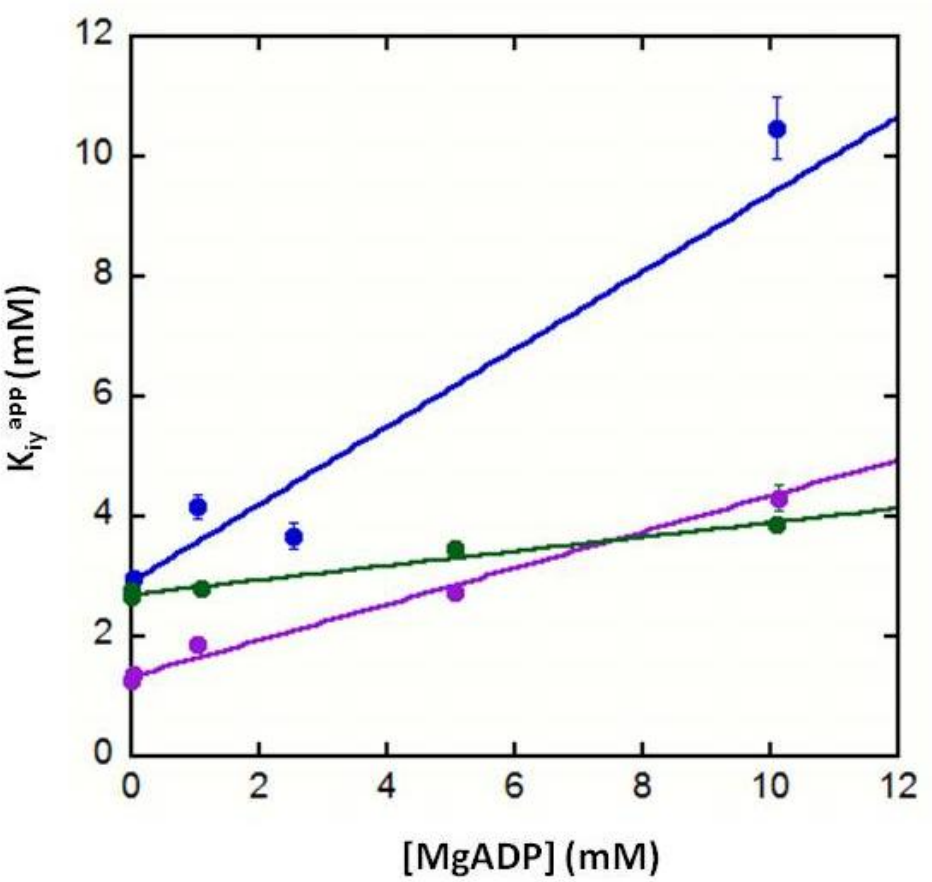

Figure 6-4. PEP/MgADP competition assay for LbPFK variants at 25 °C, pH 8.0. The $K_{1/2}$ for F6P was measured as a function of PEP and the data were fit to equation 2-3 (PFKs1s2 and D12A) or 2-4 (PFKs1s2D12A) to determine the $K_{i,app}$ for PEP at each [MgADP] for PFKs1s2 (green), D12A (blue) and PFKs1s2D12A (purple). The apparent K_i for PEP (K_{iy}^{app}) was plotted as a function of MgADP and fit to equation 2-6 to determine the apparent K_i for MgADP (K_{ix}^{app}) to give values in Table 6-2.

Table 6-2. Determination of K_i for MgADP and PEP for wild-type and LbPFK variants at 25°C, pH 8.0

LbPFK	$K_{ix}°$ (mM)[a,b,c]	K_{ix}^{app} (mM)[b,d,e]	$K_{iy}°$ (mM)[b,c]	K_{iy}^{app} (mM)[b,d,e]
WT	28 ± 8	N.D.	27 ± 2	N.D.
PFKs1s2	32 ± 6	23 ± 3	2.8 ± 0.1	2.7 ± 0.05
D12A	2.6 ± 0.2	4.5 ± 0.4	3.0 ± 0.1	2.9 ± 0.09
PFKs1s2D12A	3.4 ± 0.2	4.5 ± 0.3	1.3 ± 0.05	1.3 ± 0.03

[a] $K_{ix}°$ for WT from (*82*). [b] Values determined at [MgATP] = 15mM for LbPFK, 10mM for PFKs1s2 and 3mM for D12A and PFKs1s2D12A. [c] Values determined from coupling experiments between F6P and either PEP or MgADP. [d] Values determined from competition experiment between PEP and MgADP. [e] N.D. = not determined.

creatine kinase being present which would regenerate any MgADP formed from the reaction to MgATP. Figure 6-4 is a replot of the K_{iy}^{app} as a function of MgADP and fitting of the data to equation 2-6 the K_i for MgADP (K_{ix}^{app}) was determined for D12A, PFKs1s2 and PFKs1s2D12A. Table 6-2 compares the values for PEP and MgADP binding to the allosteric site from the two types of experiments and these numbers compare nicely indicating that the values for MgADP binding, as well as PEP binding, determined from the coupling experiments is measuring binding to the allosteric site.

Values for MgADP determined from the competition experiment with PEP are slightly weaker than that determined from the coupling experiments which might indicate that the inhibition measured in the coupling experiment could be a combination of both product and allosteric inhibition. Therefore, the binding affinity for MgADP to the active site was determined by measuring the K_b for MgATP at various concentrations of MgADP for PFKs1s2D12A (Figure 6-5A). By fitting the data to equation 2-4 a binding affinity for MgADP to the active site of 0.29 ± 0.02 mM was determined, 12-fold tighter than the binding affinity for MgADP at the allosteric site. The value for MgADP binding determined from the competition experiment between PEP and MgADP is much closer to the value of MgADP binding at the allosteric site than it is to the value for the active site. These results indicate that the inhibition measured in the coupling experiment between MgADP and F6P is due to the binding of MgADP at the allosteric site and not product inhibition.

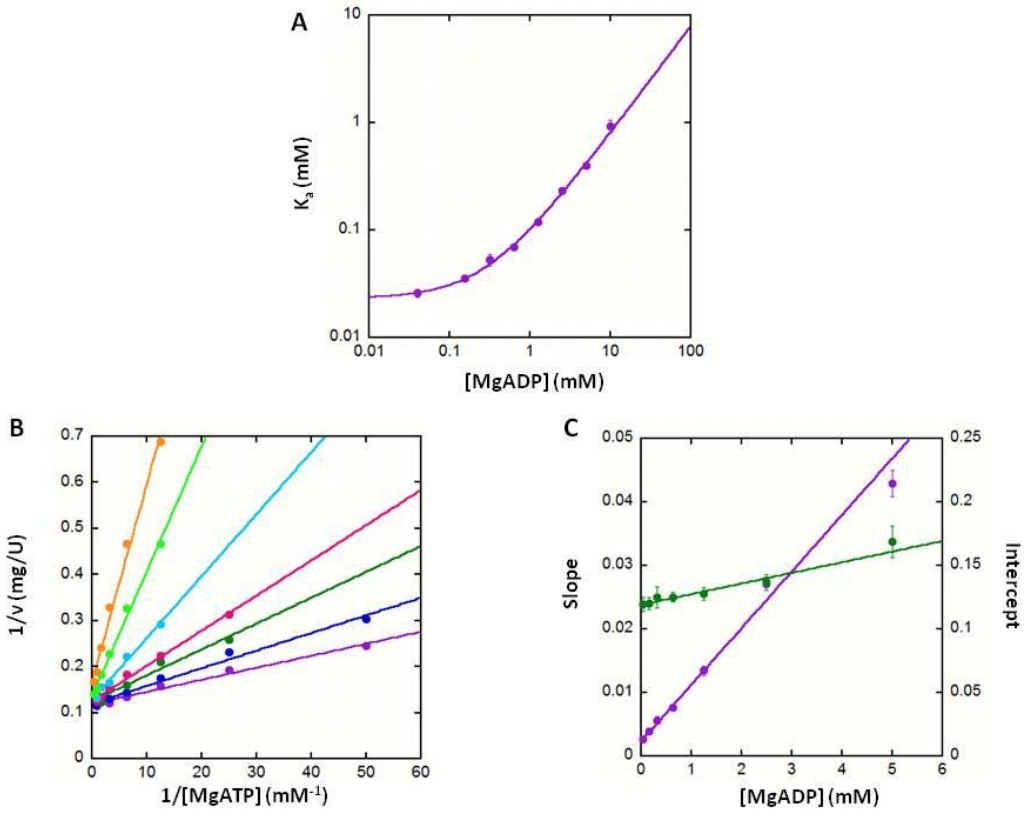

Figure 6-5. Effect of MgADP on binding of MgATP at the active site at 25°C, pH 8.0. (A) The K_b for MgATP was measured at various concentrations of MgADP and plotted as a function of [MgADP]. Data were fit to equation 2-4 to determine a K_i for MgADP at the active site of 0.29 ± 0.02 mM. (B) A double-reciprocal plot of initial velocity (ν) versus MgATP concentrations at the following MgADP concentrations: 0.04mM (purple), 0.156mM (blue), 0.313mM (dark green), 0.625mM (pink), 1.25mM (cyan), 2.5mM (light green) and 5mM (orange). Data were plotted to a linear equation to find the slope and intercept at each [MgADP]. (C) Replot of the slope (purple) and intercept (green) as a function of [MgADP].

Titrations curves for MgATP at [MgADP] from 0.04 to 5mM were plotted using a double-reciprocal plot of initial velocity (v) versus MgATP concentration (Figure 6-5B) and the pattern indicates a non-competitive relationship between MgATP and MgADP (*115*). In EcPFK, MgADP and MgATP have a competitive relationship which is described by a random kinetic mechanism at sub-saturating concentrations of F6P (*91, 114, 116*). In a random kinetic mechanism, saturating with substrate A will cause substrate B and the corresponding product Q to bind to different forms of the enzyme. The binding of B and Q to different forms of the enzyme will cause an change in the intercept and along with the change in slope, would give a non-competitive relationship between B and Q (*115*). Therefore, the non-competitive relationship between MgATP and MgADP in LbPFK could be explained simply by having saturating concentrations of F6P. Therefore, the dissociation constant determined for MgADP in the MgATP/MgADP experiment is likely to be at the active site, which is much tighter than that measured at the allosteric site (Figure 6-4 and 6-5). Comparing the dissociation constants for MgADP at both the active site and allosteric site indicate that the inhibition of F6P by MgADP is more likely to be allosteric inhibition than product inhibition.

Discussion

Two remote regions within the non-allosteric LbPFK were mutated in order to enhance binding affinity for the allosteric ligands PEP and MgADP. First, the allosteric binding site was targeted based on this region being the least conserved region when comparing LbPFK to the known allosteric PFKs, EcPFK, BsPFK and TtPFK. Residues

within the large cassettes 52-61 and 206-218 were changed from the sequence of LbPFK to the corresponding sequence of TtPFK. PFKs1s2 enhanced binding affinity of PEP 10-fold compared to WT LbPFK with no enhancement for the activator MgADP (see Chapter V). D12, located 15 Å away from the nearest allosteric site and along the active site interface, was changed to an alanine and enhanced binding for both PEP and MgADP 9-fold compared to LbPFK (see Chapter IV). Finally, combining both mutations to form PFKs1s2D12A caused a 21-fold enhancement in PEP binding that appears to be additive as it combines the 10-fold enhancement from Tt/Lb 2 with the 9-fold enhancement from D12A. The 21-fold enhancement in PEP binding was accompanied by a $Q_{ay} = 0.007 \pm 0.0008$ and this is the first time the inhibition of PEP has been quantified in the non-allosteric LbPFK.

Inhibition by PEP in PFKs1s2D12A is approximately 2-fold stronger than EcPFK ($Q_{ay} = 0.016 \pm 0.003$), 10-fold stronger than TtPFK ($Q_{ay} = 0.068 \pm 0.002$) even though the binding for PEP to Tt/Lb 2 + D12A is much weaker than either EcPFK or TtPFK (*72, 78, 81*). In 1991, La Bras did the first kinetic analysis of LbPFK and indicated that LbPFK is a non-allosteric PFK (*97*). However from the current study it is clear that LbPFK is an allosteric form of PFK with weak binding affinity for the allosteric ligands PEP and MgADP, though likely causing little allosteric control in the cell. It is possible that *Lactobacillus delbrueckii* subspecies *bulgaricus* no longer requires the allosteric regulation of PFK since it only metabolizes four sugars and the main role of its metabolism is to form lactic acid (*97*). There is evidence of an allosterically regulated glyceraldehydes-3-phosphoate dehydrogenase in *Lactobacillus*

delbrueckii subspecies *bulgaricus* and this could potentially be a more efficient way to regulate glycolysis in the lactic acid bacteria (*56*). However the weak binding for both PEP and MgADP make LbPFK a great template in better understanding of phenomenon of allostery.

Not only did PFKs1s2D12A have enhanced binding for the inhibitor PEP, it also exhibited 8-fold tighter binding for MgADP compared to WT LbPFK. PFKs1s2 had similar binding for MgADP as LbPFK but D12A showed a 9-fold enhanced binding for MgADP (see Chapters IV and V), indicating the change in MgADP binding to also be additive. Even more interesting than the enhanced binding for MgADP is the inhibitory effect by MgADP since MgADP acts as an activator in EcPFK. MgADP is also a product of the reaction, therefore it was important to ensure that the inhibition being measured is not product inhibition. Several approaches were taken and together indicate that the binding affinity measured at the allosteric site is much weaker than that for the active site and the inhibition of F6P binding by MgADP is an allosteric effect. The role of allosteric inhibition by MgADP in *Lactobacillus delbrueckii* subspecies *bulgaricus* is unclear but would likely not be seen in the cell due to the extremely weak binding for MgADP to LbPFK.

In conclusion, the current study indicates that the weak binding for PEP and MgADP to the allosteric binding site of LbPFK can be overcome by introducing changes within the residues in the allosteric site along with D12A into LbPFK. Mutating both regions within LbPFK causes enhanced binding for both allosteric ligands, though to different extents, and each region is responsible for its own contribution of the binding

affinity. Since no crystal structure has been solved for PFKs1s2D12A it is unclear how the mutations within each region affect the binding for PEP and MgADP and whether the changes in the binding affinities are even due to large structural changes or smaller dynamic changes. Further studies of PFKs1s2D12A are needed to not only define the reason for the enhancement in binding affinities but also to determine the minimum number of mutations required for the observed enhancement.

CHAPTER VII

SUMMARY

Phosphofructokinase (PFK) from the bacteria *E. coli* (EcPFK), *Bacillus stearothermophilus* (BsPFK) and *Thermus thermophilus* (TtPFK) is allosterically regulated by the inhibitor phospho(enol)pyruvate (PEP) and the activator MgADP. However, PFK from *Lactobacillus delbrueckii* subspecies *bulgaricus* (LbPFK) is non-allosteric PFK due to weak binding for both PEP and MgADP, approximately 27 mM for both ligands. Comparisons of the structures and sequences between LbPFK and the allosteric EcPFK and BsPFK show an overall conservation in structure and high sequence identity (47% identity with EcPFK and 56% identity with BsPFK) with the exception of the allosteric binding site. LbPFK, like EcPFK, BsPFK and TtPFK, is a homotetramer formed as a dimer-of-dimers. Along one dimer-dimer interfaces are the active sites and the allosteric sites along the other dimer-dimer interface. Another region identified in the Reinhart lab to be involved in PEP binding to BsPFK is along surrounding the 100% conserved D12 (*73, 85*). D12 interacts with various residues, including T156 and H160 that are located across the active site interface from D12 as well as R252 which is located within the active site and also interacts with the substrate fructose-6-phosphate (F6P). Mutating D12 to an alanine in BsPFK enhanced PEP binding 100-fold even though D12 is located 15 Å from the nearest allosteric binding site (*85*). Structural studies with D12A BsPFK showed that a large quaternary shift along the active site interface occurred when D12A was introduced as well as smaller

secondary structural changes within the allosteric binding site and the region surround D12A (*85*). In the current study mutations were introduced within the allosteric site as well as the region along the active site interface that includes D12, T156 and H160 to better understand the weak binding for PEP and MgADP in LbPFK.

First, two new structures of LbPFK were solved to add to the structural library of bacterial PFKs. The first structure was solved to 1.83 Å resolution and has phosphates bound to all four active sites, all four allosteric sites and one on the surface of each monomer. There is also a chloride ion bound to the four active sites. The surface phosphates and chloride ions are most likely due to the crystallization conditions which included $MgCl_2$ and ammonium mono-phosphate. The second structure was solved to 2.2 Å resolution and has phosphate bound to the same locations as the first structure with the differences being F6P bound to the four active sites as well as a magnesium ion in the place of the chloride ion. As with the first structure, the surface phosphates and magnesium ions are due to the crystallization conditions. The two new structures of LbPFK are similar in overall secondary, tertiary and quaternary structure to the sulfate-bound LbPFK structure published in 2005 (*82*). Only the B-factor, which is a measurement of how much an atom oscillates or vibrates around the position specified by the model, is different between the two structures. The phosphate-bound LbPFK is much more flexible overall compared to the substrate-bound LbPFK. The increased rigidity in structure upon F6P binding if LbPFK is opposite from what is seen in BsPFK where the F6P bound structure is the most flexible when comparing the substrate-bound, apo and inhibitor-bound structures (*85*). These two new structures of LbPFK are a more

useful comparison to the other bacterial PFK structures which have F6P and phosphate bound, which is a more physiologically relevant ion compared to sulfate.

Next, a mutagenesis study was performed on the D12 as well as the surrounding residues in LbPFK. D12 was mutated to an alanine in LbPFK and enhanced binding for both PEP and MgADP 9-fold compared to LbPFK. The change in PEP binding was weaker compared to that seen in BsPFK, so a crystal structure was solved of D12A LbPFK to 2.2 Å resolution. D12A LbPFK contained sulfates bound to the four active sites, four allosteric sites and one on the surface of each monomer. The presence of the sulfate on the surface of each monomer is likely due to the high concentration of ammonium sulfate in the crystallization conditions. No major structural changes were observed upon comparing the structures of D12A LbPFK and the sulfate-bound LbPFK. No structural change in opposite of the large structural change observed in BsPFK upon the mutation D12A. The lack of large structural perturbations might explain the smaller enhancement in PEP binding for D12A LbPFK compared to D12A BsPFK.

T156 and H160 form hydrogen bonds with D12 across the active site interface and introducing D12A into LbPFK would break these hydrogen bonds. The breaking of these bonds could be the reason for the enhanced PEP binding and so T156A and H160A were also introduced into LbPFK. Neither T156A nor H160A showed an enhancement in PEP binding. LbPFK contains a histidine at position 161, right next to the histidine at 160, and to show that H161 was not taking the place for H160 when H160A was introduced, H161A LbPFK as well as H160A/H161A LbPFK were created. Like T156A and H160A, H161A and H160A/H161A exhibited no enhancement in PEP binding when

compared to wild-type LbPFK. Lack of enhanced PEP binding for these variants indicates that the breaking of the hydrogen bonds formed between D12 and T156 or D12 and H160 is not the reason for the enhanced PEP binding seen in D12A LbPFK.

Another region that was focused on in the mutagenesis study of LbPFK was the allosteric site. As mentioned previously, resides within the allosteric site are not conserved when comparing LbPFK to EcPFK, BsPFK and TtPFK. Several of these residues were changed from the residues in LbPFK to the corresponding residue in TtPFK, since PEP binding to TtPFK is 9,000-fold tighter compared to LbPFK. E55R, H59N, S211R, D214K, H215S and G216S were introduced into LbPFK with no enhancement in PEP binding. Large cassette mutations were also utilized where large sequences of amino acids from LbPFK were substituted with the amino acid sequence from TtPFK. Regions including residues 52-61 (PFKs1), 206-218 (PFKs2), as well as the combination of the two regions (PFKs1s2) were mutated. PFKs1 and PFKs2, like the single mutants, showed no enhancement in PEP binding. However, PFKs1s2 exhibited PEP binding 10-fold tighter to LbPFK. Due to the enhanced PEP binding in PFKs1s2, binding for MgADP was measured and found to be similar to LbPFK. The results of the allosteric site variants indicate the need for multiple changes within the allosteric binding site in order to enhance binding for the allosteric inhibitor PEP and more changes are needed to enhance binding for MgADP.

Finally, the PFKs1s2 and D12A variants were combined to form PFKs1s2/D12A. By creating PFKs1s2/D12A, further enhancement in PEP binding was measured (21-fold compared to LbPFK). Along with the 21-fold enhancement in PEP binding, a coupling

between PEP and F6P was measured for the first time in LbPFK (Q_{ay} = 0.007 ± 0.0008). The Q_{ay} for PFKs1s2/D12A is 7-fold weaker than the coupling measured in BsPFK (Q_{ay} = 0.001 ± 0.0001) but 2-fold stronger compared to EcPFK (Qay = 0.016 ± 0.003) and 9-fold stronger compared to TtPFK (Q_{ay} = 0.068 ± 0.002) (*72, 78, 81*). MgADP binding for PFKs1s2/D12A was similar to D12A LbPFK indicating that the enhancement in MgADP binding is due to the D12A mutation. MgADP appears to act as an allosteric inhibitor in LbPFK. Enhancing MgADP binding in D12A and PFKs1s2D12A allows that inhibition to be more evident, and the reason for this inhibition in LbPFK is unclear. MgADP is a product of the PFK reaction and does show product inhibition of the substrate MgATP, but the inhibition of F6P is clearly allosteric. A crystal structure of PFKs1s2/D12A has not been determined but would be useful in better understanding the role of these mutations in the overall enhancement in binding and inhibition measured for both PEP and MgADP.

In conclusion, the crystal structures and mutagenesis studies performed on LbPFK indicate that there are remote regions within the enzyme that are important for binding of the allosteric ligands PEP and MgADP. Multiple changes in the allosteric site are needed to enhance the binding for PEP signifying that the weak binding of PEP in LbPFK is due to numerous differences in the composition of residues, not just a single residue, in the allosteric site. The role of D12A in enhancing the binding for PEP and MgADP is still unclear but is necessary for tighter binding to the allosteric site. The distance between D12 and the allosteric site is far reaching and the pathway that is involved in linking the two sites in unknown. From the studies of PFKs1s2/D12A, it is

clear that allosteric inhibition is possible in LbPFK if PEP and MgADP can bind to the allosteric binding site. It is likely then that the weak binding of PEP and MgADP to wild-type LbPFK causes the lack of allosteric regulation in this enzyme and as long as PEP and MgADP can bind with high enough affinity, an allosteric response can be measured. Identifying the role of each mutation in PFKs1s2/D12A is needed in order to truly understand the molecular basis of the enhanced PEP and MgADP binding compared to wild-type LbPFK.

REFERENCES

1. Mozzi, F., Raya, R. R., and Vignolo, G. M., (Eds.) (2010) *Biotechnology of Lactic Acid Bacteria: Novel Applications*, Blackwell Publishing, Ames, Iowa.

2. Hutkins, R. W. (2008) Microbiology and Technology of Fermented Foods, Wiley-Blackwell, Hobeken, NJ, USA.

3. Liu, S. Q. (2003) Practical implications of lactate and pyruvate metabolism by lactic acid bacteria in food and beverage fermentations, *Int J Food Microbiol 83*, 115-131.

4. Deutscher, J., Francke, C., and Postma, P. W. (2006) How phosphotransferase system-related protein phosphorylation regulates carbohydrate metabolism in bacteria, *Microbiol Mol Biol Rev 70*, 939-1031.

5. Higgins, C. F. (1992) ABC transporters: from microorganisms to man, *Annu Rev Cell Biol 8*, 67-113.

6. Premi, L., Sandine, W. E., and Elliker, P. R. (1972) Lactose-hydrolyzing enzymes of Lactobacillus species, *Appl Microbiol 24*, 51-57.

7. Lawrence, R. C., and Thomas, T. D. (1979) The fermentation in milk by lactic acid bacteria., In *Microbilogy Technology: Current State, Future Directions* (Bull, A. T., Ellwood, D. C., and Ratledge, C., Eds.), pp 187-219, Cambridge Univeristy Press, Cambridge, England.

8. Leloir, L. F. (1971) Two decades of research on the biosynthesis of saccharides, *Science 172*, 1299-1303.

9. Kuroda, M., Wilson, T. H., and Tsuchiya, T. (2001) Regulation of galactoside transport by the PTS, *J Mol Microbiol Biotechnol 3*, 381-384.

10. Hurley, J. H., Faber, H. R., Worthylake, D., Meadow, N. D., Roseman, S., Pettigrew, D. W., and Remington, S. J. (1993) Structure of the regulatory complex of *Escherichia coli* IIIGlc with glycerol kinase, *Science 259*, 673-677.

11. Decker, K., Plumbridge, J., and Boos, W. (1998) Negative transcriptional regulation of a positive regulator: the expression of malT, encoding the transcriptional activator of the maltose regulon of *Escherichia coli*, is negatively controlled by Mlc, *Mol Microbiol 27*, 381-390.

12. Zeng, G. Q., De Reuse, H., and Danchin, A. (1992) Mutational analysis of the enzyme IIIGlc of the phosphoenolpyruvate phosphotransferase system in *Escherichia coli*, *Res Microbiol 143*, 251-261.

13. Kuroda, M., de Waard, S., Mizushima, K., Tsuda, M., Postma, P., and Tsuchiya, T. (1992) Resistance of the melibiose carrier to inhibition by the phosphotransferase system due to substitutions of amino acid residues in the carrier of *Salmonella typhimurium*, *J Biol Chem 267*, 18336-18341.

14. Kuhnau, S., Reyes, M., Sievertsen, A., Shuman, H. A., and Boos, W. (1991) The activities of the *Escherichia coli* MalK protein in maltose transport, regulation, and inducer exclusion can be separated by mutations, *J Bacteriol 173*, 2180-2186.

15. Hogema, B. M., Arents, J. C., Bader, R., Eijkemans, K., Yoshida, H., Takahashi, H., Aiba, H., and Postma, P. W. (1998) Inducer exclusion in *Escherichia coli* by non-PTS substrates: the role of the PEP to pyruvate ratio in determining the phosphorylation state of enzyme IIAGlc, *Mol Microbiol 30*, 487-498.

16. Veenhoff, L. M., and Poolman, B. (1999) Substrate recognition at the cytoplasmic and extracellular binding site of the lactose transport protein of *Streptococcus thermophilus*, *J Biol Chem 274*, 33244-33250.

17. Poolman, B., Modderman, R., and Reizer, J. (1992) Lactose transport system of *Streptococcus thermophilus*. The role of histidine residues, *J Biol Chem 267*, 9150-9157.

18. Gunnewijk, M. G., Postma, P. W., and Poolman, B. (1999) Phosphorylation and functional properties of the IIA domain of the lactose transport protein of *Streptococcus thermophilus*, *J Bacteriol 181*, 632-641.

19. Darbon, E., Servant, P., Poncet, S., and Deutscher, J. (2002) Antitermination by GlpP, catabolite repression via CcpA and inducer exclusion triggered by P-GlpK dephosphorylation control *Bacillus subtilis* glpFK expression, *Mol Microbiol 43*, 1039-1052.

20. Deutscher, J., and Sauerwald, H. (1986) Stimulation of dihydroxyacetone and glycerol kinase activity in *Streptococcus faecalis* by phosphoenolpyruvate-dependent phosphorylation catalyzed by enzyme I and HPr of the phosphotransferase system, *J Bacteriol 166*, 829-836.

21. Mijakovic, I., Poncet, S., Galinier, A., Monedero, V., Fieulaine, S., Janin, J., Nessler, S., Marquez, J. A., Scheffzek, K., Hasenbein, S., Hengstenberg, W., and Deutscher, J. (2002) Pyrophosphate-producing protein dephosphorylation by HPr kinase/phosphorylase: a relic of early life?, *Proc Natl Acad Sci U S A 99*, 13442-13447.

22. Reizer, J., Sutrina, S. L., Saier, M. H., Stewart, G. C., Peterkofsky, A., and Reddy, P. (1989) Mechanistic and physiological consequences of HPr(ser) phosphorylation on the activities of the phosphoenolpyruvate:sugar phosphotransferase system in gram-positive bacteria: studies with site-specific mutants of HPr, *EMBO J 8*, 2111-2120.

23. Eisermann, R., Deutscher, J., Gonzy-Treboul, G., and Hengstenberg, W. (1988) Site-directed mutagenesis with the ptsH gene of *Bacillus subtilis*. Isolation and characterization of heat-stable proteins altered at the ATP-dependent regulatory phosphorylation site, *J Biol Chem 263*, 17050-17054.

24. Deutscher, J. a. E., R. . (1984) Purification and characterization of an ATP-dependent protein kinase from *Streptococcus faecallis*, *FEMS Microbiol Lett 23*, 157-162.

25. Reizer, J., Sutrina, S. L., Wu, L. F., Deutscher, J., Reddy, P., and Saier, M. H., Jr. (1992) Functional interactions between proteins of the phosphoenolpyruvate:sugar phosphotransferase systems of *Bacillus subtilis* and *Escherichia coli*, *J Biol Chem 267*, 9158-9169.

26. Morel, F., Lamarque, M., Bissardon, I., Atlan, D., and Galinier, A. (2001) Autoregulation of the biosynthesis of the CcpA-like protein, PepR1, in *Lactobacillus delbrueckii* subsp *bulgaricus*, *J Mol Microbiol Biotechnol 3*, 63-66.

27. Dossonnet, V., Monedero, V., Zagorec, M., Galinier, A., Perez-Martinez, G., and Deutscher, J. (2000) Phosphorylation of HPr by the bifunctional HPr Kinase/P-ser-HPr phosphatase from *Lactobacillus casei* controls catabolite repression and inducer exclusion but not inducer expulsion, *J Bacteriol 182*, 2582-2590.

28. Jault, J. M., Fieulaine, S., Nessler, S., Gonzalo, P., Di Pietro, A., Deutscher, J., and Galinier, A. (2000) The HPr kinase from *Bacillus subtilis* is a homo-oligomeric enzyme which exhibits strong positive cooperativity for nucleotide and fructose 1,6-bisphosphate binding, *J Biol Chem 275*, 1773-1780.

29. Arutyunov, D. Y., and Muronetz, V. I. (2003) The activation of glycolysis performed by the non-phosphorylating glyceraldehyde-3-phosphate dehydrogenase in the model system, *Biochem Biophys Res Commun 300*, 149-154.

30. Cao, R., Zeidan, A. A., Radstrom, P., and van Niel, E. W. (2010) Inhibition kinetics of catabolic dehydrogenases by elevated moieties of ATP and ADP--implication for a new regulation mechanism in *Lactococcus lactis*, *FEBS J 277*, 1843-1852.

31. Hensel, R., Mayr, U., Stetter, K. O., and Kandler, O. (1977) Comparative studies of lactic acid dehydrogenases in lactic acid bacteria. I. Purification and kinetics of the allosteric L-lactic acid dehydrogenase from *Lactobacillus casei* ssp. *casei* and *Lactobacillus curvatus*, *Arch Microbiol 112*, 81-93.

32. Garvie, E. I. (1980) Bacterial lactate dehydrogenases, *Microbiol Rev 44*, 106-139.

33. Taguchi, H., and Ohta, T. (1992) Unusual amino acid substitution in the anion-binding site of *Lactobacillus plantarum* non-allosteric L-lactate dehydrogenase, *Eur J Biochem 209*, 993-998.

34. Hensel, R., Mayr, U., and Yang, C. Y. (1983) The complete primary structure of the allosteric L-lactate dehydrogenase from *Lactobacillus casei*, *Eur J Biochem 134*, 503-511.

35. Hensel, R., Mayr, U., and Woenckhaus, C. (1983) Affinity labelling of the allosteric site of the L-lactate dehydrogenase of *Lactobacillus casei*, *Eur J Biochem 135*, 359-365.

36. Jurica, M. S., Mesecar, A., Heath, P. J., Shi, W., Nowak, T., and Stoddard, B. L. (1998) The allosteric regulation of pyruvate kinase by fructose-1,6-bisphosphate, *Structure 6*, 195-210.

37. Malcovati, M., and Kornberg, H. L. (1969) Two types of pyruvate kinase in *Escherichia coli* K12, *Biochim Biophys Acta 178*, 420-423.

38. Le Bras, G., and Garel, J. R. (1993) Pyruvate kinase from *Lactobacillus bulgaricus*: possible regulation by competition between strong and weak effectors, *Biochimie 75*, 797-802.

39. Collins, L. B., and Thomas, T. D. (1974) Pyruvate kinase of *Streptococcus lactis*, *J Bacteriol 120*, 52-58.

40. Thompson, J., and Torchia, D. A. (1984) Use of 31P nuclear magnetic resonance spectroscopy and 14C fluorography in studies of glycolysis and regulation of pyruvate kinase in *Streptococcus lactis*, *J Bacteriol 158*, 791-800.

41. Sakai, H., Suzuki, K., and Imahori, K. (1986) Purification and properties of pyruvate kinase from *Bacillus stearothermophilus*, *J Biochem 99*, 1157-1167.

42. Simon, W. A., and Hofer, H. W. (1977) Allosteric and non-allosteric phosphofructokinases from Lactobacilli. Purification and properties of phosphofructokinases from *L. plantarum* and *L. acidophilus*, *Biochim Biophys Acta 481*, 450-462.

43. Doelle, H. W. (1971) Kinetic Characterization of Phosphofructokinase from *Lactobacillus casei* var. *rhamnosus* ATCC 7469 and *Lactobacillus plantarum* ATCC 14917, *Biochemica et biophysica acta 258*, 404-410.

44. Simon, W. A., and Hofer, H. W. (1981) Phosphofructokinases from Lactobacteriaceae. II. Purification and properties of phosphofructokinase from *Streptococcus thermophilus*, *Biochim Biophys Acta 661*, 158-163.

45. Le Bras, G., Deville-Bonne, D., and Garel, J.-R. (1991) Purification and properties of the phosphofructokinase from *Lactobacillus bulgaricus*: A non-allosteric analog of the enzyme from *Escherichia coli*, *European Journal of Biochemistry 198*, 683-687.

46. Branny, P., De La Torre, F., and Garel, J. R. (1993) Cloning, sequencing, and expression in *Escherichia coli* of the gene coding for phosphofructokinase in *Lactobacillus bulgaricus*, *J Bacteriol 175*, 5344-5349.

47. Kotlarz, D., and Buc, H. (1981) Regulatory properties of phosphofructokinase 2 from *Escherichia coli*, *Eur J Biochem 117*, 569-574.

48. Guixe, V., Rodriguez, P. H., and Babul, J. (1998) Ligand-induced conformational transitions in *Escherichia coli* phosphofructokinase 2: evidence for an allosteric site for MgATP2, *Biochemistry 37*, 13269-13275.

49. Guixe, V., and Babul, J. (1985) Effect of ATP on phosphofructokinase-2 from *Escherichia coli*. A mutant enzyme altered in the allosteric site for MgATP, *J Biol Chem 260*, 11001-11005.

50. Guixe, V., and Babul, J. (1988) Influence of ligands on the aggregation of the normal and mutant forms of phosphofructokinase 2 of *Escherichia coli*, *Arch Biochem Biophys 264*, 519-524.

51. Johnson, J. L., and Reinhart, G. D. (1992) MgATP and fructose 6-phosphate interactions with phosphofructokinase from *Escherichia coli*, *Biochemistry 31*, 11510-11518.

52. Fenton, A. W., and Reinhart, G. D. (2003) Mechanism of substrate inhibition in *Escherichia coli* phosphofructokinase, *Biochemistry 42*, 12676-12681.

53. Cabrera, R., Ambrosio, A. L., Garratt, R. C., Guixe, V., and Babul, J. (2008) Crystallographic structure of phosphofructokinase-2 from *Escherichia coli* in complex with two ATP molecules. Implications for substrate inhibition, *J Mol Biol 383*, 588-602.

54. Cabrera, R., Baez, M., Pereira, H. M., Caniuguir, A., Garratt, R. C., and Babul, J. (2010) The crystal complex of phosphofructokinase-2 of *Escherichia coli* with fructose-6-P: kinetic and structural analysis of the allosteric ATP inhibition, *J Biol Chem*.

55. Makarova, K., Slesarev, A., Wolf, Y., Sorokin, A., Mirkin, B., Koonin, E., Pavlov, A., Pavlova, N., Karamychev, V., Polouchine, N., Shakhova, V., Grigoriev, I., Lou, Y., Rohksar, D., Lucas, S., Huang, K., Goodstein, D. M., Hawkins, T., Plengvidhya, V., Welker, D., Hughes, J., Goh, Y., Benson, A., Baldwin, K., Lee, J. H., Diaz-Muniz, I., Dosti, B., Smeianov, V., Wechter, W., Barabote, R., Lorca, G., Altermann, E., Barrangou, R., Ganesan, B., Xie, Y., Rawsthorne, H., Tamir, D., Parker, C., Breidt, F., Broadbent, J., Hutkins, R., O'Sullivan, D., Steele, J., Unlu, G., Saier, M., Klaenhammer, T., Richardson, P., Kozyavkin, S., Weimer, B., and Mills, D. (2006) Comparative genomics of the lactic acid bacteria, *Proc Natl Acad Sci U S A 103*, 15611-15616.

56. van de Guchte, M., Penaud, S., Grimaldi, C., Barbe, V., Bryson, K., Nicolas, P., Robert, C., Oztas, S., Mangenot, S., Couloux, A., Loux, V., Dervyn, R., Bossy, R., Bolotin, A., Batto, J. M., Walunas, T., Gibrat, J. F., Bessieres, P., Weissenbach, J., Ehrlich, S. D., and Maguin, E. (2006) The complete genome sequence of *Lactobacillus bulgaricus* reveals extensive and ongoing reductive evolution, *Proc Natl Acad Sci U S A 103*, 9274-9279.

57. Wood, B., and Warner, P. (2003) *Genetics of Lactic Acid Bacteria*, Kluwer Academic, Plenum, New York.

58. Jamet, E., Ehrlich, D., Duperray, F., and Renault, P. (2001) Study of the duplicated glycolytic genes in *Lactococcus lactis* IL1403, *Lait 81*, 115-129.

59. Siebers, B., Klenk, H. P., and Hensel, R. (1998) PPi-dependent phosphofructokinase from *Thermoproteus tenax*, an archaeal descendant of an ancient line in phosphofructokinase evolution, *J Bacteriol 180*, 2137-2143.

60. Asanuma, N., Kanada, K., and Hino, T. (2008) Molecular properties and transcriptional control of the phosphofructokinase and pyruvate kinase genes in a ruminal bacterium, *Streptococcus bovis*, *Anaerobe 14*, 237-241.

61. Crispie, F., Anba, J., Renault, P., Ehrlich, D., Fitzgerald, G., and van Sinderen, D. (2002) Identification of a phosphofructokinase-encoding gene from *Streptococcus thermophilus* CHRZ1205 - a novel link between carbon metabolism and gene regulation?, *Molecular Genetics and Genomics 268*, 500-509.

62. Luesink, E. J., van Herpen, R. E., Grossiord, B. P., Kuipers, O. P., and de Vos, W. M. (1998) Transcriptional activation of the glycolytic las operon and catabolite repression of the gal operon in *Lactococcus lactis* are mediated by the catabolite control protein CcpA, *Mol Microbiol 30*, 789-798.

63. van den Bogaard, P. T., Kleerebezem, M., Kuipers, O. P., and de Vos, W. M. (2000) Control of lactose transport, beta-galactosidase activity, and glycolysis by CcpA in *Streptococcus thermophilus*: evidence for carbon catabolite repression by a non-phosphoenolpyruvate-dependent phosphotransferase system sugar, *J Bacteriol 182*, 5982-5989.

64. Viana, R., Perez-Martinez, G., Deutscher, J., and Monedero, V. (2005) The glycolytic genes pfk and pyk from *Lactobacillus casei* are induced by sugars transported by the phosphoenolpyruvate:sugar phosphotransferase system and repressed by CcpA, *Archives of Microbiology 183*, 385-393.

65. Llanos, R. M., Harris, C. J., Hillier, A. J., and Davidson, B. E. (1993) Identification of a novel operon in *Lactococcus lactis* encoding three enzymes for lactic acid synthesis: phosphofructokinase, pyruvate kinase, and lactate dehydrogenase, *J Bacteriol 175*, 2541-2551.

66. Gouy, M., and Gautier, C. (1982) Codon usage in bacteria: correlation with gene expressivity, *Nucleic Acids Res 10*, 7055-7074.

67. Branny, P., De La Torre, F., and Garel, J. R. (1996) The genes for phosphofructokinase and pyruvate kinase of *Lactobacillus delbrueckii* subsp. *bulgaricus* constitute an operon, *J Bacteriol 178*, 4727-4730.

68. Changeux, J. P. (1961) The feedback control mechanisms of biosynthetic L-threonine deaminase by L-isoleucine, *Cold Spring Harb Symp Quant Biol 26*, 313-318.

69. Gerhart, J. C., and Pardee, A. B. (1962) The enzymology of control by feedback inhibition, *J Biol Chem 237*, 891-896.

70. Monod, J., Wyman, J., and Changeux, J. P. (1965) On the Nature of Allosteric Transitions: A Plausible Model, *J Mol Biol 12*, 88-118.

71. Koshland, D. E., Jr., Nemethy, G., and Filmer, D. (1966) Comparison of experimental binding data and theoretical models in proteins containing subunits, *Biochemistry 5*, 365-385.

72. Johnson, J. L., and Reinhart, G. D. (1997) Failure of a two-state model to describe the influence of phospho(enol)pyruvate on phosphofructokinase from *Escherichia coli*, *Biochemistry 36*, 12814-12822.

73. Ortigosa, A. D., Kimmel, J. L., and Reinhart, G. D. (2004) Disentangling the web of allosteric communication in a homotetramer: heterotropic inhibition of phosphofructokinase from *Bacillus stearothermophilus*, *Biochemistry 43*, 577-586.

74. Reinhart, G. D. (1983) The determination of thermodynamic allosteric parameters of an enzyme undergoing steady-state turnover, *Arch Biochem Biophys 224*, 389-401.

75. Weber, G. (1972) Ligand binding and internal equilibria in proteins, *Biochemistry 11*, 864-878.

76. Weber, G. (1975) Energetics of ligand binding to proteins, *Adv Protein Chem 29*, 1-83.

77. Reinhart, G. D. (2004) Quantitative analysis and interpretation of allosteric behavior, *Methods Enzymol 380*, 187-203.

78. Shubina-McGresham, M. (2011) Allosteric Regulation of Phosphofructokinase in the extreme thermophilic bacterium *Thermus thermophilus*, Disseratation in preparation, Texas A&M University, College Station, TX.

79. Tlapak-Simmons, V. L., and Reinhart, G. D. (1994) Comparison of the inhibition by phospho(enol)pyruvate and phosphoglycolate of phosphofructokinase from *B. stearothermophilus*, *Arch Biochem Biophys 308*, 226-230.

80. Johnson, J. L., and Reinhart, G. D. (1994) Influence of MgADP on phosphofructokinase from *Escherichia coli*. Elucidation of coupling interactions with both substrates, *Biochemistry 33*, 2635-2643.

81. Kimmel, J. L., and Reinhart, G. D. (2000) Reevaluation of the accepted allosteric mechanism of phosphofructokinase from *Bacillus stearothermophilus*, *Proc Natl Acad Sci U S A 97*, 3844-3849.

82. Paricharttanakul, N. M., Ye, S., Menefee, A. L., Javid-Majd, F., Sacchettini, J. C., and Reinhart, G. D. (2005) Kinetic and structural characterization of phosphofructokinase from Lactobacillus bulgaricus, *Biochemistry 44*, 15280-15286.

83. Shirakihara, Y., and Evans, P. R. (1988) Crystal structure of the complex of phosphofructokinase from Escherichia coli with its reaction products, *J Mol Biol 204*, 973-994.

84. Schirmer, T., and Evans, P. R. (1990) Structural basis of the allosteric behaviour of phosphofructokinase, *Nature 343*, 140-145.

85. Mosser, R. E. (2010) A Structural and Kinetic Study into the Role of the Quaternary Shift in *Bacillus stearothermophilus* Phosphofructokinase, Dissertation, Texas A&M University, College Station, TX.

86. Hill, L., and Flack, M. (1910) The influence of oxygen inhalations on muscular work, *J Physiol 40*, 347-372.

87. Briggs, G. E., and Haldane, J. B. (1925) A Note on the Kinetics of Enzyme Action, *Biochem J 19*, 338-339.

88. Reinhart, G. D. (1988) Linked-function origins of cooperativity in a symmetrical dimer, *Biophys Chem 30*, 159-172.

89. Cleland, W. W. (1986) *Enzyme kinetics as a tool for determination of enyzme mechanisms*, John Wiley and Sons, New York.

90. Lovingshimer, M. R., Siegele, D., and Reinhart, G. D. (2006) Construction of an inducible, pfkA and pfkB deficient strain of *Escherichia coli* for the expression and purification of phosphofructokinase from bacterial sources, *Protein Expr Purif 46*, 475-482.

91. Blangy, D., Buc, H., and Monod, J. (1968) Kinetics of the allosteric interactions of phosphofructokinase from *Escherichia coli*, *J Mol Biol 31*, 13-35.

92. Byrnes, M., Zhu, X., Younathan, E. S., and Chang, S. H. (1994) Kinetic characteristics of phosphofructokinase from *Bacillus stearothermophilus*: MgATP nonallosterically inhibits the enzyme, *Biochemistry 33*, 3424-3431.

93. Blangy, D. (1968) Phosphofructokinase from *E. Coli*: Evidence for a tetrameric structure of the enzyme, *FEBS Lett 2*, 109-111.

94. Evans, P. R., Farrants, G. W., and Hudson, P. J. (1981) Phosphofructokinase: structure and control, *Philos Trans R Soc Lond B Biol Sci 293*, 53-62.

95. Rypniewski, W. R., and Evans, P. R. (1989) Crystal structure of unliganded phosphofructokinase from *Escherichia coli*, *J Mol Biol 207*, 805-821.

96. Riley-Lovingshimer, M. R., Ronning, D. R., Sacchettini, J. C., and Reinhart, G. D. (2002) Reversible ligand-induced dissociation of a tryptophan-shift mutant of phosphofructokinase from *Bacillus stearothermophilus*, *Biochemistry 41*, 12967-12974.

97. Le Bras, G., Deville-Bonne, D., and Garel, J. R. (1991) Purification and properties of the phosphofructokinase from *Lactobacillus bulgaricus*. A non-allosteric analog of the enzyme from Escherichia coli, *Eur J Biochem 198*, 683-687.

98. Thaller, C., Weaver, L. H., Eichele, G., Wilson, E., Karlsson, R., and Jansonius, J. N. (1981) Repeated seeding technique for growing large single crystals of proteins, *J Mol Biol 147*, 465-469.

99. Otwinowski, Z., Minor, W., and Charles W. Carter, J. (1997) Processing of X-ray diffraction data collected in oscillation mode, *Methods Enzymol 276*, 307-326.

100. McCoy, A. J., Grosse-Kunstleve, R. W., Adams, P. D., Winn, M. D., Storoni, L. C., and Read, R. J. (2007) Phaser crystallographic software, *J Appl Crystallogr 40*, 658-674.

101. Adams, P. D., Grosse-Kunstleve, R. W., Hung, L. W., Ioerger, T. R., McCoy, A. J., Moriarty, N. W., Read, R. J., Sacchettini, J. C., Sauter, N. K., and Terwilliger, T. C. (2002) PHENIX: building new software for automated crystallographic structure determination, *Acta Crystallogr D Biol Crystallogr 58*, 1948-1954.

102. Emsley, P., and Cowtan, K. (2004) Coot: model-building tools for molecular graphics, *Acta Crystallogr D Biol Crystallogr 60*, 2126-2132.

103. Davis, I. W., Leaver-Fay, A., Chen, V. B., Block, J. N., Kapral, G. J., Wang, X., Murray, L. W., Arendall, W. B., 3rd, Snoeyink, J., Richardson, J. S., and Richardson, D. C. (2007) MolProbity: all-atom contacts and structure validation for proteins and nucleic acids, *Nucleic Acids Res 35*, W375-383.

104. Rhodes, G. (2006) *Crystallography Made Crystal Clear: A Guide for Users of Macromolecular Models*, Third ed., Elsevier, Inc., Burlington, MA.

105. Parthasarathy, S., and Murthy, M. R. (2000) Protein thermal stability: insights from atomic displacement parameters (B values), *Protein Eng 13*, 9-13.

106. Raaijmakers, H. C., Versteegh, J. E., and Uitdehaag, J. C. (2009) The X-ray structure of RU486 bound to the progesterone receptor in a destabilized agonistic conformation, *J Biol Chem 284*, 19572-19579.

107. Kundrot, C. E., and Evans, P. R. (1991) Designing an allosterically locked phosphofructokinase, *Biochemistry 30*, 1478-1484.

108. Pham, A. S., and Reinhart, G. D. (2001) MgATP-dependent activation by phosphoenolpyruvate of the E187A mutant of *Escherichia coli* phosphofructokinase, *Biochemistry 40*, 4150-4158.

109. Paricharttanakul, N. M. (2004) Pathway to Allostery: Differential Routes for Allosteric Communication in Phosphofructokinase from *Eschericia coli*, Dissertation, Texas A&M University, College Station, TX.

110. Kimmel, J. L., and Reinhart, G. D. (2001) Isolation of an individual allosteric interaction in tetrameric phosphofructokinase from *Bacillus stearothermophilus*, *Biochemistry 40*, 11623-11629.

111. Lau, F. T., and Fersht, A. R. (1989) Dissection of the effector-binding site and complementation studies of *Escherichia coli* phosphofructokinase using site-directed mutagenesis, *Biochemistry 28*, 6841-6847.

112. Byrnes, W. M., Hu, W., Younathan, E. S., and Chang, S. H. (1995) A Chimeric Bacterial Phosphofructokinase Exhibits Coopertivity in the Absence of Heterotropic Regulation, *The Journal of Biological Chemistry 270*, 3828-3835.

113. Tlapak-Simmons, V. L., and Reinhart, G. D. (1998) Obfuscation of allosteric structure-function relationships by enthalpy-entropy compensation, *Biophys J 75*, 1010-1015.

114. Johnson, J. L., and Reinhart, G. D. (1994) Influence of substrates and MgADP on the time-resolved intrinsic fluorescence of phosphofructokinase from *Escherichia coli*. Correlation of tryptophan dynamics to coupling entropy, *Biochemistry 33*, 2644-2650.

115. Cook, P. F., and Cleland, W. W. (2007) *Enzyme Kinetics and Mechanism*, Garland Science, New York, New York.

116. Deville-Bonne, D., Laine, R., and Garel, J. R. (1991) Substrate antagonism in the kinetic mechanism of *E. coli* phosphofructokinase-1, *FEBS Lett 290*, 173-176.

VITA

Scarlett Blair Ferguson

Department of Biochemistry and Biophysics
103 Biochemistry/Biophysics Building
Texas A&M University
2128 TAMU
College Station, TX, 77843-2128

Education:

Angelo State University, San Angelo, TX	Chemistry	B.S., 2003
Texas A&M University, College Station, TX	Biochemistry	Ph.D., 2011

Publications:

Ferguson, S.B. and Reinhart, G.D. (2011) The effect of remote regions on the binding and allosteric inhibition for PEP in Phosphofructokinase from *Lactobacillus delbrueckii* subspecies *bulgaricus* (In preparation)

Ferguson, S.B. and Reinhart, G.D. (2011) Introducing allosteric inhibition and enhanced PEP binding in the non-allosteric PFK from *Lactobacillus delbrueckii* subspecies *bulgaricus* (In preparation)

Presentations:

Scarlett A. Blair (2005) Conferring Allosteric Response in a Non-Allosteric Phosphofructokinase. Department of Biochemistry/Biophysics Research Competition, Texas A&M University, College Station, TX.

Scarlett A. Blair (2007) Conferring Allosteric Response in a Non-Allosteric Phosphofructokinase: The Story from *Lactobacillus delbrueckii* subspecies *bulgaricus*. Texas Protein Folder's Annual Meeting, Camp Allen, Navasota, TX.

Scarlett B. Ferguson (2010) Remote regions involved in the binding of phospho(enol)pyruvate to Phosphofructokinase from *Lactobacillus delbrueckii* subspecies *bulgaricus.* Chemistry/Biology Interface Group Annual Conference, Texas A&M University, College Station, TX.